UNIVERSITY OF SOUTHAMPTON

School of Engineering Sciences

Hydroelastic Investigation of a Fast Patrol Boat made of Fibre Reinforced Plastic

by

Francisco Machado dos Santos

Thesis for the degree of Master of Philosophy

July 2005

To my wife, my parents,

and the loving memory

of my grandfather Manuel Praia and uncle Jose Quita-Quita.

ABSTRACT

The aim of this document is to investigate the dynamic behaviour of a fast patrol boat due to wave induce loads using a hydroelastic approach. This includes two and three dimensional idealisations for *dry hull* analysis and three-dimensional *wet hull* analysis for both idealisations. Regarding *dry hull* analysis a preliminary two-dimensional beam analysis is conducted by means of the Prohl-Myklestad method where it is intended to derive a first estimate of the first four symmetrical mode shapes. Later a more complex three-dimensional finite element model is developed in order to evaluate the *in vacuo* modal characteristics until the fourth node symmetrical vertical mode shape, although, the latter analysis does not exclude antisymmetric and coupled distortions. The *wet hull* analysis includes a three dimensional hydrodynamic analysis, based on a singularity distribution on the mean wetted surface, for both non-uniform beam and three dimensional structural model idealisations. The algorithm used for the evaluation of the Green's function for the pulsating source is based on a method using asymptotic and Taylor series. Three heading angles are investigated, i.e. 180, 135 and 90 degrees for regular waves of varying frequency. Results from full scale trials are also presented in order to compare rigid body motions transfer functions with numerical predictions. The evaluation of the dynamic behaviour of the fast patrol boat, with small length to beam ratio, by means of a unified hydroelastic analysis, showed some inherent limitations of a beamlike approach for this particular type of vessels.

Contents

List of Tables

List of Figures

Acknowledgements

I am fully thankful for the motivation, scientific support and endless patience always demonstrated by my co-supervisors Professor Guedes Soares and Professor Temarel during the development of this investigation.

I am also thankful for the crucial support given by my colleagues at the Ship Science Department, during my stay at Southampton University, in particular to Spyro Hirardis, Paolo Manganelli, Leigh Sutherland, Marco Salas Inzunza and Frédéric Louarn.

I wish to thank my portuguese colleagues of the Unit of Marine Technology and Engineering, of IST, in particular to important support provided by Dr. Nuno Fonseca, Dr. Yordan Gorbatov and Capt.Lt. Alves Francisco, and to the always competent team work produced by Ricardo Pascoal, Miguel Costa and Filipe Duarte during the difficult working conditions experienced in the seakeeping trials.

I make a very special reference to my late and missed colleague José Carlos Goncalves that largely facilitate my integration in Southampton University.

I finally thank the Commander and Crew of NRP Dragao for their full cooperation during sea trials. These trials were included in the project named *Prediction of Ship Operationality Considering Wave Climate and Ship Behaviour* funded by the Portuguese Defence Ministry and by the Portuguese Universities Foundation.

Chapter 1

Introduction

Ship responses to environmental conditions have a fundamental role in safety, performance and capability. In commercial type vessels like cargo, fishing or passenger, there is, in most cases, the possibility of taking evasive manoeuvres to avoid the influence of heavy weather. Most common actions taken by the Master are voluntary speed reduction or rudder action for heading change. However, these actions cannot be taken by naval vessels when on rescue or military missions. Therefore, motions and structural responses play an important role in the latter.

Throughout history, Fast Patrol Boats have been designed for speed, manoeuvrability and structural robustness in heavy seas. In fact, mission requirements demand that this kind of high performance craft operate under conditions where the fluid-structure interaction could be quite remarkable.

In conventional seakeeping studies, ships are considered as rigid bodies that will respond with six degrees of freedom corresponding to surge, sway, yaw, and, in a more relevant oscillatory behaviour, roll, pitch and heave, that in practical terms refer to the fact that only hull shape matters. However, the ship also distorts due to static and dynamic loading of the flexible hull in waves, implying that the ship internal structure must play an important role in defining the seaworthiness of a vessel.

Hull stressing can be induced in a continuous and steady way when the frequency associated with the dynamic pressure distribution along the hull matches the fundamental first vertical mode shapes. Semi-empirical formulations have described this phenomenon as *springing*, and if the structure responds in transient decay of amplitudes of vibration, after a slamming or deck wetting at bow or stern, is often called *whipping*. However, the basic principles of the dynamics of flexible bodies should be used to characterize both. These principles will allow the identification of time-dependent strains that are superimposed on those present in still water.

It is of much importance that, if possible in the design stage, the investigation of resonance frequencies and characterization of natural modes should be made. One well known action is to avoid hull resonance frequencies to be near blade rate frequency or frequencies from other sources of excitation. Knowing the mode shapes, and consequently nodal positions, is also useful to the designer in selecting the appropriate location for the installation of rotating machinery and mass distribution.

For the fluid structure interaction, variables like speed and heading can be taken into consideration to avoid resonance. In other words, not only the characterization of the rigid body response to waves, *seakeeping* is fundamental, but also the knowledge of the flexible response is crucial for the ship's safety, providing the shipmaster the necessary information to prevent excessive hull stressing. This thesis is intended to characterize both rigid and flexible body responses, by means of the application of a unified three-dimensional hydroelastic theory, towards the assessment of the dynamic behaviour of a Fast Patrol Boat.

Summary of Chapters' Contents

The aim of chapter 2 is to present a brief overview of the research developed towards the development of present day hydroelasticity theories. An introductory summary is given on the chronological progression until present, together with a brief description of the current trends of structural design methodologies used in naval architecture. The evolution of the hydrodynamic methodologies, from classical strip theory to more advanced panel methods, is also presented. References are reviewed for the assessment of a unified approach between rigid and flexible body dynamics.

In chapters 3 and 4 are presented the general formulations adopted to characterize the fluid structure interaction problem. They contain, respectively, the formulation of the generalized equations of motion to evaluate the *in vacuo* modal characteristics of the ship structure and a summary description of the formulation of the potential flow around the hull of a ship advancing and oscillating in waves.

The geometry of a three dimensional model is validated against data from the actual ship in chapter 5. Chapter 6 deals with estimation of mechanical properties of the patrol boat, whith fibre reinforced plastic requiring a particular theoretical formulation. Included in the *dry analysis*, a preliminary investigation of the characteristic modal behaviour of the structure for a two dimensional non uniform beam model is analysed by means of the Prohl-Myklestad method, and results are presented in chapter 7. For a more detailed *in vacuo* three dimensional modal analysis, chapter 8 explains the assumptions made for choice of finite element type, the development of the three dimensional model geometry and results obtained for natural frequencies and characteristic mode shapes.

Chapter 9 contains calculations for the principal coordinates for the two model idealisations for Froude numbers of 0.53 and 0.66 at three different headings. This also includes the rigid body motions, which are part of the unified hydroelastic theory. Experimental results from full scale trials are presented in chapter 10. This chapter also contains a brief description of the instrumentation procedure and validation of some sensors, in particular the wave height meter. Finally, experimental results are compared to theoretical predictions in chapter 11, and conclusions are in chapter 12.

Chapter 2

Literature Review

2.1 Introduction

Dynamic systems which can be decomposed in a set of physical components, idealised as fields operating in different continuums that interact with each other, are often called *coupled field problems*, or *multiphysics problems*. The general description of physical interaction problems comprises a wide range of particular engineering disciplines. The basis of the present investigation is often called a *fluid-structure interaction* (FSI); however, other coupled field problems are found in other engineering disciplines, like *control-structure interaction* (CSI), *flow in porous media* (FPM), *thermomechanical extrusion* of metal, among others. They can be defined as classes containing particular areas of scientific research. For the case of the FSI problem, two main areas can be found in engineering applications: aeroroelasticity, which studies the interaction of air with the aircraft structure, and hydrolelasticity, that investigates the interaction between the seaway and the floating structure.

Hydroelasticity theory has been consistently developed in the last three decades, and it has proven to be an effective alternative to quasi-static and traditional hydrodynamic prediction methods used for the evaluation of seaway dynamic loading and corresponding structural dynamic response of floating structures. The methodology behind FSI analysis involves the idealisation of distinct physical components, the fluid domain and the structural domain. The interaction of the two domains, that in the case of hydroelasticity will be regarded as hydrodynamic loading and dynamic structural response, will be the basis for the solution of the numerical prediction problem.

2.2 Fluid Structure Interaction Problem

To investigate the fluid-structure interaction system, the naval architect should consider that the hydrodynamic loading on an ocean going ship will generate two types of responses: rigid body motion and flexible body distortion. To solve this problem in a unified way, hydroelasticity theory has been developed over the years, and reference must be made to the landmark book of Bishop and Price (1979), [1]. Summarizing, the present theory predicts loads, or fluid actions, induced by waves and consequent responses for both rigid and flexible body motions.The solution can be obtained either in frequency or time domains. The former is more appropriate for linear, or weakly non-linear, problems. On the other hand, time domain solution procedures are more adequate for highly non-linear problems, like, for instance, the idealisation of transient effects occurring on ships (e.g. slamming, green water on decks, etc.).

Solution assessment of FSI problems passes trough the mathematical modelling of the common interface treatment of the two domains, Bergan et al. (1999), [2], which is the case of the free surface effects and the wetted hull area, in which the velocities are meant to be continuous. Proper boundary and initial conditions are to be used as constitutive relations. Traditionally, the structural domain is modelled by the finite element method and the fluid domain by potential flow theory. The latter, particularly sensitive, in terms of complexity, to modelling assumptions, in particular linearity and viscous flow effects. Dynamic solution techniques are used in order to assess frequency or time domain responses, [2].

The interpretation of the FSI problem is particularly relevant for present-day lightweight ship structures. The problem becomes more significant for high operational speeds and all around performance even in rough seas. The case of naval vessels and pleasure craft are definitely a proven fact of this. Several problems of practical design significance should not be disregarded in design stages or operational assessment, where their implications in safety and operational conditions are of crucial importance. Following the work done by Faltinsen (1990), [3], they can be summarised as follows:

- Estimation of local motions and accelerations
- Effect of breaking waves
- Green water on decks
- Slamming
- Sloshing
- Springing (resonant hull vibration)
- Wave induced bending moments

- Wave induced torsional moments
- Wave induced shear forces

Although, it should be emphasized that the main objective of the assessment of the overall structural response of the ship is to measure her load in operation. In particular, analysing the still water conditions and, furthermore, low and high frequency wave-induced distortions and impact loading, in which the first two represent, in most cases, the more significant classes of loads, [4]. The following itemization can be adopted to describe the subdivision of ship structural loading, as shown in figure 2.1, [5].

Static loading dependent on ship weight distribution:

- Weight of the ship and its contents;
- Static buoyancy of the ship at rest or moving at constant speed in still water;
- Thermal loads arising from non-linear temperature gradients on the ship structure;
- Concentrated loads caused by dry-docking and grounding.

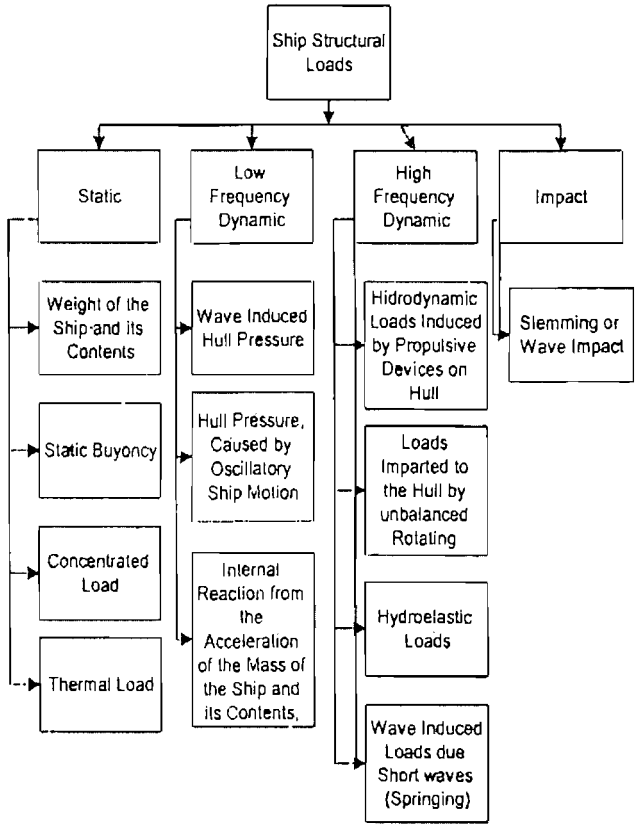

Figure 2.1: Classification of Loads

Low frequency dynamic loading correspond to loads that vary with periods that range in time from few seconds to several minutes and, therefore, occurring at lower frequencies than hull fundamental vibratory response. Loading is considered to be dynamic since it arises from wave influence, and therefore oscillatory.

- Wave induced hull pressure variations;
- Hull pressure variations due to ship oscillation;
- Internal reactions resulting from inertial forces due to ship three-dimensional mass distribution.

High frequency dynamic loading correspond to time-varying loads that excite the ship in its fundamental vibratory response. Some of the loads may be quite small in amplitude , although because of resonant amplification, they can produce large stresses and deflections.

- Hydrodynamic loading induced by propulsion devices on hull or appendages;
- Loads induced on the hull by reciprocating or unbalanced rotating machinery;
- Loading arising from interaction of hull and appendages due to the fluid flow passing through the ship;
- Wave induced loading due to high frequency of encounter waves that overlap hull natural frequencies that can produce significant resonant responses.

Impact loading typical from wave impact at bow resulting in transient hull loading that, in severe seas, can induce slamming.

- Slamming;
- Sloshing on ballast and low viscosity liquid tanks;
- Wave slap on hull sides and foredecks;
- Shock loading due to underwater explosions (mainly on Military Vessels).

2.3 Structural Design Methodologies

Two categories of design methodologies are normally adopted in present day hull strength assessment. They can be associated either with deterministic or rational-based structural design approaches. The former is mainly based on accumulated experience on

ship structural performance, where data collected has served as a basis for the development of structural design codes, i.e. classification society rules, [6]. The latter, based on physical principles and in non-linear analysis, could demand high computational effort, where several aspects should be considered simultaneously, for instance: load variations in terms of value and direction, variability of material properties and buckling constraints. Furthermore, local delamination and fatigue/fracture effects that will demand a probabilistic structural design approach for the case of composite structures.

The ultimate strength of the hull girder, in general sense, addresses the subject of behaviour of ship structures under combined loads and a rational approach can make use of different methods of analysis, [7], they are:

- Analytical;
- Numerical;
- Experimental;
- Reliability based.

Regarding the obvious limitations of analytical methods, they have proven to be an acceptable base for several structural analysis, in particular applied to composite structures, in which stresses and deflections are based on beam and plate theory formulations.

It is worth mentioning that normally, in GRP hull panels, transverse deflections due to bending are generally much larger than in-plane deflections, arising from the difference between extensional and flexural stiffness, the former being larger than the latter. Therefore the development of analytical models for prediction of bending deflection are of particular interest, Gibson (1994), [8]. Also, considering the particularity of composite structures, fabrication techniques are in constant development increasing the variability of achieving a final product. Either in contact moulding, which includes generally spray and hand lay-up, or in compression moulding which includes vaccuum bagging, autoclave and other infusion processes material properties are estimated by a standard pattern of investigation based on harmonized basic test procedures that lead to a reduced set of design rules.

Semi-empirical methods for prediction of maximum loads for several types of GRP hulls were developed, based on model and full scale experimental data, where emphasis should lay on the work made on planing craft by Heller and Jasper(1961), [9], Savitsky and Brown (1976), [10], and Allen and Jones (1978), [11]. The latter methods lead to specifications of nominal static design pressures that are multiplied by amplification factors that account for the dynamic nature of loading and structural response, Smith (1990), [12]. The concept of static design pressures also serve as reference for classification society rules development. Most commonly, scantling determination has been, in recent

years, obtained by published rules, namely LR, DNV, ABS, RINA, EACS and BV, respectively [13], [14], [15], [16], [17] and [18].

Nevertheless, several developments have contributed in recent years towards a unified rule for recreational crafts up to 24 meters. The Recreational Craft Directive (RCD), [19], that leads to the CE marked, includes all EU countries plus Iceland and Norway, represented by a group of recognised notified bodies. In particular, the structural design conformity for small craft hull construction and scantling determination are based on ISO standard 12215-1. Nonetheless, for commercial and naval vessels the former stand alone classification society rules prevail.

In the last decades, finite element analysis (FEA), has become a pillar for a composite structures rational based design procedure, and most of the design offices rely their studies on general purpose FEA codes that account for the prediction of mechanical behaviour of multilayer laminates, monolithic and/or sandwich. Some of the most broadly used commercial packages are known as ANSYS, ABAQUS and MSC NASTRAN. The first one is used in the present investigation.

Regarding limitations of the semi-empirical methodologies in properly predicting the buckling phenomena, one of the most important failure modes in composite structures, the use of numerical methods, like non-linear FEA codes, has shown to be more adapted to the three dimensional nature (anisotropy) of the composite laminate. Furthermore, interlaminar shear strength and through-thickness normal strength must be carefully estimated to prevent local delamination,[7].

2.4 Hydrodynamic Theories

Producing a summary literature review on the numerical evaluation of the dynamic behaviour of a rigid ship in a seaway, also commonly known as seakeeping, is definitely a lengthy and difficult task. Regarding the understanding of the phenomena of motion of ships in waves, early developments, in the end of the 19th century, can be attributed to the pioneering studies of William Froude (1861), [20], and his son Robert. The most relevant publications of both were later compiled in London by the Institute of Naval Architects (1955), [21]. There are numerous references to the subject and extensive works can be found in Korvin-Kroukovsky (1961),[22], Comstock (1967),[23] and Newman (1978), [24]. Also, an overall approach of the trends of ship dynamics theory can be found in the work produced by Bishop and Price (1991),[25].

The evaluation of rigid body motions requires several assumptions in which the formulation should account for proper boundary conditions and an idealisation of the three-dimensional underwater hull surface. Consequently, several simplifications regarding linearisation and hull geometry lead to the solution of the hydrodynamic problem. The

initial complexity of the problem must be simplified until the stage where there is possibility of a reliable numerical solution.

2.4.1 Two Dimensional Hydrodynamics

A proposed distribution for the domain of theoretical applicability for different seakeeping methodologies is shown in figure 2.2. This figure represent the relation between oscillation frequency of the boundaries against hull slenderness. For example, strip theory has applicability for higher frequencies and very slender hulls.

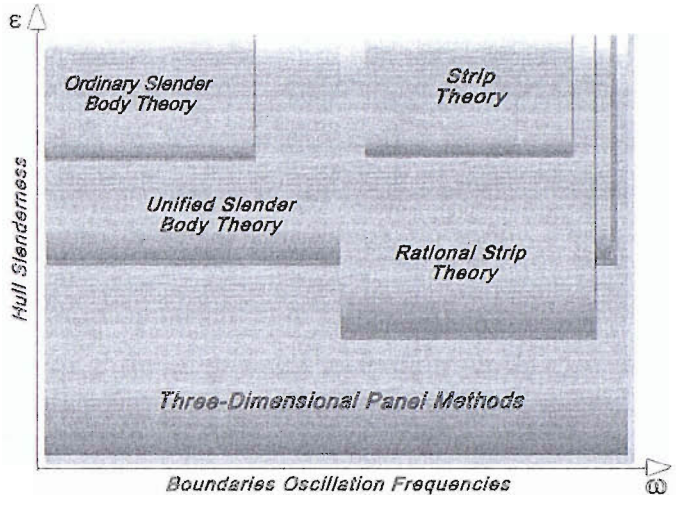

Figure 2.2: *Domains of Applicability for Seakeeping Theorethical Methodologies*

Thin Ship Theory

As already mentioned, William Froude carried the first studies on rolling motion regarding the behaviour of steam-powered vessels. Years later, Krilov (1896), [26] investigated heave and pitch motions. Both stated the differential equations of motion to predict the dynamic behaviour of the ship in waves, which include inertia and restoring components. For the component part of the exciting forces, they only accounted for the pressure field produced by the incident wave system, disregarding the presence of the ship in the water that remains static in their theoretical hypothesis. The latter forces are also known as *Froude-Krilov exciting forces.*

Developments of this hydrodynamic theory arise from the research of the problem of wave resistance, in order to model the stationary wave disturbance in calm water of the moving ship at constant forward speed. Geometric restrictions were adopted by Michell (1898), [27], to obtain a solution for the boundary condition problem with the free surface; therefore, is assumed that beam is relatively small compared to length and draught. Although the developed methodologies did not produce reliable results when compared to experiments, they were a valuable contribution for present day hydrodynamic theories.

Green's theorem was used for the first time by Haskind (1964), [28], in order to calculate the velocity potential associated with the oscillatory motions regarding heave and pitch. Haskind was also the first to separate the velocity potential in components that account for the contribution of radiation and diffraction. Small perturbations methodologies were applied to the *Thin Ship* by Peters and Stoker (1957), [29], and Newman (1961), [30]. These methodologies assumed that ship's beam and ship motions amplitude are of the same order of magnitude. But again, numerical predictions did not prove to be well correlated to experiments due to the problem of estimating the damping coefficients.

Slender Body Theory

The basic assumptions behind this theory are that the ship has beam and draught much smaller than its length and that wave length is close to ship's length. This methodology was applied to the hydrodynamic problem of wave resistance by Maruo (1962), [31], but results were only reasonable for moderate speeds, where the oscillation of the boundaries are of low frequency. Other authors like Newman (1961) and Ursell (1962), [32] investigated the applicability of this methodology; the latter applied the method towards the description of the problem of oscillatory motion without speed of advance. In addition Tuck (1964), [33] used three-dimensional singularities in order to solve the problem of the kinematic boundary condition in two different domains, one on the underwater hull surface and another on the free-surface, away from the influence of the floating ship.

Unified Slender Body Theory

In order to expand the domain of application of the slender body theory, i.e. only valid for low oscillation frequencies and moderate advance speeds, Newman and Sclavounos (1980), [34], like in the previous methodology, also assumed that the flow neighbouring the hull surface is essentially bi-dimensional, however it departs from the ordinary slender body theory because it assumes that waves can act on the hull whose lengths are less than that of the ship's. The free-surface boundary condition, sufficiently away from hull interference, is to be considered with three-dimensional behaviour when introducing in Laplace's equation. For zero forward speed Maruo and Tokura (1978), [35], and Mays (1978), [36] showed good agreement between numerical predictions and experiments. Results for the unified slender body theory presented a more consistent methodology compared to slender body and strip theories.

Strip Theory in Frequency Domain

In strip theory a simplistic approach is taken in order to represent the effects of the ship advancing at constant speed on the oscillating flow in which the stationary wave system in the ship's vicinity is disregarded. The three-dimensional hydrodynamic problem is simplified in terms of a two-dimensional analysis of a sequence of transverse slices, or strips, that define a stepped hull shape. In each strip is assumed that the flow acts only in transverse and vertical directions. With this assumption is implicit that the ship should be slender, the speed of advance moderate and the wavelength small compared to ship's length.

The first author to apply two-dimensional hydrodynamic analysis in a strip theory method was Korvin-Kroukovsky (1955), [37] in order to assess heave and pitch motions. Subsequent investigations by Timman and Newman (1962), [38], derived boundary conditions for the hull underwater surface considering the interaction effects between oscillatory and stationary flow in a way that a linear approximation was more consistent. Their studies showed that the coupling coefficients between heave and pitch are symmetric.

The development of a *Rational Strip Theory* is attributed to Ogilvie and Tuck (1969), [39], for the evaluation of vertical ship motions. The formulation is based on a systematic analysis of small perturbations for high values of wave encounter frequency. It may be helpful to note that although this rational method has a larger domain of applicability, since it was considered to be valid for a larger set of parameters, like frequency of encounter, hull slenderness and speed of advance, its numerical validation must have been small in terms of published results, and its practical application is at first sight inexistent, Fonseca (2001), [40].

Other formulations, apart from Ogilvie and Tuck's (1969) work, were also developed for coefficient determination of vertical ship motion evaluation, namely the ones by Gerritsma and Beukelman (1967), [41], and Salvesen et al. (1970), [42]. Basically what distinguishes between these theories is the type of methodologies adopted to account for viscous effects. For sway, yaw and roll motions Kaplan et al. (1969), [43] and Salvesen et al. (1970) presented two different formulations. From the aforementioned formulations only Ogilvie and Tuck (1969) and Salvesen et al. (1970) satisfy Timman-Newman symmetry relations.

A linear approach is well adapted to studies regarding hull optimization for steady ship motions or added resistance in waves. However, considering the growing tendency in the last decades to increase ship forward speed in all sea states, made non-linear responses evaluation one of the most important areas in seakeeping studies. Jensen and Pedersen (1979), [44], developed a frequency domain quadratic theory to estimate wave induced non-linear vertical ship motions responses and non-linear vertical bending moments.

Strip Theory in Combined Time and Frequency Domain

On of the main achievements in applying a time domain approach for solving the hydrodynamic equations of motion is to be able to deal with the non-linear effects. Those can include, for instance, slamming loads, water on deck and influence of controllable stabilizers.

The methodologies are based on the assumption that when using strip theory to evaluate large amplitude motions and wave loading is considered to be a computational simplification to assume radiation and diffraction forces linear. On the other hand, Froude-Krilov and time varying hydrostatic forces are kept non-linear. Combining the hydrodynamic linear coefficients with the non-linear components representing the external loading, the equation of motion is, therefore, solved by integration in time domain. Paulling and Wood (1974), [45], have used this approach for large amplitude motions induced by following seas.

It should be emphasized that this methodologies based on a *partially non-linear* strip theory although they are useful numerical tools they still remain mathematically inconsistent at a certain level. At least in terms of the use of frequency dependent hydrodynamic coefficients, that are estimated assuming harmonic oscillations, to predict irregular motions due irregular seaways. That is to say that in the case of non harmonic oscillations due to real irregular sea states the frequency dependent hydrodynamic coefficients should not be used. Instead, it should be used a memory function approach based on convolution integration of a set of impulse response functions, Fonseca (2001), [40].

In order to evaluate vertical responses Xia and Wang (1997), [46], presented a methodology based on strip theory in time domain. Developments were later carried by Xia et al. (1998), [47], where memory effects associated with the oscillation of the free surface were also accounted for. Forward speed influence, however simplified due to the limitations of strip theory, was included in the research done by Fonseca and Guedes Soares (1998a), [48], for regular waves and later Fonseca and Guedes Soares (1998b), [49], also presented a formulation for the more generalized case of an irregular wave system. The main difference of the latter formulation to the one presented by Xia and Wang (1997), is that the time domain radiation forces are estimated before the numerical evaluation by strip theory.

Two and an Half Dimensional Strip Theory

For a conventional strip theory approach it is assumed that speed of advance is relatively small ($F_n < 0.3$). Having in mind the inclusion of high forward speed effects, that is definitely the trend of the current shipping industry; such as fast ferries, two and an

half dimensional strip theory was the term adopted to define the methodology half way between two-dimensional strip theory and three-dimensional panel methods. That is to say that the basis of the formulation is the two-dimensional Laplace's equation; however, the free-surface boundary condition is considered to be three-dimensional. The methodology is sustained by the fact that for high speed and displacement ships are normally slender and the generated waves move in a direction essentially from bow to stern. Conditions must therefore be satisfied in order to ensure that waves do not propagate towards the front of the moving ship. Typically $\omega_e U/g > 0.25$, where g, U and ω_e represent respectively acceleration due to gravity, ship forward speed and encounter frequency. This approach was firstly adopted by Ogilvie (1972), [50]. Faltinsen and Zhao (1991), [51], further developed this ship motion evaluation theory in the frequency domain. Their method was based on Chapman's work (1975), [52]. Later Zhao (1994), [53], presented a more complete solution in time domain analysis.

2.4.2 Three Dimensional Hydrodynamics

Strip theory methodologies have strong limitations for high speed vessels, vessels with a small L/B ratio, and implications in which the shape of the hull induce three-dimensional effects in wave diffraction. This is considered to be the case in the present investigation, in which a Patrol Boat is an example of the aforementioned assumptions. The Panel Method formulations can be based on Green's function or Rankine's sources. Both methods can be used to determine the velocity potential and to characterize the sources, either in frequency or time domain.

Panel Methods in Frequency Domain

Regarding Green's functions panel methods in frequency domain, pioneer work is attributed to Hess and Smith (1964,1967), [54][55], who proved its applicability. However, emphasis should be made to mathematical limitations, in a frequency domain solution, when in presence of oscillatory singularities and the hull with speed of advance. To overcome this problem a time domain alternative approach can be adopted.

When in presence of zero to small speeds of advance, like currents in stationary offshore structures, for instance, Green's functions are relatively easy to calculate and three-dimensional seakeeping methods of analysis were presented by Faltinsen and Michelsen, (1974), [56], Garrison (1978), [57] Eatock, Taylor and Waite (1978),[58], and Newman and Sclavounos (1988), [59]. However, Chang (1977), [60], is considered to be the first to present a numerical solution, based on frequency domain panel method, for the problem of the ship's hull advancing in waves.

Inglis and Price (1981a,1981b), [61] [62], used a three dimensional Green's function method to determine hydrodynamic coefficients and excitation forces on a series 60

vessel with forward speed. The method is based on the determination of source strengths on the mean wetted area of the hull and the formulation of the velocity potential that allows the characterization of the fluid pressures and external forces acting on the moving hull. Forward speed effect was accounted by the type of source distribution adopted, i.e. pulsating/translating. The idealization of the hull surface by a finite number of quadrilateral panels is a fundamental step towards the numerical solution of the problem. A similar approach was adopted in the investigation presented in 1982 by Guevel and Bougis, [63]. The differences between several methodologies are dependent in the way Green's functions are computed. An example of an alternative way of determining translating or translating pulsating Green's functions is presented by Ba and Guilbaud (1995), [64].

Panel Methods in Time Domain

As mentioned earlier, assuming non-zero speed of advance, time domain Green functions are relatively simpler to evaluate numerically comparatively to the equivalent ones in frequency domain. Lin and Yue (1990,1993), [65] [66], developed a methodology based on a transient and three-dimensional time dependent Green's function to predict the response of the six degree of freedom ship moving in a seaway. The velocity potential is represented by a distribution of transient Green's functions that satisfy the linearised free-surface boundary condition due to the accounting of the exact shape of the the incoming wave. Although, the free-surface boundary condition remains linear the body boundary condition is satisfied in each instant of time on the wetted hull surface. This is possible due to the inclusion of free surface memory effects although the computational effort is considerable. Therefore, this methodology allows the estimation of large amplitude motions, although generated waves due to hull motion remain linear. The codes for this numerical procedures were named LAMP (Large Amplitude Motion Program).

Bingham et al. (1993,1994), [67] [68], proposed a different approach based on transient Green's functions in which the radiation and diffraction problem are solved, by determination of a velocity potential, or source distribution, using impulse response functions. They developed a numerical simulation code for transient wave-body interactions named TiMIT (Time-domain Investigations developed at the Massachusetts Institute of Technology). Numerical predictions, by three dimensional time-domain panel methods, have been compared to measured data and they have shown good agreement for a series 60 hull travelling at steady forward speed, Magee (1994), [69].

2.4.3 Hydroelasticity Theories

The evolution of naval structures during the last century has been towards low cost and lightweight, which consequently are simpler to produce, result in thinner hull shells and

minimal amount of structural members. Together with the later trends for the quest for all round performance, whatever the sea state, this resulted in increasing demand from naval architects regarding the assessment of both rigid and flexible body responses. This requires the coupling of structural and hydrodynamic theories to properly characterize the ship behaviour in, as many as possible, seaways. The first study known to be published considering the ship as a flexible structure, i.e modelled as an elastic beam, was presented in 1929 by Inglis, [70]. Later in 1959 Heller and Abramson, [71], proposed the term **hydroelasticy** to define the fluid-structure interaction relating the hydrodynamic loading and the corresponding elastic response of a structure.

Two-Dimensional Hydroelasticity

The unified two-dimensional hydroelasticity theory uses strip theory to model the fluid-structure interaction. Typical applications were done by investigations carried out by Bishop and Price in 1979, [1], for monohull type vessels, characterised as slender beam-like structures, with port/starboard symmetry. This theory accounts for both steady state and transient responses due to excitation loads either from regular or irregular waves at different headings and speeds. For this two-dimensional analysis the flexible dry hull is idealised as a Timoshenko beam and numerical results can be found by known algorithms, like the classic Prohl-Myklestad method or by two dimensional finite element analysis.

Using this theory, symmetric responses are predicted for rigid body motions, like pitch and heave, associated to vertical bending distortion. Likewise, antisymmetric responses are determined to characterize sway, roll and yaw rigid motions associated to coupled horizontal bending and twisting distortions, Bishop and Price (1980), [72]. Work has also been developed to investigate monohulls, such as aircraft carriers, without port/starboard symmetry, Bishop et al. (1986), [73].

Transient symmetric responses due to hull slamming were also investigated by Bishop, Price and Tam in 1978, [74]. Belik et al. (1980), [75], also produced a practical solution, based on strip theory, to numerically evaluate wave induced structural stresses including the ones due to slamming. The transient vertical bending moment, due to impact forces from slamming, is calculated in time-domain and superimposed to the linear response in order to evaluate the total non-linear structural response, although only accounting for regular incident head waves. The same authors later expanded their research for the more general case of irregular waves, [76]. The confirmation of the potential applicability of the theory come when in 1984 full-scale trial measurements and predictions have shown good agreement, Bishop et al. (1984), [77]. Guedes Soares (1989), [78], also applied a linear strip theory for relative motions between ship and waves , while impact forces due to slamming, are given by the variation rate of fluid momentum. The ship is idealised as a Timoshenko two-dimensional beam in which the vibratory response and

the correspondent vertical bending moment is superimposed to the wave induced linear bending moment, in this case at encounter frequency.

Regarding the theme of the present investigation Aksu et al. (1993), [79], published the results of their investigation over a Fast Patrol Boat travelling in irregular seas, where the hull was idealised as beam-like structure for two-dimensional hydroelastic analysis, where once again they have shown good agreement between numerical results and experiments. Research from Xia et al. in 1998, [80], also contributed to define a two-dimensional non-linear hydroelastic analysis as a valuable numerical procedure for analysis of conventional monohulls.

Three-Dimensional Hydroelasticity

To fight the limitations of the two-dimensional approach to non-slender hulls and other hull forms, like for instance catamarans and floating structures, a more powerful three-dimensional analysis has been investigated by Wu in 1984, [81]. For a three-dimensional *wet hull* analysis, instead of strip theory, the hydrodynamic actions are found in a more complex way from potential flow theory using a singularity distribution on the mean wetted surface of the structure, in which pulsating sources are used, as in section 2.4.2, in order to reduce computational times. For the preliminary *dry hull* analysis a finite element model is used to evaluate the modal characteristics. This approach served as the basis of the investigation produced by Bishop et al. in 1986, [82]. Regarding the increasing complexity of evaluation of responses due to slamming occurring due to irregular oblique seas research was later published by Aksu et al. (1991), [83].

Research comparing two- and three-dimensional theories, and accounting for the effects of wave-induced transient excitation, showed good agreement for slender hulls but confirmed the limitations of the two-dimensional hydroelastic analysis when the length to beam ratio decreases, [84]. More research has been produced for more recent ship concepts, in which flexible model measurements were compared to numerical predictions for a trimaran showing reasonably good agreement, Miao et al. (1997), [85]. Reference work on fluid structure interaction, applied to a yacht hull form made of composite material, was published by Louarn and Temarel (1999), [86] and for a patrol boat by Price et al. (2002), [89]. This theory is more suitable to multi-hulls, offshore structures and monohulls with small length/beam ratios, i.e. non-beamlike structures, Keane et al. (1991), [87]. The influence in numerical predictions, in relation to varying degrees of panel refinement of the wetted surface, have also been investigated by Louarn making a valuable contribution in sailing yacht research in 1999, [88].

2.5 Concluding Remarks

The present chapter tries to summarize, chronologically, the foundations of research that lead to the present day hydroelastic analysis.

It is considered in this text that its development is still one step behind of the measured data validation of other engineering areas like for instance in aerospace, its counter part in the fluid structure interaction group, in this case aeroelasticity. One notorious example is given by the test facilities built by the National Aerospace Agency (NASA), in particular the Langley Research Center. This is most probably in certain aspects due to the more user friendly wind tunnel testing, with easier instrumentation maintenance on a fixed and confined space within a controlled environment, than its counterpart on tank testing facilities.

However, the design and analysis of ship structures is progressively becaming more detailed, towards an increase of safety allied to cost effective constructions. Hydroelasticity theory has been proven successful for slender vessels although there is still room for research and development for monohulls with smaller length to beam ratios and high advance speeds, and that is the case of the present investigation, regarding this particular type of fast patrol boat made of fibre glass reinforced plastic. In conclusion, the general three-dimensional hydroelastic analysis applied in this investigation will allow a unified prediction of responses that include the rigid body motions, deflections, bending moments, torsional moments and stresses that can be estimated at any point on a flexible structure.

Chapter 3

Dry Hull Analysis Formulation

3.1 Generalised Equations of Motion

The equations of motion of a linear multi-degree of freedom system, such as a hull, can be expressed as follows,

$$\mathbf{M}\ddot{\mathbf{U}} + \mathbf{D}\dot{\mathbf{U}} + \mathbf{K}\mathbf{U} = \mathbf{Q} \tag{3.1}$$

where $\mathbf{Q}$ defines the vector of external forces applied. The vectors of nodal displacement, velocity and acceleration are, respectively, $\mathbf{U}$, $\dot{\mathbf{U}}$ and $\ddot{\mathbf{U}}$, mass, damping and stiffness matrices are, respectively, defined as $\mathbf{M}$, $\mathbf{D}$ and $\mathbf{K}$.

Normally the matrices have non-zero coupling terms (e.g., $K_{ij} = K_{ji} \neq 0$) making it necessary to have simultaneous solution of n equations of n unknowns. To overcome this problem one can make use of the *mode − superposition method*, or *normal − mode method*, allowing the transformation of a set of coupled equations to a set of uncoupled equations using the normal modes that describe the dynamic response of the system. It should be noted that in the case of a floating, or submerged, structure the generalised equations of motion are not uncoupled, due to fluid-structure interaction.

The undamped natural frequencies ω_r and associated principal mode shapes $\mathbf{u}_r$, for $r = 1, 2, ..., N$ satisfy the equation

$$\left(\mathbf{K} - \omega_r^2 \mathbf{M}\right) \mathbf{u}_r = \mathbf{0} \tag{3.2}$$

The modes $\mathbf{u}_r$ can be normalised in various possible procedures, Craig (1981), [90], like:

1. $(\mathbf{u}_i)_r = 1$, rth mode scaled at specified node i;
2. $(\mathbf{u}_i)_r = 1$, rth mode scaled at maximum displacement per node i where $|(\mathbf{u}_i)_r| = |max\{(\mathbf{u}_j)_r\}|$;

3. r*th* mode scaled so that the generalised mass, or *modal mass* matrix, an element of which is defined by $a_{rr} = \mathbf{u}_r^T \mathbf{M} \mathbf{u}_r$, has a specified value, where $a_{rr} = 1$ is frequently used;

Assuming a normalization of the modes by the latter scheme, generalised mass can be related to generalised stiffness as follows:

$$c_{rr} = \omega_r^2 a_{rr}. \tag{3.3}$$

The associated modes satisfy the orthogonality equations defined by equation 3.4,

$$\mathbf{u}_r^T \mathbf{M} \mathbf{u}_s = \mathbf{u}_r^T \mathbf{K} \mathbf{u}_s = 0 \qquad\qquad r \neq s. \tag{3.4}$$

The most important step in the *mode − superposition method* is to do the variable separation described by equation 3.6. According to Rayleigh's Theorem (1894), any distortion can be considered as a summation of distortions in its principal modes, [91].

Let the displacement at any point in a cartesian coordinate system be described by

$$\mathbf{u}(x, y, z, t) = \sum_{r=1}^{N} [u_r, v_r, w_r] p_r(t), \tag{3.5}$$

where $\mathbf{u}_r(x, y, z) = [u_r, v_r, w_r]$ are the *in vacuum* principal mode shapes, or the r*th* principal modal displacement vectors, and $p_r(t)$ the principal coordinates and N represents the maximum number of principal modes admitted in the analysis, then the vertical displacement can be expressed as,

$$w(x, y, z, t) = \sum_{r=1}^{N} w_r(x, y, z) p_r(t). \tag{3.6}$$

Therefore, the equation of motion, in terms of principal coordinates, describing the dynamic response of a flexible structure can be written in matrix form as,

$$\mathbf{a}\ddot{\mathbf{p}}(t) + \mathbf{b}\dot{\mathbf{p}}(t) + \mathbf{cp(t)} = \mathbf{Z(t)} \tag{3.7}$$

where $\mathbf{a}$, $\mathbf{b}$ and $\mathbf{c}$ are respectively generalised mass, structural damping and stiffness matrices with $N \times N$ dimensions. These matrices also represent the dry, or *in vacuum* structure where the elements are related as follows: $a_{rr} = a_{rr}$, $b_{rr} = 2\nu_r \omega_r a_{rr}$ and $c_{rr} = \omega_r^2 a_{rr}$, the latter referred in equation 3.3, with ω_r being the natural frequency of the hull *in vacuum* and ν_r the structural damping factor, assuming a diagonal damping matrix. Therefore, principal coordinate $\mathbf{p}(t)$ is a solution for the equation of motion 3.7. The column vector $\mathbf{Z}(t)$ with generalised components Z_r representing the external applied generalised forces due to fluid actions. It should be noted that for a structure,

such as a ship, with six rigid body motions $\omega_r = 0$ for $r = 1, ..., 6$, those indexes represent respectively surge, sway, heave, roll, pitch and yaw. The internal reactions for a three-dimensional model can also be expressed in a similar manner to equation 3.6. For example the direct longitudinal stress at a position anywhere on the vessel can be written as

$$\sigma_x(x, y, z, t) = \sum_{r=7}^{N} \sigma_{xr}(x, y, z) p_r(t) \tag{3.8}$$

where the modal direct stress is zero ($\sigma_{xr} = 0$) for the rigid body motions ($r = 1, ..., 6$). The same applies for the remaining direct and shear stress components.

Therefore, the vertical bending moment M_y can also be expressed as

$$M_y(x, t) = \sum_{r=7}^{N} M_{yr}(x) p_r(t) \tag{3.9}$$

where M_{yr} represents the modal vertical bending moment that, again, is zero for the rigid body modes. A similar approach is adopted for the remaining internal reactions like M_x, M_z, V_x, V_y and V_z which represent respectively the torsional moment, horizontal bending moment, axial force, horizontal shear force and vertical shear force.

Chapter 4

Wet Hull Analysis Formulation

In order to evaluate sea loads and motions induced on the ship the theoretical description of the problem is rather complex. This is mainly due to the non-linearity of the problem, that accounts for waves generated by wind, the waves generated by motion of the ship itself, or the ship response to large amplitude waves. The latter is not included on this investigation although this should not be disregarded in future studies since it includes the well known phenomena of slamming and some not very common occurrences, but with severe implications, like parametric rolling and broaching. Also a non-linear analysis is necessary on more particular circumstances such *as breaking waves in shallow water or locally near a ship's bow*, Newman (1977), [93]. Moreover, viscous forces are quite significant in their contribution for the wave loads induced in small bodies.

Regarding that it is possible to obtain responses to irregular seas by linear superposition of regular wave components it is assumed to be sufficient, at this stage of the investigation, to obtain responses only due to incident regular sinusoidal waves of small wave steepness. To simplify the problem in this investigation it will be assumed that the flow is ideal and therefore characterised by the more accessible potential flow theory.

4.1 Potential Flow Theory

In this section will be given a summarised description of the formulation of the potential flow around the hull of a ship advancing and oscillating in waves. The problem can be formulated in terms of a velocity potential $\Phi(x, y, z, t)$, a scalar quantity, in which its gradient is described by fluid velocity vector $\mathbf{V}(x, y, z, t)$. This will be the unknown of the set of equations representing the potential flow problem. To assess the exact solution several assumptions are to be made, therefore, in a first stage, the fluid is considered to be ideal. After this step, in the potential flow formulation, a linearisation procedure will be introduced in order to simplify and to produce a set of equations accessible for solution.

According to the ideal fluid hypothesis several points are to be satisfied therefore the fluid must be considered as:

- Homogeneous
- Incompressible
- Inviscid
- Surface tension neglected.

This simplification will permit a scalar function, the velocity potential, to be obtained that satisfies the continuity equation within the fluid domain.

Assuming an inviscid fluid and consequently irrotational motion theoretically implies that a vector with zero curl must be the gradient of the scalar function, Aris (1962), [94]. In essence, if the vorticity vector is zero,

$$\nabla \times \mathbf{V} = 0 \tag{4.1}$$

then

$$\mathbf{V} = grad\Phi = \nabla\Phi = \mathbf{i}\frac{\partial\Phi}{\partial x} + \mathbf{j}\frac{\partial\Phi}{\partial y} + \mathbf{k}\frac{\partial\Phi}{\partial z}, \tag{4.2}$$

where $\mathbf{i}$, $\mathbf{j}$ and $\mathbf{k}$ represent respectively unit vectors in directions $0x$, $0y$ and $0z$ in a fixed cartesian referential $Oxyz$.

Since water is assumed to be homogeneous and incompressible then the equation of conservation of mass reduces to the continuity equation 4.3,

$$\frac{\partial u}{\partial x} + \frac{\partial v}{\partial y} + \frac{\partial w}{\partial z} = \nabla.\mathbf{V} = 0. \tag{4.3}$$

Where u,v and w represent the cartesian components of the fluid velocity vector.

Including equation 4.2 in equation 4.3, $\nabla.\mathbf{V} = \nabla.(\nabla\Phi) = 0$, thus the velocity potential must satisfy Laplace's equation

$$\frac{\partial^2\Phi}{\partial x^2} + \frac{\partial^2\Phi}{\partial y^2} + \frac{\partial^2\Phi}{\partial z^2} = \nabla^2\Phi = 0. \tag{4.4}$$

However it should be remembered that the inviscid flow assumption may introduce some limitations that can be important in characterizing horizontal and roll motions where damping forces can not be neglected comparing to restoring forces. The same problem will arise when dealing with vertical motions on small waterplane area twin hulls, SWATH's.

In order to obtain the solution of the Laplace equation, 4.4, it is necessary to apply appropriate boundary conditions. Considering a rigid body advancing with forward speed through a free surface infinite in horizontal plane directions the boundary conditions can be summarised as follows:

1. Body wetted surface, (S_W).
2. Free Surface, (S_F).
3. Sea bottom, (S_∞).
4. Surrounding control surface far way from the rigid body, (S_∞).

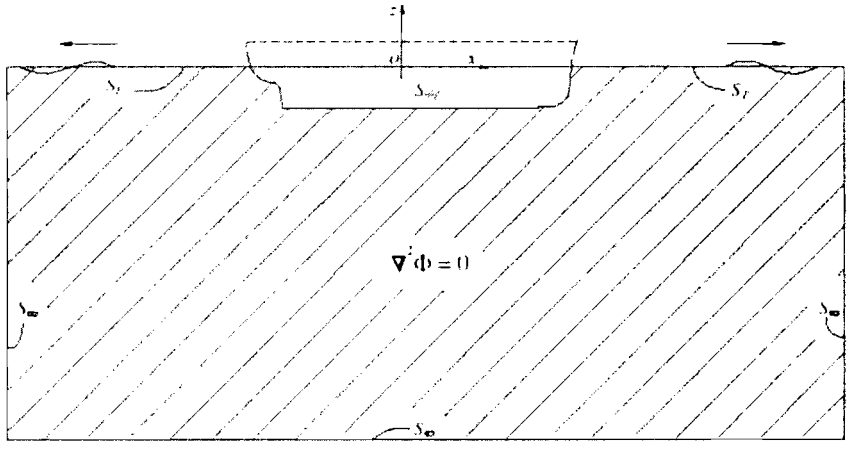

Figure 4.1: Boundary Conditions Surrounding the Fluid Domain

4.1.1 Body Boundary Condition

Without examining the forces that produce fluid motion, and in order to describe it physically, the velocity potential also satisfies the wetted surface boundary conditions, this is, either for a fixed or moving body surface.

Therefore, for a fixed body boundary condition in a moving fluid, impermeability is expressed on the body wetted surface as

$$\frac{\partial \Phi}{\partial n} = 0, \tag{4.5}$$

where $\mathbf{n}$ describing the unit positive normal direction vector, from the body surface towards the fluid domain, and $\partial/\partial n$ representing the derivative along the normal of the wetted surface, therefore, it can be said by equation 4.5 that *no fluid can flow through the boundary surface*, [93].

In the case of the boundary condition for moving body and moving fluid where $\mathbf{V}^S$ denotes the local velocity vector of the wetted surface, the velocity potential also satisfies

the boundary condition on the wetted surface "S " given in a more generalised form by

$$\frac{\partial \Phi}{\partial n} = \mathbf{V}^S.\mathbf{n}, \tag{4.6}$$

where, once again, $\mathbf{n}$ represents the outward unit normal vector. It should be noted that the local velocity of the wetted surface $\mathbf{V}^S$, will include translatory and rotational motion effects, therefore it could vary depending on the spatial position on the body wetted surface.

Therefore equation 4.6 means that the fluid velocity adjacent to the body and the body boundary move at equal normal velocity for the same point. Also the position of the boundary is not known in advance.

4.1.2 Free-Surface Boundary Conditions

Considering the fixed cartesian referential $Oxyz$ in which Oxy defines the horizontal plane lying in the undisturbed fluid free surface, and axis Oz is positive upwards. This implies that the dynamic free-surface of the fluid can be expressed by

$$z = \zeta(x, y, t), \tag{4.7}$$

where ζ represents the wave elevation.

Two conditions must be satisfied at the free surface, i.e. a kinematic and a dynamic boundary condition.

To evaluate the **kinematic free surface boundary condition** it should be noted that in order to represent the rate of change with time of a function, $F(x, y, z, t)$ describing the motion of a particle in the fluid it is necessary to make use of the substantial derivative D/Dt. Hence,

$$\frac{DF}{Dt} = \frac{\partial F}{\partial t} + \mathbf{V}.\nabla F \tag{4.8}$$

where $\mathbf{V}$ is the fluid velocity in a three-dimensional fluid domain at time t.

Then defining

$$F(x, y, z, t) = z - \zeta(x, y, t) = 0, \tag{4.9}$$

where F will represent the fluid particles that will stay on the free surface when the wave elevates, meaning that the vertical velocity of the free surface must be equal to the vertical velocity of the fluid particles on the free surface. Therefore, applying equation 4.8, the **kinematic free-surface boundary condition** can be expressed as the non-linear equation

$$\frac{DF}{Dt} = \frac{D}{Dt}(z - \zeta) = 0, \tag{4.10}$$

expanding the substantial derivative,

$$\frac{\partial}{\partial t}(z-\zeta)+\nabla\Phi.\nabla(z-\zeta)=\frac{\partial\zeta}{\partial t}+\frac{\partial\Phi}{\partial x}\frac{\partial\zeta}{\partial x}+\frac{\partial\Phi}{\partial y}\frac{\partial\zeta}{\partial y}-\frac{\partial\Phi}{\partial z}=0, \tag{4.11}$$

when $z=\zeta$.

Regarding the **dynamic free surface boundary condition** for the examination of fluid motion and forces which produce it, the particle motion can be expressed, also, by means of a non-linear condition for the free-surface boundary. The dynamic free-surface condition assumes that the water pressure on the free-surface is equal to the atmospheric pressure, p_0. Therefore, from Bernoulli's equation expressed as

$$\frac{\partial\Phi}{\partial t}+\frac{1}{2}\mathbf{V}.\mathbf{V}=-\frac{1}{\rho}(p+\rho gz)+C(t), \tag{4.12}$$

where ρgz define hydrostatic pressure at the free-surface and $C(t)$ an arbitrary function in time. Including the time dependably of $C(t)$ in the velocity potential it can be assumed as constant. Moreover, if the latter assumes the value of the ratio $\frac{p_0}{\rho}$ and $p=p_0$ will lead the term on the right hand side of equation 4.12 to be simplified as gz. Therefore, for $z=\zeta$

$$\frac{\partial\Phi}{\partial t}+\frac{1}{2}\nabla\Phi.\nabla\Phi+gz=\Phi_t+\frac{1}{2}\left|\nabla\Phi\right|^2+gz=0, \tag{4.13}$$

where g denotes the gravity acceleration and subscript t the partial time derivative. Applying the substantial derivative to equation 4.13 results in equation 4.14 expressed on $z=\zeta$ as,

$$\frac{D}{Dt}\left(\Phi_t+\frac{1}{2}\left|\nabla\Phi\right|^2+gz\right)=0. \tag{4.14}$$

which finally results in the exact free surface boundary condition represented as,

$$\Phi_{tt}+2\nabla\Phi\cdot\nabla\Phi_t+\frac{1}{2}\nabla\Phi\cdot\nabla\left(\nabla\Phi\cdot\nabla\Phi\right)+gz=0, \tag{4.15}$$

on $z=\zeta$ and where $\Phi_t=\partial\Phi/\partial t$ and $\Phi_{tt}=\partial^2\Phi/\partial t^2$. This corresponds to the description of the exact non-linear free surface boundary condition where the position of the boundary is not known a priori.

4.1.3 Bottom Boundary Condition

Assuming deep water the fluid perturbations are negligible on the sea bottom therefore fluid particles are at rest then,

$$\frac{\partial\Phi}{\partial x}=\frac{\partial\Phi}{\partial y}=\frac{\partial\Phi}{\partial z}=0 \qquad if \qquad z\to\infty, \tag{4.16}$$

Defining the wave number as $k=2\pi/\lambda$, where λ represents the wavelength, for the case of infinite depth $z\to-\infty$, a possible solution for the velocity potential Φ can be given

as,

$$\Phi = e^{kz}(A\cos kx + B\sin kx)\cos(\omega t + \alpha), \tag{4.17}$$

where A, B and α are arbitrary constants and Ox the direction of wave propagation. Thus, it can be verified that the boundary condition for infinite water depth will be characterised by "almost" static fluid particles, expressed by,

$$|\nabla\Phi| \to 0 \tag{4.18}$$

when $z \to -\infty$. It should be noted that substituting the velocity potential Φ on the single free-surface boundary condition given in equation B.4 the dispersion relation given by $\omega^2/g = k$ is obtained. Although, if the bottom is at finite distance, d, from the free surface the expression reduces only the condition of impermeability of the sea bed. Therefore, the sea bottom boundary condition is then given by,

$$\frac{\partial\Phi}{\partial z} = 0, \tag{4.19}$$

when $z = -d$, since Oz points upward from the mean free-surface.

4.1.4 Radiation Condition

In order to obtain a suitable far-field boundary condition two approaches are adopted. In the **time domain** for an initial value problem the perturbations generated by the floating body tend to vanish at large horizontal distances (r) therefore, assuming that the hydrodynamic problem is solved at a given instant of time, infinite time is not reached. In this case there is no need to satisfy the radiation condition at infinity, therefore,

$$\nabla\Phi \to 0, \qquad r \to \infty, \qquad if \qquad t < \infty, \tag{4.20}$$

in which r means the distance in the mean waterplane from the ship.

On the other hand, in the **frequency domain** waves due to body disturbances must be outgoing to infinity, and vanish, and this condition must be established in a boundary that extends from the sea bottom to the free surface at a large horizontal distance.

The waves described by the velocity potential Φ, that includes associated potentials due rigid body motions with unit amplitude, in six degrees of freedom, and a scattering potential representing the disturbance induce by the rigid body due to wave incidence. The radiation condition is therefore given by,

$$\lim_{r\to\infty} \sqrt{r}\left(\frac{\partial\Phi}{\partial r} - ik\Phi\right) = 0. \tag{4.21}$$

The radiation condition as been stated originally by Sommerfield (1949), [95], based on acoustic theory formulations.

4.1.5 Linearization of the Hydrodynamic Problem

In resume, within the ideal fluid assumption, the exact boundary value problem can be expressed by equations 4.6, 4.15, 4.19 and 4.20 satisfied by the velocity potential defined in equation 4.2. This was first shown by Newman in 1977, [93]. To obtain a numerical solution of the exact non-linear boundary value problem a high degree of complexity in the calculations is therefore required. Also to simplify numerical computations, a linearised theory can be used. It is common practice to impose some restrictions in the parameters governing the solution in order to obtain simplifications on the body and free surface boundary conditions. Some of this restrictions can be pointed as:

- Slenderness of the hull ($\epsilon = L/(\nabla)^{1/3}$);
- Speed of advance of the ship;
- Amplitude of oscillation at the boundaries (fluid free surface and wetted hull surface);
- Frequency of oscillation at the boundaries.

The boundaries previously enumerated include both the hull surface and fluid free surface. The main goal of the restrictions implies a linearisation of the problem and to remove, and/or simplify, some of the interactions between steady and unsteady flows. It should be noted that the linearisation of the problem implies that wave amplitude being much smaller than a characteristic wavelength and body dimensions, Salvesen et al. (1971), [96]. It is assumed that incident waves are regular, sinusoidal and with small wave steepness with no transient effects.

Different seakeeping formulations depend on different sets, or combinations, of restrictions resulting in different theories varying in the degree of complexity, some examples are:

- Thin Ship Theory;
- Slender Body Theory;
- Strip Theory;
- Panel Methods.

The last set includes the approach adopted in this investigation in order to characterize the Patrol Boat. Especially regarding the limitations in restrictions like hull slenderness and speed of advance.

4.1.6 Forward Speed

The velocity potential can be decomposed into a time-independent **steady flow** contribution associated with the hull advancing through the free surface in calm water, $\bar{\phi}(x, y, z)$, and a time-dependent continuation due to the **oscillatory flow** associated to the forced motion induced by incoming waves, $\tilde{\phi}(x, y, z, t)$.

The velocity potential can be represented in the equilibrium frame axis in the following form,

$$\Phi(x, y, z, t) = \bar{U}\bar{\phi}(x, y, z) + \tilde{\phi}(x, y, z, t), \tag{4.22}$$

where, once again, $\bar{\phi}$ and $\tilde{\phi}$ denote respectively the steady and unsteady perturbation potentials, [96] and [82]. The steady flow velocity vector, $\mathbf{W}$, of the steady flow with respect to the forward speed reference axis is given by,

$$\mathbf{W} = \bar{U}\nabla(\bar{\phi} - x). \tag{4.23}$$

However, for the unsteady flow, the time dependent velocity potential function $\tilde{\phi}$ must not only include contributions from incident and diffracted wave fields but also from the distortions of the structure in fluid domain. Hence, assuming small amplitude for ship motions and incident waves, the unsteady component $\tilde{\phi}$, can be linearly decomposed as incident wave potential, ϕ_0, a diffraction potential, ϕ_D, and ϕ_r, a radiation potential component associated to the rth principal mode of motion of the flexible structure, therefore the decomposition assumes the following form,

$$\tilde{\phi}(x, y, z, t) = \phi_0(x, y, z, t) + \phi_D(x, y, z, t) + \sum_{r=1}^{N} \phi_r(x, y, z, t). \tag{4.24}$$

From equation 3.5, it can be said that the deflection of the structure can be expressed by the sum of the distortions of the principal modes, a similar approach can be adopted for the radiation potentials. The radiation potentials take the form,

$$\phi_r(x, y, z, t) = \phi_r(x, y, z)p_r(t), \tag{4.25}$$

where $r = 1, 2, ...6, 7, ...$, in which 1 to 6 is related to the rigid body six degrees of freedom and from 7 forward related to the flexible structural response in the principal modes. The element $p_r(t)$ is the rth principal coordinate defined by, in regular sinusoidal waves;

$$p_r(t) = p_r.e^{i\omega_e t}, \tag{4.26}$$

or in other words, p_r is the amplitude of the motion when r assumes values from 1 to 6, that correspond respectively to surge, sway, heave, roll, pitch and yaw, [97]. Also, ω_e represents the encounter frequency due to sinusoidal wave excitation. It should be noted that linearisation is also necessary to apply on the combined free-surface boundary

condition. Using Bernoulli equation 4.12 and chosen a value for constant C as

$$C = \frac{\rho}{2}\bar{U}^2 + p_0, \tag{4.27}$$

where there is no free-surface elevation, or in other words in which equation 4.22 reduces to $\phi = \bar{U}x$. By disregarding interactions with the steady velocity potential and non-linear terms the dynamic mean free-surface boundary condition, on $z = 0$, can be expressed as

$$g\zeta - i\omega_e\phi + \bar{U}\frac{\partial\phi}{\partial x} = 0. \tag{4.28}$$

on the other hand the kinematic mean free-surface boundary condition, on $z = 0$, is given by

$$-i\omega_e\zeta + \bar{U}\frac{\partial\zeta}{\partial x} - \frac{\partial\phi}{\partial z} = 0, \tag{4.29}$$

where $\zeta e^{-i\omega_e t}$ represents the unsteady wave elevation. Equations 4.28 and 4.29 can be combined as

$$\left[\left(\bar{U}\frac{\partial}{\partial x} - i\omega_e\right)^2 + g\frac{\partial}{\partial z}\right]\tilde{\phi} = 0. \tag{4.30}$$

From equation 4.30, and accordingly to Bishop et al. (1986), [82], the **linearised free surface boundary condition** on $z = 0$, associated to the incident, diffracted and radiation potentials, respectively, ϕ_0, ϕ_D and ϕ_r, each one of them represented by the letter ϕ, can be expressed as

$$\bar{U}^2\phi_{xx} - 2i\omega_e\bar{U}\phi_x - \omega_e^2\phi + g\phi_z = 0, \tag{4.31}$$

where $\phi_{xx} = \partial^2\phi/\partial x^2$, $\phi_x = \partial\phi/\partial x$ and $\phi_z = \partial\phi/\partial z$.

Also a suitable **linearised bottom and radiation conditions at infinite distances**, i.e. far away from the oscillatory source of disturbance must be satisfied. The relation between incident and diffracted potentials, once again respectively ϕ_0 and ϕ_D, must satisfy the relation,

$$\frac{\partial\phi_0}{\partial n} = -\frac{\partial\phi_D}{\partial n}, \tag{4.32}$$

on a time-independent wetted surface $\bar{S}$ associated to the flexible body distortions. The latter will also be the domain of application of the **linearised body boundary condition** that governs the radiation potentials that can be expressed as,

$$\frac{\partial\phi_r}{\partial n} = \left[i\omega_e\mathbf{u}_r + \theta_r \times \mathbf{W} - (\mathbf{u}_r \cdot \nabla)\,\mathbf{W}\right] \cdot \mathbf{n}, \tag{4.33}$$

on $\bar{S}$, where $\mathbf{W}$ represents the steady flow velocity vector, $\mathbf{n}$ the outward unit normal and $\mathbf{u}_r$ and θ_r represent respectively the translational and rotational principal modes in the vector form.

4.1.7 Pressure Distribution

During the oscillatory motion of the flexible structure the fluid pressure may be found from Bernoulli's equation and expressed as,

$$p = -\rho\left[\frac{\partial\phi}{\partial t} + \mathbf{W}\cdot\nabla\phi + \frac{1}{2}\left(W^2 - \bar{U}^2\right) + \frac{1}{2}\nabla\phi\cdot\nabla\phi + gz\right], \tag{4.34}$$

applied on the instantaneous wetted surface S. Although approximations must be made in order to account for the variations of the wetted surface due to the oscillatory behavior of the flexible structure. The pressure of the instantaneous wetted surface, p_S, is related to the mean wetted surface pressure, $p_{\bar{S}}$, by a Taylor series expansion represented as follows,

$$p_S = \left[1 + (\mathbf{u}\cdot\nabla) + \frac{1}{2}(\mathbf{u}\cdot\nabla)^2 + ...\right] p_{\bar{S}}. \tag{4.35}$$

For the linearisation of the problem second order terms are neglected by assuming that the oscillatory motion of the structure is relatively small, as well as, the parasitic flow associated to it. The linearised pressure on the mean wetted surface, $p_{\bar{S}}$, can be expressed as,

$$p_{\bar{S}} = -\rho\left\{\frac{\partial\phi}{\partial t} + \mathbf{W}\cdot\nabla\phi + \left[\frac{1}{2}(W^2 - \bar{U}^2) + gz'\right] + \left[gw + \frac{1}{2}(\mathbf{u}\cdot\nabla)W^2\right]\right\}_{\bar{S}}. \tag{4.36}$$

As shown in expression 4.36 the flow associated to the steady forward motion still remains non-linear, [82].

4.1.8 Generalised Fluid Actions

The external force $\mathbf{Z}$ has a generalised rth component that can be expressed as,

$$Z_r(t) = -\int\int_{\bar{S}} \mathbf{n}^T\cdot\mathbf{u}_r p dS, \tag{4.37}$$

where $\mathbf{n}$ represents the unit normal vector point outward of the mean wetted surface $\bar{S}$. It is assumed that within the linear theory the integrations take place over the mean wetted surface. The component form of the rth generalised external force can be expressed in equation 4.38 when the steady and unsteady potentials are substituted in the pressure equation 4.36

$$Z_r(t) = \Xi_r(t) + H_r(t) + R_r(t) + \bar{R}_r, \tag{4.38}$$

where Ξ_r, H_r, R_r and $\bar{R}_r$ denote respectively the generalised wave exciting force, radiation force, restoring force and hydrostatic force. Regarding a regular waves assumption,

generalised wave excitation force will be sinusoidal at a determined encounter frequency, and can be expressed as,

$$\Xi_r(t) = \Xi_r e^{i\omega_e t} = (\Xi_{0r} + \Xi_{Dr})\, e^{i\omega_e t}. \tag{4.39}$$

where Ξ_{0r}, represents the amplitude of forces and moments arising from the undisturbed pressure field, i.e. the generalised Froude-Krilov contribution, and for incident regular waves,Ξ_{Dr} representing the amplitude of forces and moments arising from diffracted waves due to a disturbed pressure field related to the presence of the flexible structure. Considering the oscillatory characteristics of the principal coordinates, $p_r(t)$, the **generalised radiation force** for N rigid and flexible modes can be expressed as,

$$H_r(t) = \sum_{k=1}^{N} \left[\left(\omega_e^2 A_{rk} - i.\omega_e.B_{rk} \right) p_k e^{i\omega_e t} \right]. \tag{4.40}$$

Similarly, the **generalised restoring excitation force** assumes the following form,

$$R_r(t) = \sum_{k=1}^{N} \left[(C_{rk})\, p_k e^{i\omega_e t} \right]. \tag{4.41}$$

Finally, the contributions of the **generalised forces due to hydrostatic and gravitational effects** are expressed by,

$$\bar{R}_r(t) = \rho \int\int_{\bar{S}} \mathbf{n}^T \cdot \mathbf{u}_r \left[\frac{1}{2}(W^2 - \bar{U}^2) + gz' \right] dS. \tag{4.42}$$

which denotes the independence of all unsteady motions. Substituting all the generalised components, i.e. 4.39, 4.40, 4.41 and 4.42 into 4.38 and the generalised equations of motion 3.7 may be written in matrix form,

$$(\mathbf{a} + \mathbf{A})\ddot{\mathbf{p}}(t) + (\mathbf{b} + \mathbf{B})\dot{\mathbf{p}}(t) + (\mathbf{c} + \mathbf{C})\mathbf{p}(\mathbf{t}) = \Xi_\mathbf{r} \mathbf{e}^{\mathbf{i}\omega_\mathbf{e}\mathbf{t}} \tag{4.43}$$

which as already been found previously by Bishop and Price, [1]. this represents the behaviour of a freely flexible ship travelling in stationary regular oblique waves. This linear equations are solved to obtain the amplitudes of the principal coordinates $\mathbf{p}(t)$. Matrices **A**, **B** and **C** represent generalised added mass, hydrodynamic damping and restoring coefficients respectively, As mentioned earlier, the generalised wave excitation Ξ_r includes incident and diffracted wave contributions. Wave induced displacements, for either directions x, y, and z at any three-dimensional position in the structure can be obtained through a summation of the principal coordinates multiplied by the associated modal characteristics in the corresponding direction [1]. For example, the displacement at any position in the structure, due to distortion and rigid body motion,

can be expressed in the form

$$\mathbf{u}(x,y,z;t) = \sum_{k=1}^{N} \left[\mathbf{u}_r(x,y,z).p_r e^{i\omega_e t}\right] \tag{4.44}$$

It should be noted that disregarding rigid body motions, $r = 1..6$, therefore excluding this motions from equation 4.44, i.e. only considering $r = 7,..,N$, is possible to evaluate the total structure distortion in any direction. It may be helpful to note that, for the particular case of symmetrical responses, the rigid modes (distortion free) are obviously reduced to heave ($r = 0$) and pitch ($r = 1$) only, thus the flexible modes become with indexes $r = 3,..,N$. The approach described previously can be adopted to access also internal reactions. Again, equation 4.44 is used only taking into consideration the flexible mode shapes. For the cartesian referential adopted in the hydroelastic analysis vertical bending moment, horizontal bending moment and torsional moment are respectively defined as M_y, M_z and M_x. Similarly, shear forces in vertical, horizontal and axial directions are respectively defined as V_z, V_y and V_x. For example at any position in the structure the vertical bending moment can be defined as

$$M_y(x;t) = e^{i\omega_e t} \sum_{k=7}^{N} \left[M_{yr}(x).p_r\right] \tag{4.45}$$

where M_{yr} is the modal vertical bending moment obtained in the dry analysis. The vertical shear force can be obtained by

$$V_z(x;t) = e^{i\omega_e t} \sum_{k=7}^{N} \left[V_{zr}(x).p_r\right] \tag{4.46}$$

Once again, V_{zr} defines the modal vertical shear force. To this end, wave induced stresses are obtained in a similar formulation, making use once again of the principal of modal summation. For the case of the longitudinal direct stress,

$$\sigma_x(x,y,z;t) = e^{i\omega_e t} \sum_{k=7}^{N} \left[\sigma_{xr}(x,y,z).p_r\right] \tag{4.47}$$

Likewise, σ_y and σ_z represent stresses in horizontal and vertical directions respectively. The subscript r denotes the modal stress in the corresponding direction.

Chapter 5

Patrol Boat Description, Model Definition and Validation

5.1 Fast Patrol Boat Description

The subject of this investigation is class *ARGOS* Fast Patrol Boat of the Portuguese Navy made of fibre reinforced plastic. Among its various missions, this boat mainly protects the Portuguese Exclusive Economic Zone and enforces the domestic fisheries law on the continental coast line. The first Fast Patrol Boat of this class, out of five, was built in the beginning of the nineties.

Figure 5.1: Class *ARGOS*

Main Dimensions	
Length:	27.2 m
Breath:	5.9 m
Depth:	3.5 m
Draft:	1.4 m
Maximum Displacement:	94 tonnes
Propulsion	
2 Engines MTU 12V 396 TE84 diesel	
Speed:	28 knots
Autonomy:	1350 miles at 15 knots
Autonomy:	200 miles at 28 knots
Weapon System	
2 Mg's	12.7 mm
Auxiliary Equipment	
Navigation Radar	FURUNO 1505 DA
Crew	
Officers	1
Sergeants and Sailors	7

Table 5.1: Principal Particulars

5.2 Hull Geometry Definition

In common engineering analysis, the definition and validation of the system under investigation is an essential step. The approach adopted in this work is to generate a three-dimensional geometry of the patrol boat and to validate it in comparison with intact stability data. All drawing plans and available intact stability data were provided by the Portuguese Navy. To describe the Patrol boat in detail, for appropriate hydrostatic calculations, the commercial software *ShipShape* was used, this software has been developed by the Wolfson Unit for Marine Technology and Industrial Aerodynamics, that uses a group of network curves as a schematic representation of the ship, i.e., a set of specific nodes defines all the curves that allow the generation of the surfaces. One of the major advantages of this particular software is that for a movement of a chosen point of a curve, during the fairing procedure, the neighbouring curves will also move to maintain compatibility, and before fairing, a geometry file is structured for a transverse section offset distribution, i.e., for a given abscissa value, a group of half breadths for the relevant waterlines are supplied. The hull form can be characterised as follow:

- The deadrise angle at the transom is considerably high, i.e. about 24 degrees.
- The after body of the hull, behind amidships, has a constant deadrise angle.
- The chine breadth is about 84% of maximum breath in the after body.

- Chine line exists along all the side shell.
- There is no convexity in bow sections.

In the model, and for each section, the specific nodes were defined as discrete points (i.e. keel, chine, sheer and deck three dimensional positions). The profile points define mesh boundary line. The layout by sections does not give the best approach for fairing the lines plan, due to the nature of a chined semi-planning hull used. Therefore, special attention was paid to the longitudinal fairing of the water lines, so that almost all of the offsets in the chine line do not lie on a particular waterline, but follow a three-dimensional longitudinal cubic spline. Figures 5.2 and 5.4 shows the first hull form, *Model A*, developed from the offset table and lines plan. This model is similar to the actual hull form of the Patrol Boat, defining the chine, keel and sheer shapes as the original, although does not account for the docking space that occupies the aft body, figure 5.4, this only happens in *Model C*, as can be seen in figure 5.7. On the other hand, *Model B*, figure 5.3 and 5.5 shows a simplified form of the hull with reduced detail in keel, chine and sheer geometric definitions, where differences can be seen in figure 5.6. Again no docking space is modelled, figure 5.5. Both models showed good agreement with the intact stability data of the actual ship, this can be seen in table 5.2.

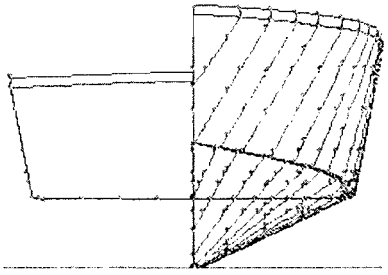

Figure 5.2: *Model A*: Detailed

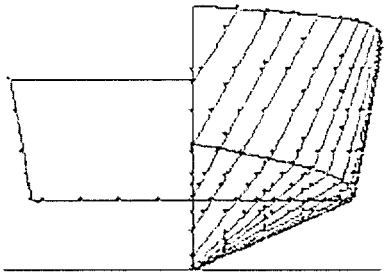

Figure 5.3: *Model B*: Simplified

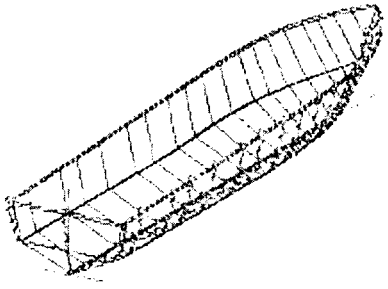

Figure 5.4: *Model A*

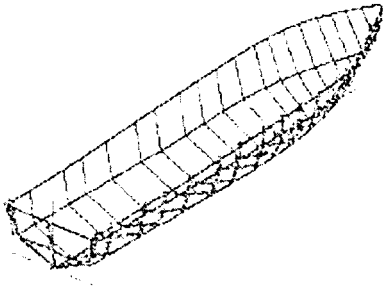

Figure 5.5: *Model B*

The reason for using a simplified model is to avoid unnecessary complexities when applying a hydroelastic analysis. Furthermore, a third model, *Model C*, figure 5.7 was run in *ShipShape*, taking into consideration the fact that the after-body has a floodable

docking space between the stern panel and the no.3 transverse bulkhead. This is mainly due to the transport of a rapid intervention semi-inflatable boat. In order to validate the intact stability data collected from the trials, this latter model should also be the most appropriate to compare, (see table 5.2). However, it should be noted that in order to accomplish a representation for *Model C* that would follow the schematic network used by *ShipShape*, it was necessary to consider the after-body as a catamaran type hull at water plane having zero half-breadth between hulls in the submerged double-bottom.

Assuming that the number of geometrical frames adopted is sufficient for a good surface fairing, the models were reduced to the minimum possible set of nodes that could properly define the geometry, this is, in order to consider the future implications on the development of the finite element model. Also, with the finished model, it is possible to generate an output file of offsets for sections, waterlines and buttocks defined at a particular position. This is a powerful tool that allows the definition of the precise offsets of a particular structural item in the ship, that will permit a less time consuming finite element geometric modelling of the internal structure.

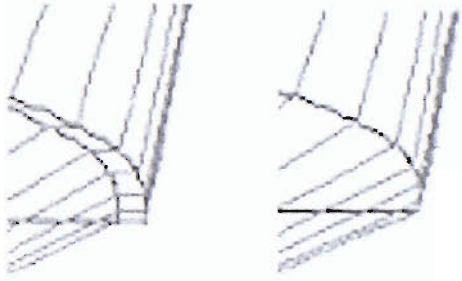

Figure 5.6: The cross-section dissimilitude

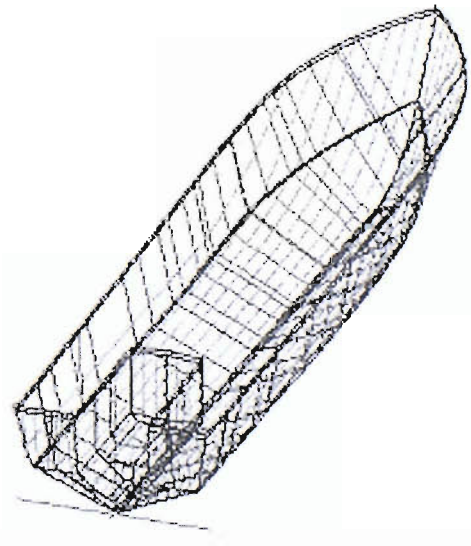

Figure 5.7: *Model C*: Detailed with Docking Area

5.3 Intact Stability Validation

To validate the model, the basic hydrostatics of the ship - including displacement, form parameters, metacentric and centres of buoyancy and flotation - are determined. To define equivalent hull characteristics for the finite element *in vacuum* structural dynamic analysis and fluid structure interaction, the following data from drawing plans and stability trials are the main references for the present investigation:

- Geometry;
- Displacement (Δ);
- Longitudinal position of the centre of buoyancy (LCB);
- Longitudinal position of the centre of flotation, centroid of the waterplane area (LCF);
- Vertical position of the centre of buoyancy above the base line (VCB);
- Vertical position of the transverse metacentre above the base line (KM_T);
- Moment to change trim in one centimetre (MCT);
- Transverse metacentric height (GM_T);
- Static trim (t_s);
- Draft (T).

The ship's stability data describe four load conditions:

1. Light Weight;
2. Normal;
3. Heavy Loaded;
4. Limit.

Initially, a normal loading condition was chosen as the basis of the analysis. The comparisons in table 5.2 were made for the actual ship and the three developed models. Calculations were made in order to access the original displacement for *models A* and *B* since they do not have the real aft body configuration. On the other hand, immersion was chosen as the reference comparison variable with *model C*. The underwater definition adopted, in the calculations, for the three models includes 20 sections, 10 waterlines and 5 buttocks. From the analysis of table 5.2 it can be seen that 1.38 metres is the appropriate value for the water line definition for the analysis using models A and B,

	Original	Model A	Model B	Model C
Δ(ton)	87.97	87.97	87.97	88.03
LCB (m)	11.05	10.50	10.52	10.90
LCF (m)	11.65	10.84	10.95	11.60
VCB (m)	0.93	0.91	0.92	0.93
KM_T (m)	3.50	3.47	3.48	3.52
MCT (ton.m/cm)	1.53	1.67	1.71	1.42
GM (m)	1.31	1.28	1.29	1.31
Trim t_s (m)	-0.02	-0.02	-0.02	-0.03
T (m)	1.44	1.38	1.38	1.44
KM_L (m)	46.02	53.00	51.17	45.91

Table 5.2: Intact Stability Data Comparison

where the after-body is not defined in detail. It can also be noted that the more detailed representation of model C agrees closer with the original hull, in which the draft assumes the value of 1.44 metres.

Chapter 6

Estimation of the Mechanical Properties

6.1 Theoretical Background

By definition, a composite material is made up of more than one phase, figure 6.1. For the materials used in the marine industry, the so-called *reinforcing phase* is in the form of chopped or continuous fibres that are stronger than the *matrix phase*. On the other hand, the *matrix phase* surrounds these fibres, figure 6.1 giving them both structural stability and protection.

Two types of fibre reinforcement have been used in the Patrol Boat structure:

- $ChoppedStrandMat$ - Discontinuous Fibres
- $WovenRoving$ - Continuous Fibres

Due to the marine environment this kind of fibre is susceptible to abrasion, moisture and internal delamination. Therefore, special coatings ("sizes") are used, but generally they do not have a significant role in the mechanical properties of the composite, unless the detail chosen for the numerical analysis takes into account mechanical properties like inter laminar shear strength. Thus, coating will not be included in calculations. The type of matrix material that constitutes the composite structure of the boat is unknown, therefore E-glass polyester is chosen since it is the most common resin used in marine industry. The less expensive orthopthalic form of polyester resin was considered. The properties estimation of the structural elements is determined with simple engineering

formulations developed from solid mechanics theory that could be found in Gibson's work published in 1994, [8].

Fibre composites have a relatively high modulus along the axis of their fibres and a low modulus perpendicular to this axis. The modulus of the composite, this is, matrix plus reinforcing fibre, is governed by the *Rule of Mixtures*. Considering the ideal situation as

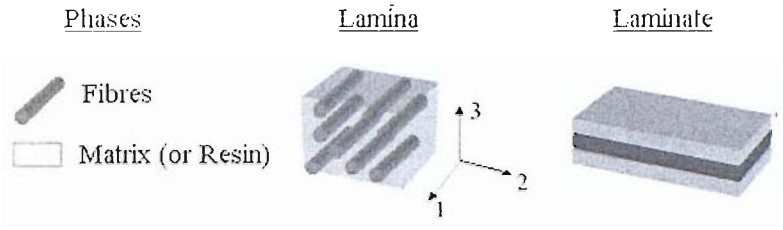

Figure 6.1: Composite Idealization and Reference Axes

continuous fibre layout, the assumptions are as follows. For longitudinal loading (applied force parallel to fibre direction) an "Isostrain" condition is assumed, where,

$$\epsilon_1 = \epsilon_m = \epsilon_f. \tag{6.1}$$

Since,

$$\sigma_1 = \sigma_m V_m = \sigma_f V_f \tag{6.2}$$

then,

$$E_1 = E_m V_m = E_f V_f. \tag{6.3}$$

For transverse loading an *isostress* condition is assumed, where,

$$\sigma_2 = \sigma_m = \sigma_f. \tag{6.4}$$

Since,

$$\epsilon_2 = \epsilon_m V_m = \epsilon_f V_f \tag{6.5}$$

then,

$$E_2 = \frac{E_m E_f}{E_m V_f + E_f V_m}, \tag{6.6}$$

where σ, E and V stand for tensile strength, modulus of elasticity and volume fraction, respectively. The subscripts m and f denote matrix and fibres, respectively. Three distinct cases are considered for in plane fibre distribution:

- Aligned and continuous;
- Aligned and discontinuous;
- Randomly orientated.

In this investigation the first case represents the basis to the theoretical approach. Knowing that η is a stress-partitioning parameter, given by equations 6.7 and 6.8,

$$\eta = \frac{\frac{E_f}{E_m} - 1}{\frac{E_f}{E_m} + \xi} \tag{6.7}$$

and

$$\eta = \frac{\frac{G_f}{G_m} - 1}{\frac{G_f}{G_m} + \xi}, \tag{6.8}$$

for longitudinal and transverse loading, respectively. Where the parameter and ξ represents a curve-fitting parameter which accounts for the degree of reinforcement of the matrix by the fibres.

K	Fibre Orientation	Stress Direction
1	All fibres parallel	Parallel to fibres
0		Perpendicular to fibres
3/8	Random in the plane	Any direction in the plane
1/5	Random in 3D	Any direction in 3D

Table 6.1: Values of constant "K" for discontinuous fibres in a Lamina

In practical calculations, Chop Strand Mat (CSM) will be assumed as a typical case of random orientated fibre, and Woven Roving (WR) as an unidirectional continuous fibre with in plane random stress direction with the correspondent value of constant "K", table 6.1. Woven Roving will be defined as two orthogonal unidirectional layers.

6.2 Lamina Properties

The following schemes broadly illustrate the formulation behind the material property estimation for a Lamina. A more refined approximation of the longitudinal and trans-

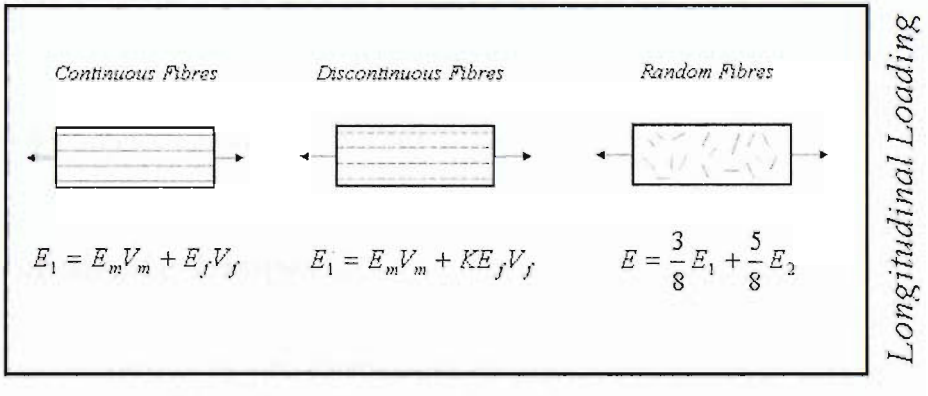

Figure 6.2: Longitudinal Young's Modulus of a Lamina - Direction 1

verse Young's moduli is due to Halpin and Tsai's semi-empirical equations, [98] and

[99], illustrated respectively in figures 6.2 and 6.3. Also, figure 6.4 illustrates the shear loading formulation. In the latest equations the value of ξ is function of the average

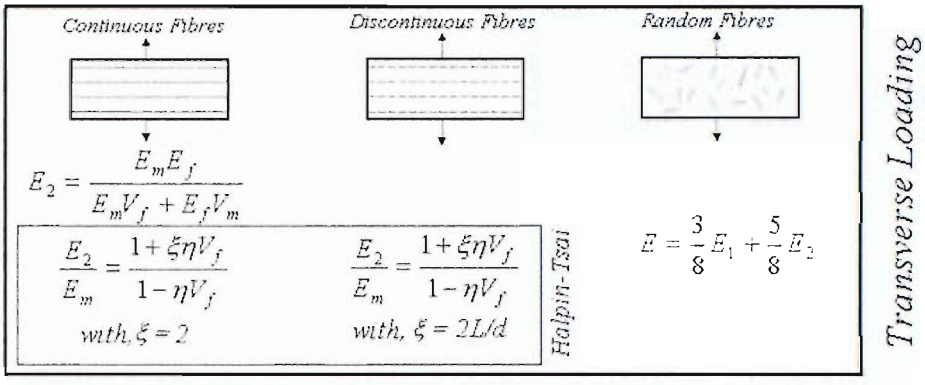

Figure 6.3: Longitudinal Young's Modulus of a Lamina - Direction 2

fibre length L and also of the average fibre diameter d, as can be seen in figure 6.3 and 6.4. For the Random Fibres case the empirical equations are derived from the moduli of aligned short-fibre composites, Agarwal and Broutman (1980), [100], and Hull (1981), [101]. Noting as well that $G_{12} = G_{21}$ for continuous fibres. The values for Poisson's

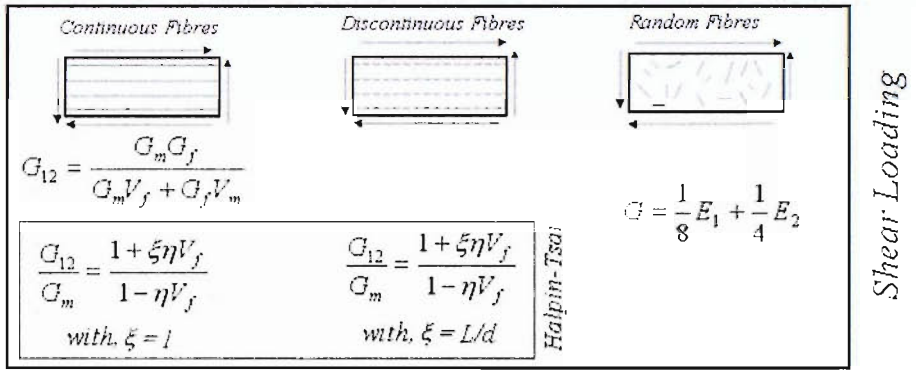

Figure 6.4: Shear Modulus of a Lamina

ratios of all type of fibre arrangement are given by,

$$\nu_{12} = \nu_m V_m + \nu_f V_f \tag{6.9}$$

Equation 6.9 applies for both continuous and discontinuous lamina.

6.3 Laminate Properties

Each lamina, or ply, is considered to be in a state of plane stress when forces are applied. Benham and Crawford (1996), [102], define the reduced stiffness matrix for a

lamina by,

$$\mathbf{K} = \begin{bmatrix} K_{11} & K_{12} & K_{16} \\ K_{21} & K_{22} & K_{26} \\ K_{61} & K_{62} & K_{66} \end{bmatrix} \tag{6.10}$$

where,

$$K_{11} = \frac{E_1}{1 - \nu_{12}\nu_{21}}, \tag{6.11}$$

$$K_{22} = \frac{E_2}{1 - \nu_{12}\nu_{21}}, \tag{6.12}$$

$$K_{66} = G_{12}, \tag{6.13}$$

$$K_{12} = K_{21} = \frac{\nu_{12}E_2}{1 - \nu_{12}\nu_{21}} = \frac{\nu_{21}E_1}{1 - \nu_{21}\nu_{12}}, \tag{6.14}$$

and

$$K_{16} = K_{61} = K_{26} = K_{62} = 0. \tag{6.15}$$

The laminate has a total thickness h and the thickness of the k_{th} ply with $k = 1, 2 \ldots n_p$ has a thickness h_k. Matrices $\bar{\mathbf{A}}$, representing direct and shear rigidities, $\tilde{\mathbf{D}}$, flexural and twisting rigidities and $\bar{\mathbf{D}}$, representing coupling terms, are obtained as;

$$\bar{A}_{ij} = \int_{-h/2}^{h/2} K_{ij} dz = \sum_{k=1}^{n_p} K_{kij} h_k, \tag{6.16}$$

$$\bar{B}_{ij} = \int_{-h/2}^{h/2} K_{ij} z dz = \sum_{k=1}^{n_p} K_{kij} h_k z_k, \tag{6.17}$$

and

$$\bar{D}_{ij} = \int_{-h/2}^{h/2} K_{ij} z^2 dz = \sum_{k=1}^{n_p} K_{kij} (h_k z_k^2 + \frac{1}{12} h_k^3). \tag{6.18}$$

The compliance matrix $\bar{\mathbf{Q}} = \bar{\mathbf{A}}^{-1}$ will give the coefficients for the determination of the laminate mechanical properties that may be found from

$$E_1 = \frac{1}{h \cdot \bar{Q}_{11}}, \tag{6.19}$$

$$E_2 = \frac{1}{h \cdot \bar{Q}_{22}}, \tag{6.20}$$

$$G_{12} = \frac{1}{h \cdot \bar{Q}_{66}}, \tag{6.21}$$

$$\nu_{12} = -\frac{\bar{Q}_{12}}{\bar{Q}_{11}}, \tag{6.22}$$

and

$$\nu_{21} = -\frac{\bar{Q}_{12}}{\bar{Q}_{22}}. \tag{6.23}$$

Furthermore, assuming that the lamina is anisotropic, with three planes of symmetry, the relation between Poisson's ratio is given by,

$$\nu_{21} = \nu_{12} \cdot \frac{E_2}{E_1}, \tag{6.24}$$

regarding that orthotropic materials do not allow relations between Young's modulus and Shear modulus.

The following comment, regarding all the previous calculations, should be made at the lamina analysis stage, orthotropic behaviour is assumed, but for the laminate calculation stage general solid mechanics theory is used, considering anisotropy. Only during the final phase, and due to the high number of plies randomly orientated by the hand layout fabrication process, it is assumed that the global laminate has isotropic in-plane elasticity modulus, that allows the use of semi-empirical formulations in order to determine their mechanical properties.

6.4 Characteristics of Fibres, Resins and Composites

Typical properties of thermosetting resins and unidirectional fibres are shown in tables 6.2 and 6.3.

Material	Specific Gravity d_m (g/cm^3)	Young's Modulus E_m (GPa)	Poisson's Ratio ν
Polyester (orthophthalic)	1.23	3.2	0.36
Polyester (isophthalic)	1.21	3.6	0.36

Table 6.2: Typical Properties of Thermosetting Resins

Material	Specific gravity d_f (g/cm^3)	Young's modulus E_f (GPa)	Shear modulus G_f (GPa)	Poisson's Ratio ν
E-Glass	2.55	72	30.00	0.2
S-Glass	2.5	88	36.67	0.2
HS Carbon (Thornel T-40)	1.74	297	-	
Aramid (Kevlar 49)	1.45	124	-	

Table 6.3: Typical Properties of Unidirectional Fibre

For typical chop-strand mat (CSM) laminates with weight in the range 300-600 g/m^2 and woven roving (WR) laminates with weight 400-800 g/m^2, the fibre weight fraction W_f ranges from 0.25-0.35 and 0.45-0.55 respectively, as illustrated in table 6.4, Smith (1990), [12].

Material	Fibre Volume Fraction V_f	Specific Gravity $d_f(g/cm^3)$	Young's Modulus $E(GPa)$	Shear Modulus $G(GPa)$	Min. Weight per Unit Area $w_f(g/m^2)$	Min. Fibre Weight Fraction W_f	Max. Weight per Unit Area w_f (g/m^2)	Max. Fibre Weight Fraction W_f
E-Glass polyester (CSM)	0.18	1.5	8	3	300	0.25	600	0.35
E-Glass polyester (WR)	0.34	1.7	15	3.5	400	0.45	800	0.55

Table 6.4: Mechanical Properties of the FRP Laminate

6.5 Laminate Scantlings

Ignoring voids, thickness per layer may be estimated from the following expression [6]

$$t_p = w_f \cdot \left[\frac{1}{d_f} + \left(\frac{1 - W_f}{W_f} \right) \cdot \frac{1}{d_m} \right] \tag{6.25}$$

where:

- w_f = Weight per Unit Area;
- W_f = Fibre Weight Fraction;
- W_m = Resin Weight Fraction;
- d_f = Fibre Density;
- d_m = Resin Density.

The data collected in this section will be used for the structural details of the three-dimensional idealization and for the beam-like ship analogy. In this boat, there is mainly a sequential combination of alternate layers of CSM and WR that were often used in high performance hulls at the beginning of the last decade. Also included in the structure are sandwich panels that use core materials such as Polyurethane and patented Core-Mat.

According to the structural data and drawings, an estimate for shell and stiffeners thickness is presented in table 6.5. Calculations for laminates from A to J include hull shell, bulkheads, buttocks, main deck, floors, double bottom and superstructure that are to be used as distinct panels, like the original structural drawing, in the three-dimensional finite element idealization.

Structural Element	No. of plies of WR	Weight per Unit Area (g/m^2)	No. of plies of WR a) Core-Mat 4 mm b) Polyurethane 50 mm c) Polyurethane 100 mm d) Polyurethane 200 mm	No. of plies of CSM	Weight per Unit Area (g/m^2)	Estimated Thickness (mm)
Laminate A	14	800	-	16	300	29
Laminate B	9	800	-	11	300	19
Laminate C	6	800	-	8	300	14
Laminate D	2	500	3 a)	5	300	18
Laminate E	4	500	3 a)	7	300	22
Stiffener Type 2	4	500	-	5	300	8
Stiffener Type 3	4	500	-	5	300	8
Stiffener Type 8	4	500	-	5	300	8
Frame Type 5	3+4	800+500	-	8	300	14
Frame Type 6	3+4	800+500	-	8	300	14
Laminate F	2	500	1 a)	4	300	9
Laminate G	4	500	1 b)	5	300	58
Laminate H	4	500	1 c)	5	300	108
Laminate I	8+2	800+500	1 d)	11	300	220
Laminate J	2	500	1 b)	1	300	54
Frame Type 9	7+4	800+500	-	8	300	18
Frame Type 10	7+2	800+500	-	10	300	18
Frame Type 11	7+2	800+500	-	10	300	18
Frame Type 12	5+3	800+500	-	9	300	16

Table 6.5: Thickness of Laminates, Longitudinal Stiffeners and Frames

6.6 Stiffener Scantlings

According to the nomenclature represented in figure 6.5, the determination of the equivalent stiffener scantlings was calculated considering equal values for sectional inertias and height of neutral axis.

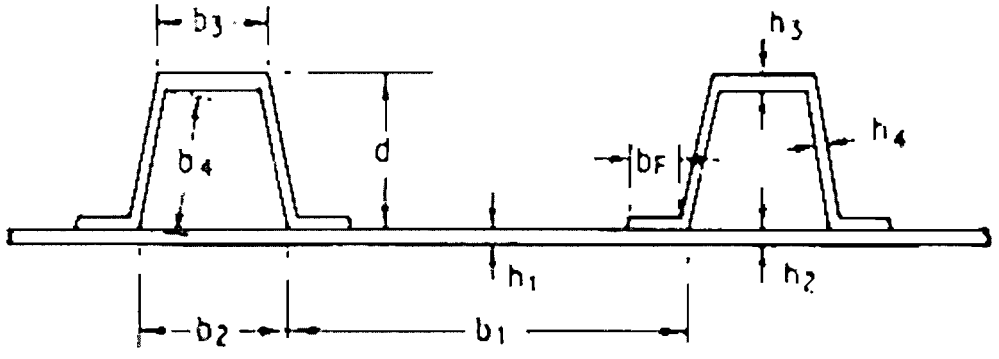

Figure 6.5: Stiffener Scantling Nomenclature

[mm]	Longitudinal Stiffeners			Frames	
Type No.	2	3	8	5	6
b_1	*	*	*	*	*
b_2	100.0	130.0	80.0	220.0	100.0
b_3	80.0	95.0	60.0	180.0	80.0
b_4	114.0	117.6	75.0	190.7	187.5
b_F	80.0	95.0	60.0	90.0	80.0
h_1	*	*	*	*	*
h_2	*	*	*	*	*
h_3	7.7	7.7	7.7	13.6	13.6
h_4	7.7	7.7	7.7	13.6	13.6
d	120.0	120.0	80.0	200.0	200.0

Table 6.6: Stiffener Scantling Values
*Dependent on the correspondent structural panel.

6.7 Assumed Material Properties

Chopped-strand mat laminates are commonly used in marine construction and this particular case is no exception. Smith [12] assumes isotropic in-plane modulus for random fibre orientation, which can be derived empirically from the modulus of an aligned short-fibre composite, as

$$E = \frac{3}{8}E_1 + \frac{5}{8}E_2 \tag{6.26}$$

$$G = \frac{1}{8}E_1 + \frac{1}{4}E_2. \tag{6.27}$$

The calculated values can be seen in table 6.7.

Properties Units	E_1 GPa	G_{12} GPa	ν_{12}	ν_{21}	E_2 GPa	E GPa	G GPa	ν	Density g/cm^3
Laminate A	20.423	1.241	0.422	0.094	4.569	10.515	3.695	0.422	1.597
Laminate B	20.157	1.281	0.419	0.095	4.569	10.414	3.662	0.421	1.593
Laminate C	19.814	1.333	0.415	0.096	4.567	10.285	3.619	0.415	1.589
Laminate D	15.462	1.615	0.366	0.108	4.548	8.641	3.070	0.366	0.578
Laminate E	16.266	1.466	0.374	0.105	4.553	8.946	3.172	0.374	0.736
Membrane	-	-	-	-	-	8.641	3.070	0.366	0.578
Long.Type 2	17.131	1.306	0.383	0.102	4.558	9.273	3.281	0.383	1.578
Long.Type 3	17.131	1.306	0.383	0.102	4.558	9.273	3.281	0.383	1.578
Long.Type 8	17.131	1.306	0.383	0.102	4.558	9.273	3.281	0.383	1.578
Frames Type 5	21.042	4.926	0.167	0.101	12.766	15.869	5.822	0.167	1.589
Frames Type 6	21.042	4.926	0.167	0.101	12.766	15.869	5.822	0.167	1.589
Laminate F	15.950	1.524	0.371	0.106	4.551	8.826	3.132	0.371	0.918
Laminate G	17.131	1.291	0.383	0.102	4.558	9.273	3.281	0.383	0.298
Laminate H	17.131	1.291	0.383	0.102	4.558	9.273	3.281	0.383	0.206
Laminate I	15.875	6.016	0.183	0.117	10.142	12.312	4.527	0.183	0.236
Laminate J	16.652	1.379	0.378	0.103	4.555	9.091	3.220	0.378	0.217
Frames Type 9	22.792	4.619	0.200	0.096	10.902	15.396	5.587	0.200	0.882
Frames Type 10	20.806	4.849	0.177	0.097	11.337	14.910	5.443	0.177	1.128
Frames Type 10	20.806	4.849	0.177	0.097	11.337	14.910	5.443	0.177	1.128
Frames Type 12	20.907	4.882	0.172	0.099	11.951	15.342	5.613	0.172	0.938

Table 6.7: Mechanical Properties of the Ship Structure

Chapter 7

Two Dimensional Dry Hull Analysis

7.1 Introduction

This chapter describes a study comparison between a classic longitudinal load analysis and a numerical prediction method in which the dry hull is idealised as a free-free Timoshenko beam, in order to extract mode shapes and natural frequencies using an analytical formulation for a two dimensional analysis, namely the Prohl-Myklestad technique. Euler beam approximation was an hypothesis at the beginning but a closer look to the problem soon shows that shear effects were far from being neglected. Especially regarding large deck openings and structural discontinuities. This preliminary analysis for symmetric response has the main objective of finding the order of magnitude of the variables that characterize the dry flexible body with a relatively simple algorithm before the use of a commercial finite element analysis package. Also this demonstrates a first step when approaching this investigation, especially regarding the identification of the problematic structural areas of the vessel in this preliminary phase. The approach here adopted is similar to the one presented by Bishop and Price (1979), [1].

7.2 Equivalent Mechanical Properties for Two Dimensional Beam Idealization

After the determination of laminate scantlings, and inherent mechanical properties, of the principal structural components that are present in the Patrol Boat, chapter 6, it is necessary to combine the properties of each structural element for each strip of hull in order to define global equivalent cross section properties. There are several structural numerical prediction methods available to evaluate the characteristic linear

elastic behaviours of laminated composite beams under bending and torsion. Although, it is not the intent of this document to explore exhaustively this field of solid mechanics. The objective is by a brief literature review to identify explicit design equations, function of panel mechanical properties, that have presented satisfactory results for the prediction of equivalent beam flexural stiffness, in composite panels of various structural shapes. Some prediction methods are based in the laminate stiffness matrix, which inverted will give the compliance matrix, equivalent to the method adopted in chapter 6. Therefore, the effective mechanical properties for the laminate are computed from the reciprocals of the components of the corresponding laminate compliance matrix, equations 6.19 to 6.23. In order to simplify the analysis the bending response of FRP beams is evaluated by means of the Mechanics of Laminated Beams (MLB), Barbero et al. (1993), [103]. This methodology considers that the stiffness coefficients, of the equivalent beam are determined by adding the stiffness's of each of the component panels. The complete model accounts for membrane and flexural stiffness's of the thin walled panels. Bending deflections are determined from Timoshenko's beam solution. For the Classical Laminate

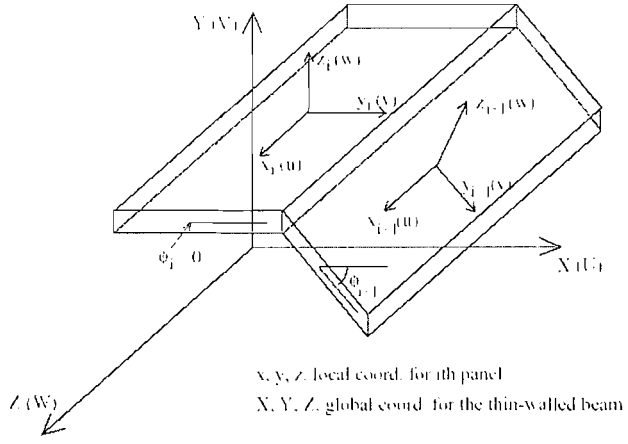

Figure 7.1: Global (beam) and local (panel) coordinate systems

Theory (CLT) the general constitutive relations for direct and shear forces per unit width, N_x, N_y, N_{xy}, together with bending and twisting moments,M_x, M_y, M_{xy}, and corresponding stress-resultants, combined with strains ϵ_x, ϵ_y, γ_{xy} and curvatures κ_x, κ_y and κ_{xy}, are given by the following matricial equation,

$$\begin{bmatrix} N_x \\ N_y \\ N_{xy} \\ M_x \\ M_y \\ M_{xy} \end{bmatrix} = \begin{bmatrix} A_{11} & A_{12} & A_{16} & B_{11} & B_{12} & B_{16} \\ A_{12} & A_{22} & A_{26} & B_{12} & B_{22} & B_{26} \\ A_{16} & A_{26} & A_{66} & B_{16} & B_{26} & B_{66} \\ B_{11} & B_{12} & B_{16} & D_{11} & D_{12} & D_{16} \\ B_{12} & B_{22} & B_{26} & D_{12} & D_{22} & D_{26} \\ B_{16} & B_{26} & B_{66} & D_{16} & D_{26} & D_{66} \end{bmatrix} \begin{bmatrix} \epsilon_x \\ \epsilon_y \\ \gamma_{xy} \\ \kappa_x \\ \kappa_y \\ \kappa_{xy} \end{bmatrix}. \tag{7.1}$$

Assuming that plane sections remain plane under membrane and flexural deformation direct and shear rigidities, A_{ij}, flexural and twisting rigidities, D_{ij}, and coupling coefficients B_{ij} are determined respectively by equations 6.16, 6.17 and 6.18. Assuming a similar approach according to the theory of Mechanics of thin-walled Laminated Beams, or in other words transferring the same methodology from micro to macromechanics, is assumed that the stress resultants are compatible with beam theory, therefore resultant forces and moments due to stresses in the y_i direction, figure 7.1, are negligible:

$$N_y = M_y = 0 \tag{7.2}$$

Assuming also bending without torsion, it fallows that

$$M_{xy} = 0 \tag{7.3}$$

Now the over-line identifies a panel quantities, where $\overline{A}_i$, $\overline{B}_i$ and $\overline{D}_i$ are respectively extensional, coupled (bending-extension) and bending relaxation coefficients. The *ith* panel of a thin-walled laminated beam has the relaxation matrix defined in equation 7.4.

$$\begin{bmatrix} \overline{N}_x \\ \overline{M}_x \\ \overline{N}_{xy} \end{bmatrix} = \begin{bmatrix} \overline{A}_i & \overline{B}_i & 0 \\ \overline{B}_i & \overline{D}_i & 0 \\ 0 & 0 & \overline{F}_i \end{bmatrix} \begin{bmatrix} \overline{\epsilon}_x \\ \overline{\kappa}_x \\ \overline{\gamma}_{xy} \end{bmatrix} \tag{7.4}$$

Furthermore, assuming that bending-extension coupling is not present the axial , bending and shear stiffness's of the *ith* panel are determined by equations 7.5, 7.6 and 7.7 respectively.

$$\overline{A}_i = (E_x)_i t_i \tag{7.5}$$

$$\overline{D}_i = (E_x)_i \frac{t_i^3}{12} \tag{7.6}$$

$$\overline{F}_i = (G_{xy})_i t_i \tag{7.7}$$

where t_i is the thickness, or the smaller dimension, of what is to be considered the thin-wall, and E_x and G_{xy} respectively the equivalent young and shear modulus obtained from micromechanics based on the classical laminate theory. From beam variational formulation expressions for the beam relaxation coefficients that account from the contribution of all the panels that constitute the thin-walled section can be determined from equation 7.8 to 7.10.

$$\widehat{A} = \sum_{i=1}^{n} \overline{A}_i b_i \tag{7.8}$$

$$\widehat{D} = \sum_{i=1}^{n} \left[\overline{A}_i \left(\left[(\overline{z}_{panel}) - (z_{na}) \right]^2 + \frac{b_i^2}{12} sin^2\Phi_i \right) + \overline{D}_i cos^2\Phi_i \right] b_i \tag{7.9}$$

$$\widehat{F} = \sum_{i=1}^{n} \overline{F}_i b_i sin^2\Phi_i \tag{7.10}$$

where b_i represents the larger dimension, of what is to be considered the thin-wall, Φ_i the orientation and $[(\overline{z}_{panel}) - (z_{na})]$ the distance from the neutral axis to the centroid of the cross sectional area of the *ith* panel. Therefore, in a macromechanic approach the prediction of the cross section equivalent modulus of elasticity, E_{eq}, and shear modulus, G_{eq}, are respectively determined by equations 7.11 and 7.12.

$$E_{eq} = \frac{\widehat{D}}{I} \tag{7.11}$$

$$G_{eq} = \frac{\widehat{F}}{A} \tag{7.12}$$

where A represents the total area and I the total second moment of inertia of the corresponding cross section of the non-uniform beam. The methodology previously described also allows the simplification of a stiffened panels, with girders and/or longitudinals, in an equivalent panel for a less detailed finite element model construction.

7.3 Hull Structural Data Relevant for Symmetric Response

Data presented in this section is evaluated from the most detailed *Model C*, referred in chapter 5. The structure was divided in 23 sections along the longitudinal axis, recalling that the hull fixed cartesian reference axis were x, y and z are respectively the longitudinal, transverse and vertical axis. The sections are not equally spaced because an intent was made to recognize which strips of the hull can be considered as homogeneous. Therefore, all discontinuities in deck openings, superstructure, bulkheads, double bottoms, framing and longitudinals where identified. The variation of nondimensionalised mass per unit length for the normal operation condition is given by figure 7.2.

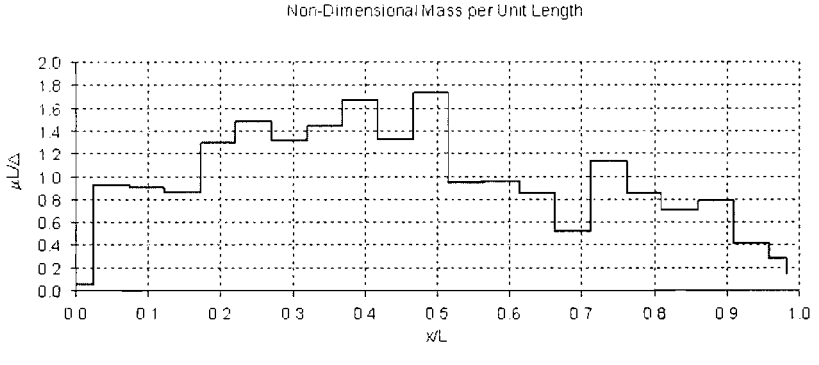

Figure 7.2: Non Dimensional Mass per Unit Length

For each of the 22 homogeneous strips, spreadsheet-based calculations were made in order to determine all relevant sectional characteristics.

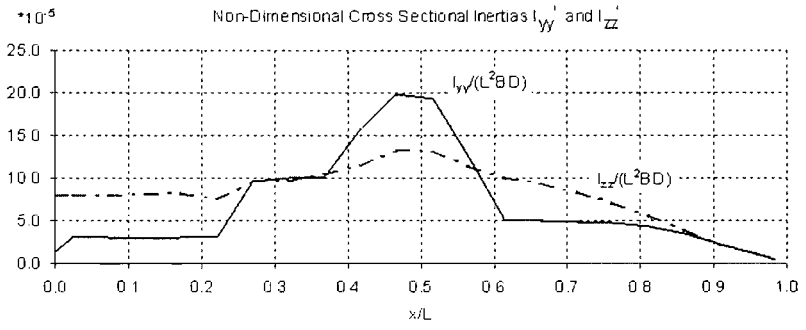

Figure 7.3: Non Dimensional Second Moments of Area

These are nondimensionalised dividing the original values by L^2BD, in which L, B, D, represent respectively length, beam and depth.

Observing figure 7.3, it is possible to identify the position of the docking deck from about 0 to 20 %, the deck opening over the engine room between 25 and 40 %, and the forward end of the superstructure at about 60 % of hull length L. Assuming that, for transverse cross sections, dimensions are not small compared to the length of the hull, it is necessary to account for the effects of rotatory inertia and shear deformation. The formulation for this problem is known as Timoshenko Beam Theory or also called thick beam theory. For the determination of the rotatory inertia, the following equation is used;

$$I_y = \int z^2 dm. \tag{7.13}$$

Hence, the graphic representation of the non dimensional distribution of rotatory inertia is given by figure 7.4 in which the ordinate values are calculated as $I_y/(L^2\Delta)$.

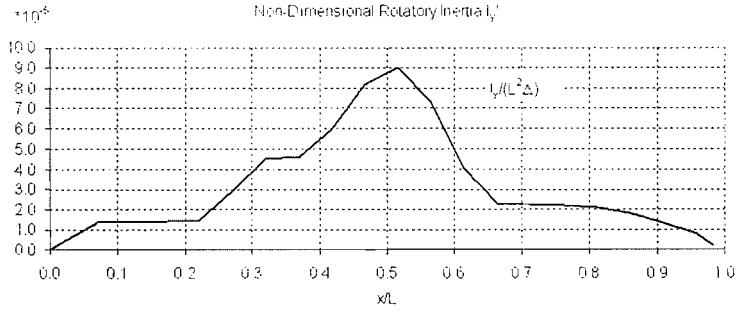

Figure 7.4: Non Dimensional Rotatory Inertia

Calculated values for shear coefficient k were determined by equation 7.14 and have a range from 0.44 to 0.76 which can be seen in figure 7.5. The shear coefficient for cross sectional area A is calculated by equation 7.14 assuming dependency of shape of the cross section.

$$k = \frac{SA}{bI} \tag{7.14}$$

where b is the cross sectional width at neutral axis and S is the upper half static moment of area of the cross section, given by equation 7.15

$$S = \int_{z \geq 0} z dA \tag{7.15}$$

However, a more accurate determination of k is given by Cowper's work published in 1966, [104], which reveals that k depends also on the Poisson's ratio. This shows that it is not purely a geometrical factor. Nevertheless, in the scope of this study, and due to simplification purposes, only the geometrical dependency was assumed.

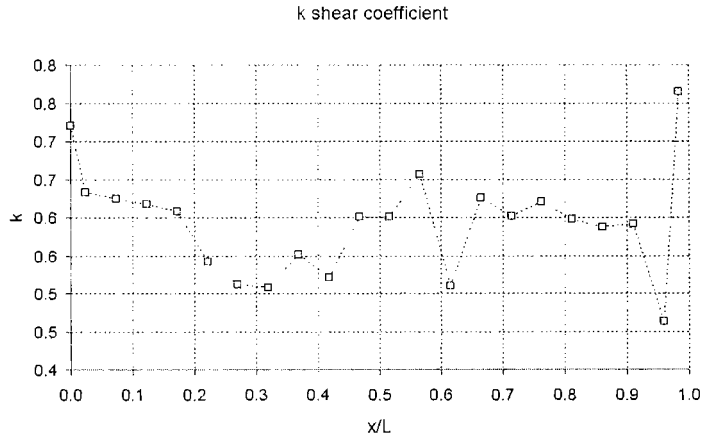

Figure 7.5: Shear Coefficient

Likewise, having already the values for the total cross sectional area $A(x)$ with corresponding longitudinals, the shear area $kA(x)$ is represented in fig.7.6

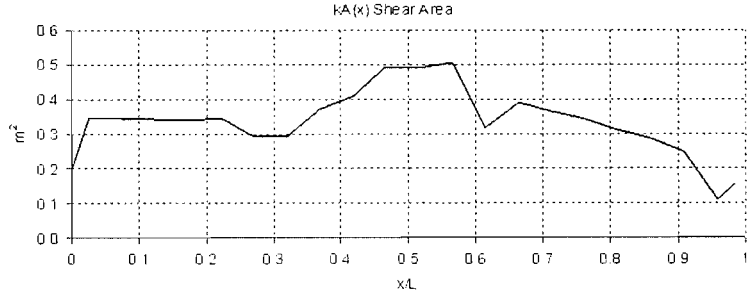

Figure 7.6: Cross Sectional Shear Area

If one assumes corrections made for shear deflections in the Prohl-Myklestad method, it is therefore also necessary to have the vertical position of the shear centre where a comparison between the latter and neutral axis position is given in fig. 7.7. Observing figure 7.7 is clear the discrepancy of values for the transom area, again, in about 20 percent of ship's length. Sections in which this structural characterisation is relevant can be seen in appendix C, more precisely in figures C.1, C.2 and C.3.

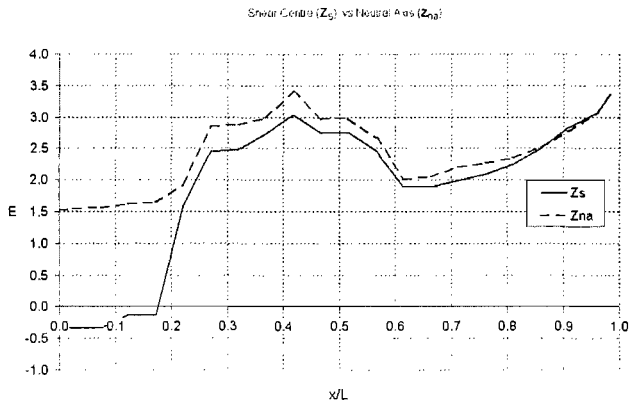

Figure 7.7: Vertical Position of Shear Centre and Neutral Axis

To obtain the values presented in fig. 7.7 a software tool module named *Cross Sections* was used as part of the package of *Ansys*, [105]. This algorithm also allows the determination of other properties, like the warping constant (I_w), the transverse cross sectional inertias (I_{yy},I_{yz} and I_{zz}), the centroid position and the non dimensional torsional constant shown in figure 7.8.

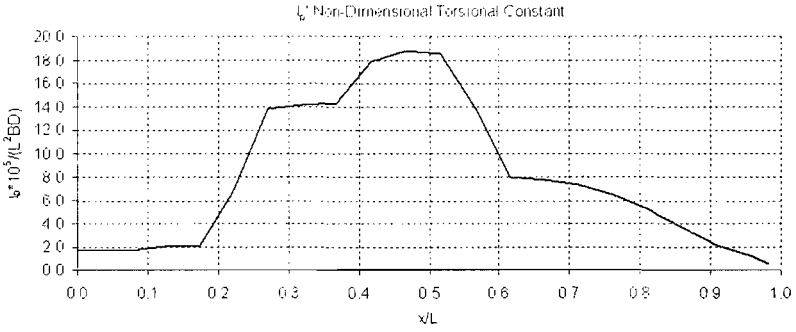

Figure 7.8: Non Dimensional Torsional Constant

The polar moment of inertia I_s about a longitudinal axis which passes through the shear centre is shown in figure 7.9.

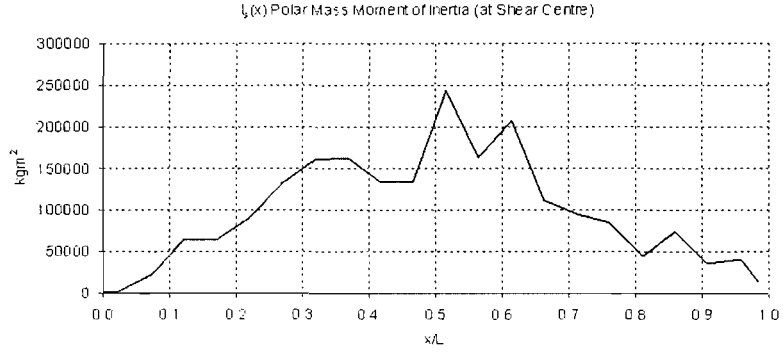

Figure 7.9: Polar Mass Moment of Inertia

To define each cross section through finite elements, which model a homogeneous strip, a section mesh file was created and the result for each station can be seen in Appendix C. The approach adopted was to calculate all beam properties by means of a finite element analysis and then converting to two-dimensional beam theory. Equivalent thickness's for finite element calculations are based on equivalent reinforced panels estimated the regarding structural geometric characteristics of table 6.7.

7.4 Longitudinal Load Analysis of Hull Girder in Still Water

The proper representation of a ship in still water must respect the Archimedes principle, which in a simplified interpretation, states that the total values of buoyancy and weight should cancel each other. But as it is known, both weight and buoyancy distributions along the length are in fact non-uniform. The resultant distortion for the particular load condition depends also of the environment, like water salinity and temperature, among others, Bishop and Price [1].

The *Hull Girder* is idealised as hollow thin-walled beam. This idealisation actually allows the use of simpler assumptions in the determination of ship global stress and consequently strains. The assumptions are based on simple beam theory, and they are as follows:

- One independent variable, longitudinal position x, gives one single value of load and deflection at each cross section.
- The Hull Girder is considered elastic, deflections are small, and longitudinal strain varies linearly over the section.
- Bending in the vertical plane is the most predominant.

Therefore to define the still water loading it is assumed that the net upward force per unit length is given by the equation

$$\overline{Z}(x) = Z_0(x) - \mu(x)g \tag{7.16}$$

Integrating Z(x) the static shearing force is obtained

$$\overline{V}(x) = -\int_0^x \overline{Z}(x)dx \tag{7.17}$$

Integrating once more the static bending moment is obtained

$$\overline{M}(x) = -\int_0^x \overline{V}(x)dx \tag{7.18}$$

For the *Normal* load condition with 1.44 metres draft the buoyancy force $Z_0(x)$ and weight $\mu(x)g$, both per unit length, are shown in figure 7.10. The data represented in this graphic is tabulated in Appendix A.3

For the buoyancy curve the values between stations are interpolated by *AutoHydro* allowing a well behaved line, i.e. non stepped. However, for the station at 4.13 metres forward from aft perpendicular, there is a notorious jump in the buoyancy curve. This

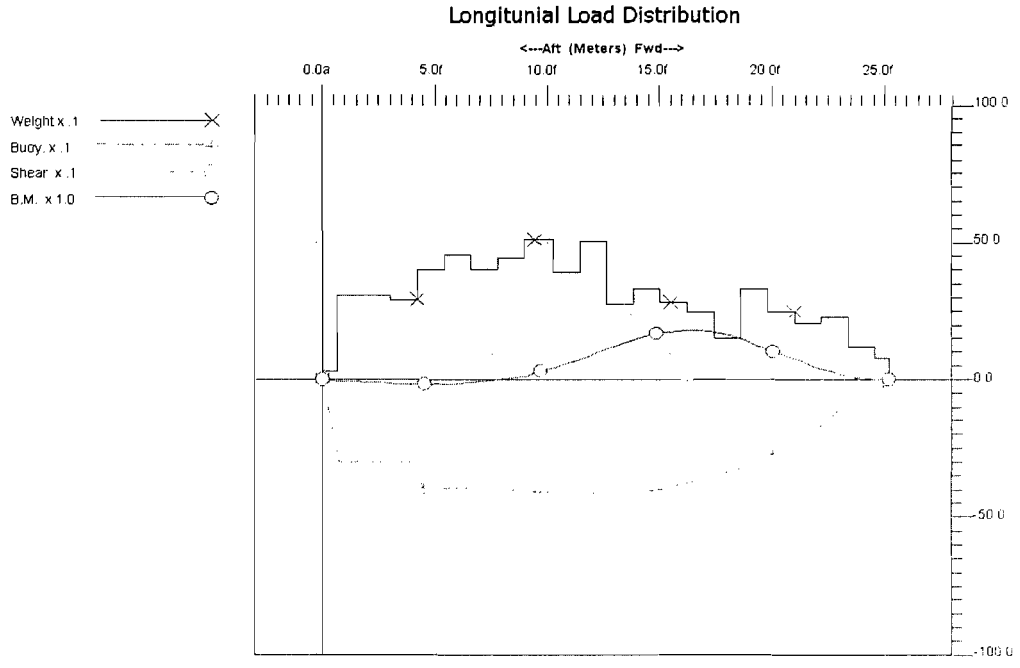

Figure 7.10: Still Water Longitudinal Load per Unit Length

is due to the aft body compartment that is not watertight. Naturally, for zero forward speed condition, or going astern, this compartment has water inside.

Data from *Trim and Stability Booklet* gives precise positions for weight items. The commercial program *AutoHydro* allows the use of a non equal spaced weight distribution, therefore the classical *20-slice* representation was not used in which the results can be seen in figure 7.10.

Diagrams for shearing force and bending moment, here determined, will be latter compared in section 7.5.2 towards the mode summations of the principal coordinates, i.e. after modal analysis results have been processed.

7.5 Prediction by the Prohl-Myklestad Method

The Prohl-Myklestad method is classical sequence of calculation adapted when the structure in analysis is due to respond with coupled flexure-torsion. The hull is represented by a set of masses connected by massless elastic rods. *The elastic axis of the beam about which the torsional rotation takes place is assumed to be initially straight. Although it is able to twist, its displacement due bending is restricted to the vertical plane*, [106]. The idealised beam, figure 7.11 is discretized by a set of lumped masses m_i with its centre of mass at a distance $(z_{cg})_i$ from the elastic neutral axis. The mass

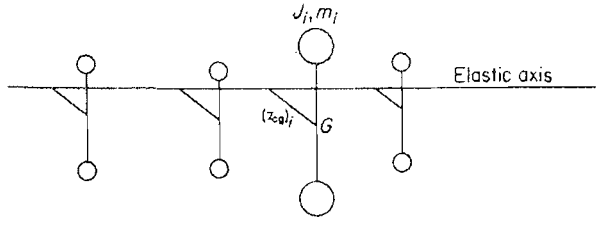

Figure 7.11: Lumped Mass Idealisation

moment of inertia through the centre of gravity, J_{cg}, can be related to the mass moment of inertia about the elastic axis, J_i, by the following expression:

$$J_i = (J_{cg})_i + m_i(z_{cg})_i^2. \tag{7.19}$$

The idealized ith segment with length L_i and adjacent stations i and $i+1$ can be seen in figure 7.12. Based in references [106] and [107], the relations between two consecutive

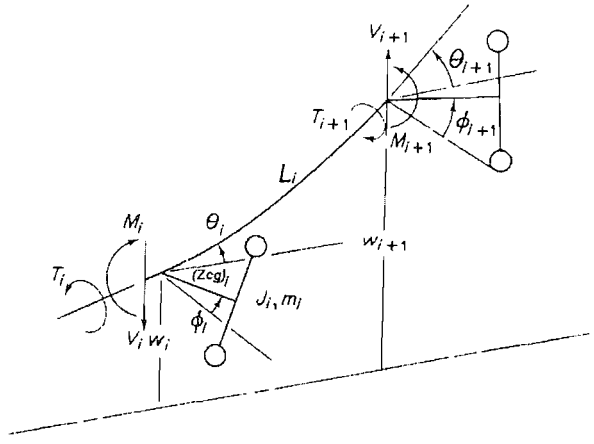

Figure 7.12: Adjacent Sections in Myklestad's Method

stations (i and $i+1$) in the idealised beam are given by expressions 7.20, 7.21, 7.22, i.e. respectively shear force, bending moment, twisting moment;

$$V_{i+1} = V_i - m_i\omega^2 \left[(w_i + \phi_i(z_{cg})_i\right], \tag{7.20}$$

$$M_{i+1} = M_i - V_{i+1} L_i, \tag{7.21}$$

$$T_{i+1} = T_i + \omega^2 \left[J_i \phi_i + m_i w_i (z_{cg})_i \right]. \tag{7.22}$$

In addition, equations 7.23, 7.24 and 7.25, respectively bending rotation, vertical deflection and torsional rotation given by;

$$\theta_{i+1} = \theta_i + M_{i+1} \frac{L_i}{(EI)_i} + V_{i+1} \frac{L_i^2}{2(EI)_i}, \tag{7.23}$$

$$w_{i+1} = w_i + \theta_i L_i + M_{i+1} \frac{L_i^2}{2(EI)_i} + V_{i+1} \frac{L_i^3}{6(EI)_i} - \frac{V_i}{k(AG)_i}, \tag{7.24}$$

$$\phi_{i+1} = \phi_i + T_{i+1} \frac{L_i}{(GI_p)_i}, \tag{7.25}$$

where I represents the cross sectional inertia and I_p the polar moment of inertia. Accounting for free-ended beams the starting condition for numerical computations are stated as follows:

- $V_1 = M_1 = T_1 = 0$
- $\theta_1 = \theta$
- $w_1 = 1.0$

Using the Prohl-Myklestad method, two dimensional modal analysis results where obtained with a *Matlab* based routine. The lowest four flexible modes, symmetrical and vertical, are calculated and their mode shapes can be observed in figure 7.13.

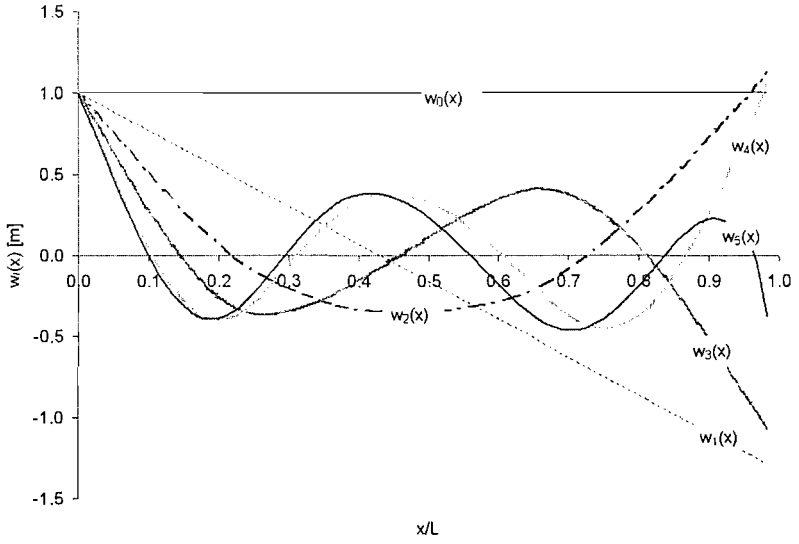

Figure 7.13: Symmetric Mode Shapes

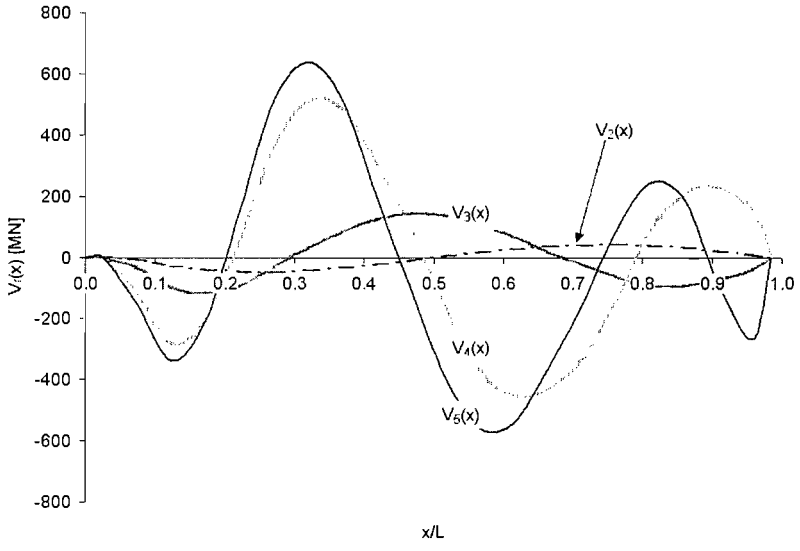

Figure 7.14: Modal Shearing Force

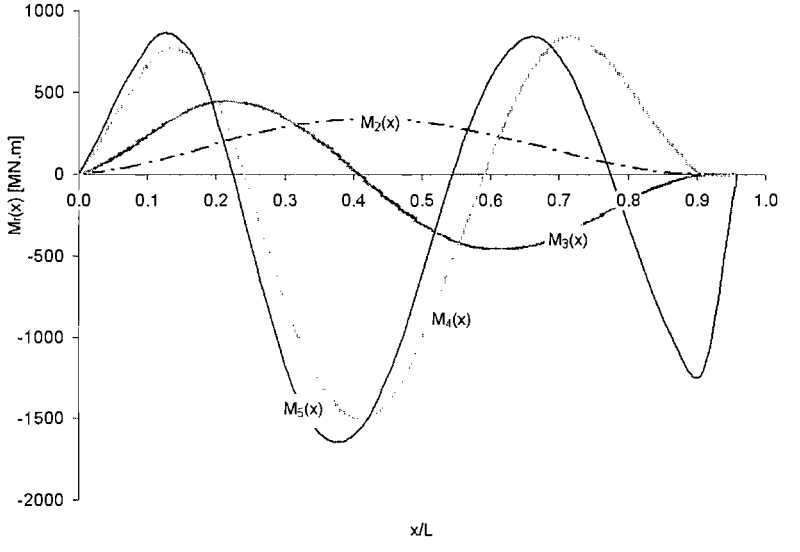

Figure 7.15: Modal Bending Moment

Note that indexes 0 and 1 define rigid body modes, respectively heave and pitch. The intersection of the latter with the abscissa axis defines the longitudinal position of the centre of mass of the patrol boat. As seen, the normalisation adopted is unit displacement at stern. With the same approach described previously, the corresponding modal shearing force and bending moment diagrams are given in figures 7.14 and 7.15, respectively.

It should be reminded that the inclusion of several parcels like rotatory inertia, sprung-mass and shear terms are considered to be optional, [107]. In equation 7.24 the inclusion of the shear term was adopted due to the fact of the existence of a significant number of effective longitudinal bulkheads and bottom girders that where assumed to contribute

significantly in the restraining of the flexible response especially regarding vertical symmetrical deflections. The contribution of longitudinal effective structural elements for shear rigidity can easily be identified by the cross sections presented in appendix C. However, it should be emphasized that the methodology used here, i.e. to account for a shear term, became inaccurate for the determination of higher modes. Although, for higher modes, shear effects became increasingly important but again more difficult to estimate correctly, [107], and that was one of the main reasons in determine a limited set of mode shapes in this preliminary two dimensional investigation.

7.5.1 Generalised Dynamic Characteristics

Assuming an undamped system and with no external forces applied, the mechanical system in study is considered to be conservative thus allowing the use of the principle of orthogonality.

Using orthogonality conditions the generalised masses can be shown as,

$$a_{rr} = \int_0^L (\mu w_r^2 + I_y \theta_r^2) dx, \tag{7.26}$$

where I_y represents the rotatory inertia.

Given the net upward force, $\bar{Z}(x)$, as being the difference between weight force per unit length $\mu(x)g$ and buoyancy curve $Z_0(x)$, and knowing the generalised characteristics of the hull structure, Bishop and Price [1] shown that the rth principal coordinate is given by,

$$\bar{p}_r = \frac{1}{\omega_r^2 a_{rr}} \int_0^L \bar{Z}(x) w_r(x) dx. \tag{7.27}$$

Furthermore, the generalised applied force $\bar{P}_r$ can be evaluated as follows,

$$\bar{P}_r = \int_0^L \bar{Z}(x) w_r(x) dx. \tag{7.28}$$

The values, given in table 7.1, as stated before, stand for natural frequencies, generalised masses, generalised forces and generalised coordinates defined respectively as ω_r, a_{rr}, $\bar{P}_r$ and $\bar{p}_r$, where the over bar stands for still water condition.

Modal index r	Natural Frequency ω_r (rad/s)	Natural Frequency (Hz)	Generalised Mass a_{rr} $(kg.m^2)$	Generalised Force $\bar{P}_r$ $(kN.m)$	Generalised Coordinate $\bar{p}_r$
2	89.22	14.2	12785	306	0.00300
3	189.75	30.2	10052	-501	-0.00138
4	390.16	62.1	10309	261	0.00016
5	447.36	71.2	9580	211	0.00011

Table 7.1: Two dimensional Symmetric Analysis Natural Frequencies and Generalised Masses

7.5.2 Two Dimensional Modal Summation

Considering w the vertical displacement, in $z - direction$, Rayleigh's theorem (1984) states that for a beam-like structures any distortion can be expressed as an aggregate of distortions in its principal modes, [1]. Thus, the symmetric responses, like vertical displacement, bending moment and shear force respectively $w(x,t)$, $M(x,t)$ and $V(x,t)$ can be expressed by,

$$w(x,t) = \sum_{r=0}^{N} p_r(t) w_r(x), \tag{7.29}$$

$$M(x,t) = \sum_{r=2}^{N} p_r(t) M_r(x), \tag{7.30}$$

and

$$V(x,t) = \sum_{r=2}^{N} p_r(t) V_r(x). \tag{7.31}$$

It may be helpful to note that for symmetric vertical response the rigid body modes for $r = 0, 1$, with zero natural frequencies, define heave and pitch responses are given by the following expressions,

$$w_0(x) = 1 \tag{7.32}$$

and

$$w_1(x) = 1 - \left(\frac{x}{\bar{x}}\right), \tag{7.33}$$

where $\bar{x}$ represent the longitudinal position of the centre of gravity. For $r = 0..N$ the boundary conditions are equivalent to a $free - free$ beam-like structure with length L, i.e. $M_r(0) = M_r(L) = V_r(0) = V_r(L) = 0$, for all r. Also equations 7.29 to 7.31 can be used to obtain still water distortions and internal actions. It has been found that the summations using the first four principal modes and the respective generalised dynamic characteristics give in figure 7.16 and 7.17 the representations for shearing force and bending moment diagrams respectively.

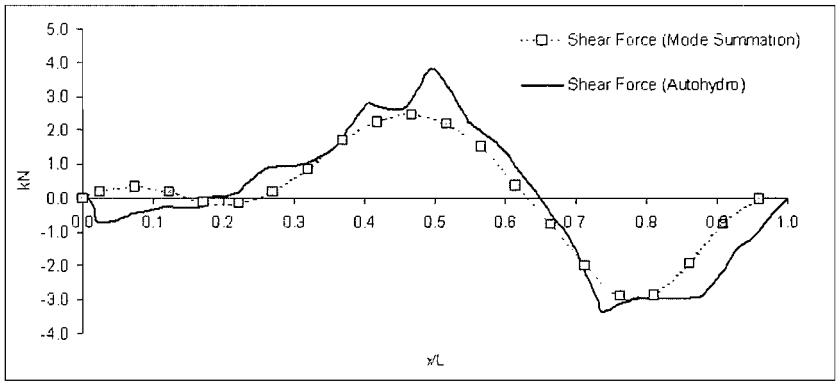

Figure 7.16: Still Water Shearing Force by Modal Summation

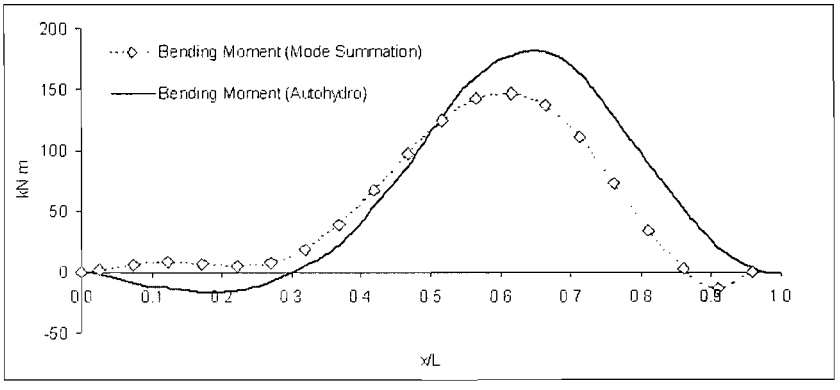

Figure 7.17: Still Water Bending Moment by Modal Summation

7.6 Concluding Remarks

Results obtained by mode summation and longitudinal static balance analysis compare relatively well however it is possible that using two more symmetric mode shapes, i.e. fifth and sixth, could lead to a relatively better convergence of values in the shearing force and bending moment diagrams. On the other hand it may be helpful to note that is known that the Prohl Myklestad method has some problems in properly defining high order modes and corresponding frequencies. Trial runs, using the later numerical prediction algorithm, confirmed the assumption and that was the reason why only the first fourth flexible modes where used.

Chapter 8

Three Dimensional Dry Hull Analysis

8.1 Introduction

The development of computer technology has generated a huge potential for the analysis of complex ship structures. One of the most widely used tool for structural dynamic analysis is the finite element method, that enables the study of a continuous system, subdividing into in a finite number of discrete elements connected by nodes.

Assuming that an individual finite element is continuous, that internal forces are in balance and nodal displacements are compatible between adjacent elements, the structure can therefore behave like a flexible body. The finite element method allows the derivation of the equations of motion for the complete structure by assembling the individual equations of motion for each element. Also the motion of any point inside the element can be estimated by interpolation, [108].

In the finite element modal analysis it is expected to assess the *in vacuum* **rigid body** motions for zero natural frequencies, i.e. the six degrees of freedom, and for the **flexible body** responses, like bending, twisting and their coupling for the non-zero natural frequencies. As usual in ship structural dynamics, the ship is considered as an undamped structure with free ends *in vacuum*, and modal analysis of the model will determine the natural frequencies and mode shapes as dynamic characteristics of the ship.

For the hull dry-modes analysis, several objectives are to be accomplished:

1. Interaction with the finite element program *Ansys*;
2. Definition of a proper mesh geometry, size and distribution;
3. Node numbering optimisation (3D Plate Model);

4. Selecting the appropriate internal behaviour of the finite element;

5. Selecting the appropriate solution procedure;

6. Mode shapes identification.

Therefore, at a first stage the main goal was to validate the geometry of the model and gather indications about their structural dynamic behaviour. A three dimensional plate and beam models, *3D Plate* and *3D Beam* respectively, will be evaluated by the eigen value problem solved by means of the subspace iteration method as a solution procedure, latter briefly explained in section 8.5.

8.2 Theoretical Background

For the determination of natural frequencies and mode shapes of free vibration of an undamped structure, the differential equations can be expressed in matrix form,

$$\mathbf{M}\ddot{\mathbf{u}} + \mathbf{K}\mathbf{u} = \{\mathbf{0}\} \tag{8.1}$$

where $\mathbf{u}$, $\ddot{\mathbf{u}}$ represent respectively the displacement and acceleration vectors. Again, $\mathbf{M}$ and $\mathbf{K}$ represent the inertia and stiffness matrices respectively.

For this undamped multi-degree of freedom system, all elements will experience simple harmonic motion.

The n second-order linearly independent homogeneous equations 8.1 will have general solutions of the form,

$$\mathbf{u} = \mathbf{\Phi}_r cos(\omega_r t), \tag{8.2}$$

where $\mathbf{u}$ is function of time t, the rth natural frequency ω_r, and $\mathbf{\Phi}_r$ as the eigenvector of the rth natural mode shape. It can also be called natural modal vector if it obeys the orthogonality condition with respect to the inertia matrix,

$$\mathbf{\Phi}_s^T \mathbf{M} \mathbf{\Phi}_r = 0 \qquad r, s \neq 1, 2, \ldots n \tag{8.3}$$

and also the stiffness matrix,

$$\mathbf{\Phi}_s^T \mathbf{K} \mathbf{\Phi}_r = 0. \qquad r, s \neq 1, 2, \ldots n \tag{8.4}$$

Following the reference to *Ansys* theory manual [105], equation 8.1 adopts the form,

$$\left(\mathbf{K} - \omega_s^2 \mathbf{M}\right) \mathbf{u} = \{\mathbf{0}\}. \qquad s = 1, 2, \ldots n \tag{8.5}$$

To avoid the trivial solution, $\mathbf{\Phi}_s = \{\mathbf{0}\}$, the determinant of $(\mathbf{K} - \omega_s{}^2\mathbf{M})$ should be zero. This eigenvalue problem for n degrees of freedom gives n values for natural frequencies and respective eigenvectors.

Afterwards, the eigenvectors can be normalised by the mass matrix, i.e.

$$\mathbf{\Phi}_s^T \mathbf{M} \mathbf{\Phi}_r = 1. \qquad\qquad s = 1, 2, \ldots n \tag{8.6}$$

Or they can be normalised assuming that the largest value obtained in each rth mode shape becomes unity.

8.3 Model Pre-Processing

8.3.1 Type of Finite Elements Choice

The fairly slender geometry of conventional ships usually satisfies to the simple Bernoulli-Euler beam theory, which follows the listed assumptions, Hughes (1988), [6]:

1. The plane cross sections remain plane after bending;
2. The beam has a prismatic configuration; [1]
3. The material is homogeneous and elastic.

However, the Fast Patrol Boat has a relatively small *length/beam* ratio and *length/depth* ratio, respectively equal to 4.6 and 7.8. Moreover, she has a planning hull shape without similar adjacent cross-sections, which shows that item number 2 can be of difficult applicability.

The complexity of the structure, due to the purpose of this type of vessel, could possibly demand a more detailed analysis rather than a two-dimensional approach, adopted as a starting point in chapter 7.

For the three dimensional beam model the Beam4 element was adopted , from *Ansys* [105]. The element is uniaxial and has two nodes, each with six degrees of freedom, figure 8.1, and its capabilities involve tension, compression, torsion and bending. Real constants that are used to characterise elements that represent each longitudinal portion of the naked hull, that include in the current analysis cross-sectional area, area moment of inertia about z- and y-axis, thickness's along z- and y-axis and torsional moment of inertia. Also mechanical properties like tension and shear modulus, in independent directions, are defined. At this stage the use of two-dimensional beam elements for the definition of the finite element model was not the main concern of this investigation, since it was understood that the assessment of a three dimensional response was the principal aim of this investigation. Nevertheless it is obviously identifiable as a simpler and less time consuming tool that deserves to be explored in terms of practical applications on a day to day basis in the design office.

Hence, for the three dimensional plate model it is useful to remind that shell elements are normally identifiable as entities having one dimension, namely thickness, that is much smaller than the other two dimensions, figure 8.2. Assuming that the shell element is integrated in a ship structure, the variation of stress through its thickness is practically negligible; the stress value will only depend on the element spatial position. Therefore,

[1] hull girder approximation, i.e. ignoring openings or discontinuities

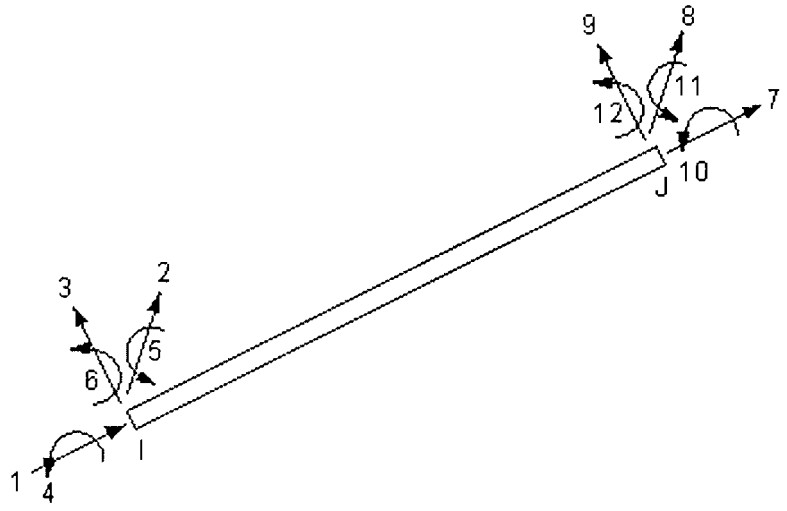

Figure 8.1: Order of Degrees of freedom for Beam4 Element

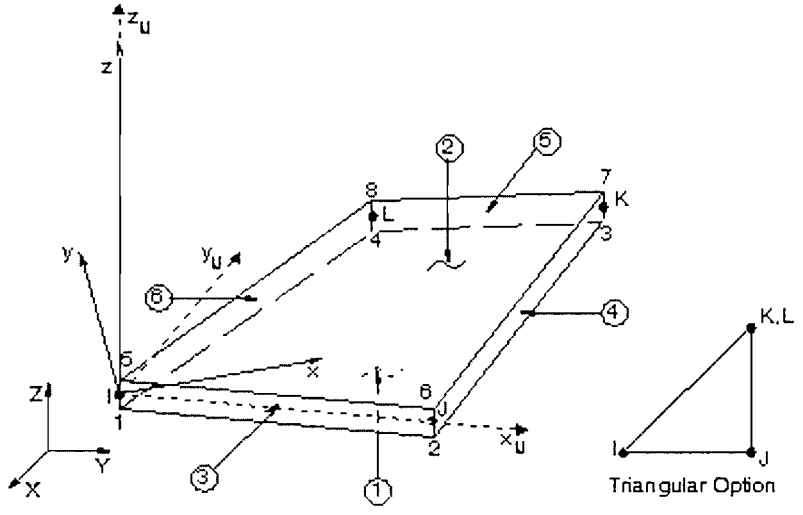

Figure 8.2: Reference axis on Shell63 Element

from basic structural analysis, stresses in x direction only depend on the distance from the cross section neutral axis.

Since a composite material is being dealt with, several assumptions are to be made in order to simplify the analysis. The basic idea consists in ignoring the laminate layers and to assume an equivalent set of directional material properties using stress-strain relationships with conjunction with the rule-of-mixtures, explained in chapter 6. Therefore, the following assumptions are disregarded:

- Interlaminar shear stress
- Through thickness stress variations

- Through thickness weight variations

These largely simplify the problem avoiding the use of mid-side nodes in thickness direction edges reducing the number of nodes, and degrees of freedom (DOF) and, consequently, computational times.

Expecting from the shell element a three-dimensional behaviour it is necessary to have rotational DOF. However, in a shell element where an edge in the thickness direction is identified by one node, two additional out-of-plane rotational DOF's are necessary. They define rotations around x and y axis assuming the shell surface parallel to xy plane
.

The third rotational in-plane DOF around z axis, also known as *Drilling DOF*, has a "fictitious" rotational stiffness. This in-plane rotational DOF is used to prevent the singularity of the stiffness matrix, [109].

It has already been pointed out that in classical ship structural analysis the membrane action of flat plates and shells is more predominant than bending action. However, for this fast patrol boat dimensional ratios demand some care in the analysis. That is why the study of both actions, membrane and bending should be taken in consideration. To allow the former study, in *Ansys*, element type *Shell* 63 was chosen.

This element has six DOF in each node, has both bending and membrane capabilities and allows the input of orthotropic material properties.

The hull modelling of the fast patrol boat was done by a combination of triangular and quadrilateral shell elements. Internal structures like longitudinal stiffeners, frames, girders, bulkheads, pillars and openings were modelled as precisely as possible. Also outer shell discontinuities, like the keel, chine and sheer have been modelled.

In particular, to model pillars positioned in the accommodation area, the *Pipe* 16 element was used, furthermore *Solid* 45 has been used to model, as "lumped mass", the twin propulsion engines and generators.

In order to obtain the correct base dimension limits (engine mountings position), weights and centre of masses position of main and auxiliary engines, calculations were made to define an equivalent volume, density and shape, respectively.

In summary, the following *Ansys* finite elements were used for the analysis:

- *Shell 63*, for hull shell modelling, internal and external structural elements;
- *Pipe 16*, for particular off centre line pillars at the accommodation area;
- *Solid 45*, engines and generators.

8.4 Model Geometry and Loading

The three-dimensional model generated in *Shipshape* served as base to the more refined finite element model in *Ansys*. To achieve some detail in the model definition, the amount of nodes and elements tend to be relatively large due to the complexity of the ship structure. In order to simplify the analysis nodal spatial positions were chosen to accommodate all known structure discontinuities.

Keeping in mind the future fluid structure interaction numerical calculations, using hydrodynamic panel idealization, nodes and element edges coincide both with the centre line and where relevant with the waterline (for normal operation condition), the former for questions of port-starboard symmetry and the latter in order to define the limit of the panels on the mean wetted surface.

A simplified command input file was produced using a transversal *strip type* grouping of the values. This approach allows identification of the geometry in the development of the internal structure. Also an appropriate node numbering permits the easy assessment of the weights for each two successive cross-sections. In this phase, special care was given to achieve the best compromise between the internal structure of the full scale boat and the model.

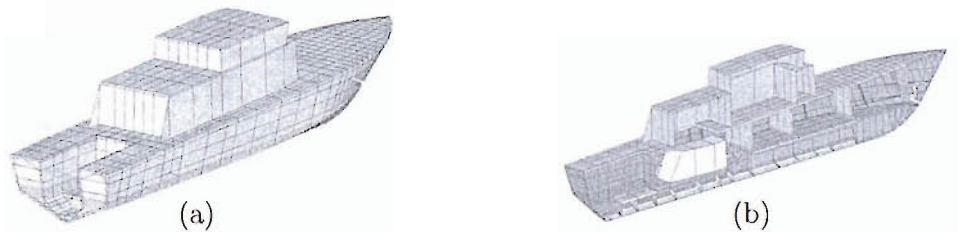

Figure 8.3: Finite Element Model

As shown in figure 8.3, the mesh size at the superstructure is relatively large compared to the surface under the waterline and also at the forward body. The latter was mainly due to an essential refined mesh in the definition of high curvature surfaces.

In preliminary studies, and for what was thought to be a simplified approach , the superstructure was not considered a critical area for the analysis. Several trial runs in *Ansys* were computed without the superstructure showing that this area can be very sensitive to all of the torsional modes, in other words there was always a distortion node in the vicinity of the deck opening. However, the superstructure must exist to prevent unrealistic particular local dynamic behaviour in the relatively large deck opening, at main deck level over the engine room. For the internal structure of the boat, it should be noted that all the frames were represented as not being uniform. This can be seen by the different grey colour along the contour of each frame, see figure 8.4. Also, bulkheads do not have the same thickness as the floors at the same cross section. Vertical stiffeners

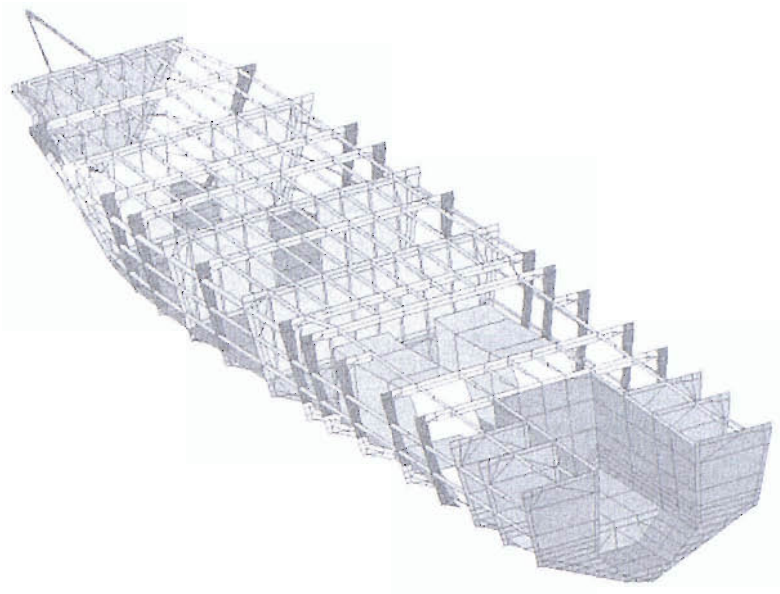

Figure 8.4: Internal Structure

were modelled following the structural drawings and conveniently prevent the use of "zero density membrane" elements.

The modelling of the stern, that usually carries a rigid inflatable boat, was especially time consuming phase. As figures 8.5 illustrate the internal structure at the aft body is quite dense. Therefore, all efforts were made to avoid excess of rigidity in this zone. In addition, surface loads were defined on the fuel and fresh water tanks with *Ansys* command *SFE*, *Specifies Surface Loads on selected Elements*; the values of the hydrostatic internal pressure were estimated respecting the height of the fluid column over the panel. In figure 8.5, the engines are represented as a *"lumped masses"* idealisation. As mentioned before, the fore body, figure 8.6, has supporting steel pillars and they were modelled as *Pipe* 16 elements. All of them are off the centre line, and the most forward are the only ones to exist as a symmetrical pair in the same cross section. The finite element model has the following characteristics: The even number of elements, in table

Number of	
Elements (PS and SB)	6947
Nodal Points (PS)	5219

Table 8.1: FE Model Characteristics

8.1 are justified by the inclusion of the steel pillars.

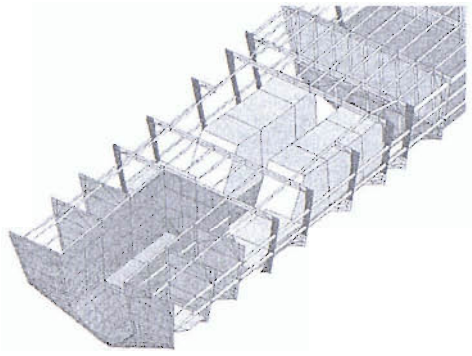

Figure 8.5: Engine Room

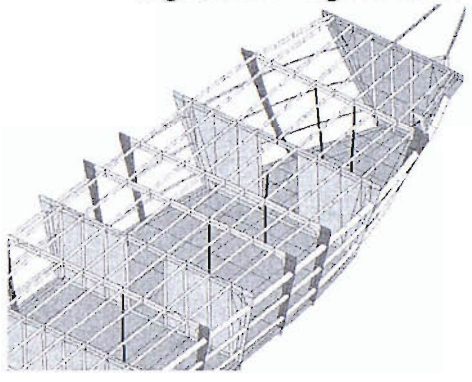

Figure 8.6: Accommodation Area

8.5 Solution Procedure

Using *Ansys* capabilities, in order to determine *in vacuum* natural frequencies and mode shapes of the structure, the solution method adopted is the Subspace Iteration Method. This method is commonly used in the solution of large eigenvalue problems, i.e. several thousand degrees of freedom. Although, for systems having a *moderate number* of degrees of freedom, say a few hundred, it is possible to make use of methods to reduce unwanted degrees of freedom before the solution of the eigenvalues problem. Nevertheless, the latter approach does not apply to this investigation, where the number of degrees of freedom reaches more the 30000.

8.5.1 Subspace Iteration Method Description

The Subspace Iteration Method is a very effective method of determining the lowest r*th* eigenvalues and corresponding eigenvectors with large multi-degree of freedom problems, Petyt (1990), [110].

The method can be resumed in the following steps:

1. Assume a starting matrix $[X]_1$ with a number j of columns greater than the lowest number of r eigenvalues required.

2. For $k = 1, 2, ...$

   (a) Solve equation 8.7 for $[\bar{X}]_{k+1}$

   $$[K][\bar{X}]_{k+1} = [M][X]_k \tag{8.7}$$

   (b) Calculate

   $$[K]_{k+1} = [\bar{X}]_{k+1}^T [K][\bar{X}]_{k+1} \tag{8.8}$$

   $$[M]_{k+1} = [\bar{X}]_{k+1}^T [M][\bar{X}]_{k+1} \tag{8.9}$$

   (c) Solve the reduced eigenvalue problem

   $$[K]_{k+1}[W]_{k+1} = [M]_{k+1}[W]_{k+1}[\Lambda]_{k+1} \tag{8.10}$$

   where $[\Lambda]_{k+1}$ and $[W]_{k+1}$ represent the eigenvalues' diagonal matrix and eigenvectors' matrix, respectively.

   (d) Determine a better approximation for the eigenvectors in the starting matrix

   $$[X]_{k+1} = [\bar{X}]_{k+1}[W]_{k+1} \tag{8.11}$$

   The eigenvalues should converge to lowest values of the original eigenvalue problem. The process is terminated as soon as predefined accuracy is achieved.

3. Sturm sequence check in order to determine if the number eigenvalues are in a specified range.

8.6 Results of Natural Frequencies and Mode Shapes

According to the data obtained from *Ansys*, the values for the natural frequencies and type of mode shape identified, which correspond to the first 19 flexible mode shapes, are presented in table 8.2. Letters "V", "T", "H" will define vertical, torsional and horizontal mode shapes, respectively.

Figure 8.7 characterizes the modal response in the natural frequency of the lumped masses that were used to model the main engines. A more detailed investigation should be taken into consideration due to this possible modelling problem. However, for the time being it is out of the scope of the present investigation. The first 2-node vertical mode, were the darkest gray represent higher stress values in the x-direction can be seen in figures 8.8 and 8.20.

Modal index r	Natural Frequency $\omega'_r = \omega_r(L/g)^{1/2}$	Natural Frequency (Hz)	Predominant Distortion	Coupled Distortion	Comments
7	163.70	16.402	-	-	Engines Lateral Oscillation
8	174.74	17.508	2-node V	-	1st symmetric
9	186.30	18.667	2-node H	1-node T	1st antisymmetric
10	244.09	24.458	1-node T	1-node H	2nd antisymmetric
11	273.20	27.375	1-node T	2-node H	3rd antisymmetric
12	282.93	28.350	3-node V	-	2nd symmetric
13	323.79	32.443	3-node H	1-node T	engine room + bottom
14	334.16	33.483	4-node V	-	3rd symmetric
15	378.48	37.924	2-node T	2-node H	4th antisymmetric
16	403.56	40.436	-	-	deck opening on engine room
17	424.02	42.486	-	-	engine room
18	439.22	44.009	-	-	stern twist
19	454.53	45.543	3-node H	1-node T	5th antisymmetric

Table 8.2: Three Dimensional Analysis Natural Frequencies and Modal Shape Identification

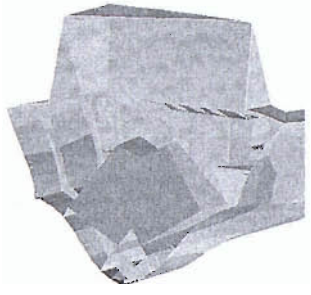

Figure 8.7: Engine Room(16.402 Hz)

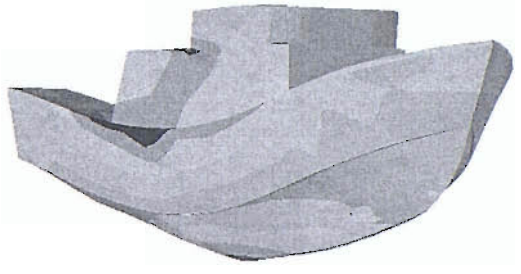

Figure 8.8: 2-node vertical(17.508 Hz)

The first horizontal mode shape, fig. 8.9, has coupled twist at the aft body. On the other hand, the first torsional mode shape has a coupled two-node horizontal mode, fig. 8.10.

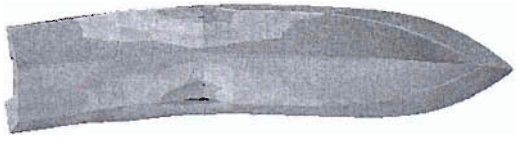

Figure 8.9: 2-node horizontal(18.667 Hz)

Figure 8.10: 1-node torsional(24.458 Hz)

Figure 8.11: mode coupling(27.375 Hz)

Figure 8.12: 3-node vertical(28.350 Hz)

In fig. 8.11, the keel shows a relatively well balanced coupling between one-node torsional and two-node horizontal modes. For the four-node vertical mode observed in fig. 8.14,

Figure 8.13: engine room(32.443 Hz)

Figure 8.14: 4-node vertical(33.483 Hz)

the vertical structure at stern, delimiting the docking area, oscillates transversely (*phase opposition*). The latter observation is predominant at 44.009 Hz, fig. 8.16. Regarding

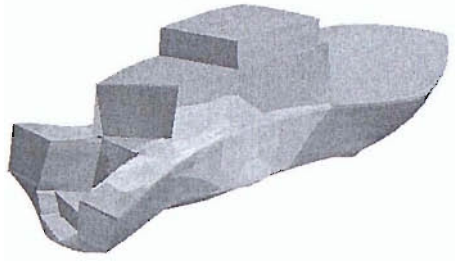

Figure 8.15: 2-node torsional(37.924 Hz)

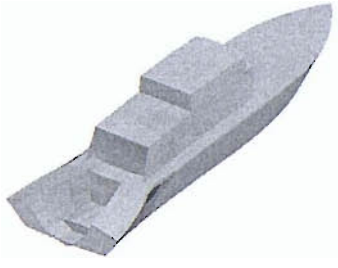

Figure 8.16: stern oscillation(44.009 Hz)

the previous work done by Price et al. [73], in their analysis in a similar type of GRP vessel ($L/B = 4.7$) the first set of flexible mode shapes contained a large number of symmetrical mode shapes, i.e. vertical bending related distortions. Conclusions, were then drawn regarding their greater flexibility in terms of symmetrical distortions. On the contrary, by the results obtained, in the present investigation, the vessel seems to be more flexible to antisymmetric distortions, most probably due to their stern configuration and the large deck opening above the engine room.

8.7 Dry Hull Dynamic Characteristics Comparison

From the previous section, this new set of results, of a full three-dimensional finite element analysis, and recalling the two-dimensional results presented in section 7.5, it can be seen in figures 8.17, 8.18 and 8.19, respectively 2^{nd}, 3^{rd} and 4^{th} the comparison of symmetrical vertical mode shapes. Furthermore, it should be emphasized that the deformed shaped acquired for the tree-dimensional case presented on the latter figures were obtained at waterline. The non-dimensional natural frequencies and generalized masses, respectively ω_r', given by $\omega_r(L/g)^{1/2}$, and a_{rr}/a_{00}, are presented in table 8.3. Unit displacement mode normalization at stern panel was adopted and for the present case a linearised set of nodes at waterline level was chosen for calculations, regarding its proximity in terms of elevation towards the neutral axis. The differences observed between natural frequencies are important for the 2- and 3-node symmetric modes, respectively 18.9% and 85.5% and it is difficult to identify the source of the problem,

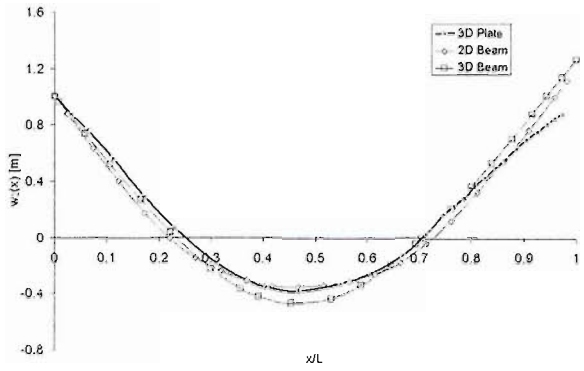

Figure 8.17: Mode shape curve comparison between 2D and 3D for $r = 2$

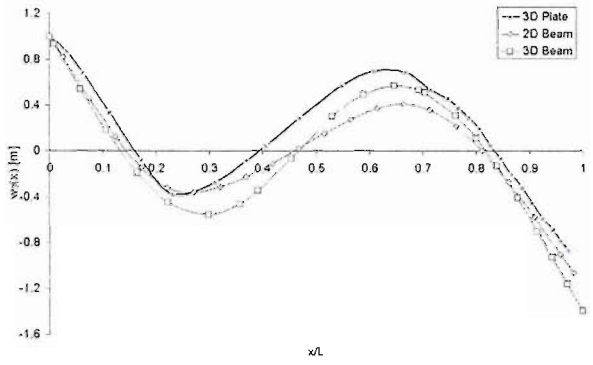

Figure 8.18: Mode shape curve comparison between 2D and 3D for $r = 3$

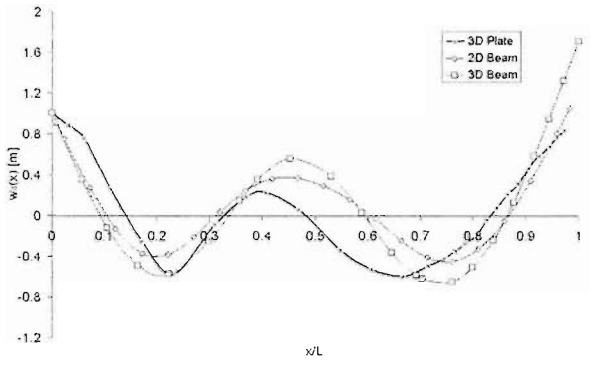

Figure 8.19: Mode shape curve comparison between 2D and 3D for $r = 4$

although several thoughts seem to be pointed to the actual interference of the superstructure in the flexible response of the forward body. This could be a modelling problem either for the three dimensional plate structure above deck or some problem related to the refinement of station spacing adopted for the two dimensional beam model. Probabily due to the variability of the cross section properties between 20 to 60% of hull length. Also, an averaged constant modulus of elasticity was adopted for the two dimensional model analysis by the Prohl-Myklestad method. Adding to this, there is a trend that when a node remains in the vicinity of 30% of boat length, i.e. under the large deck oppening, above main engine, it is difficult to obtain similar results for the

natural frequencies. Further research should be evaluated in order to compute a more accurate representaion of the two dimensional beam model. Furthermore, as expected the generalized masses seem to fallow the same trend which leads to relatively constant difference between the two models with the exception of the 3-node symmetric mode shape that produces good agreement.

Mode Shape	Non-dimensional Natural Frequency $\omega'_r = \omega_r(L/g)^{1/2}$			Non-dimensional Generalised Mass a_{rr}/a_{00}		
	3D Plate	3D Beam	2D Beam	3D Plate	3D Beam	2D Beam
2-node (S)	174.73	137.65	141.71	0.242	0.154	0.148
3-node (S)	282.93	347.90	301.39	0.117	0.141	0.117
4-node (S)	334.16	606.50	619.72	0.191	0.119	0.120
5-node (S)	684.94	907.07	710.58	0.169	0.112	0.111

Table 8.3: Comparing Non-dimensional Natural Frequencies and Generalised Masses

8.7.1 Results of Modal Internal Actions

In this section the results of the longitudinal modal stress analysis are presented. Three distinct, longitudinally distributed, sequences of panels were chosen in the finite element model for the determination of the modal internal actions. They are the keel bottom panels, the sheer strake panels (hull-deck joint line) and finally the uppermost centre line panels in the structure comprising the superstructure and the forward upper deck, thus defining a discontinuous line.

The sheer strake line is always above the neutral axis as can be seen in appendix C, and therefore, is expected to naturally have stress values with opposing sign to the bottom ones. It is also seen in the illustrations here presented that the superstructure appears to have extra rigidity compared to the deck panels. On the other hand, the load paths also appear to avoid the superstructure ceiling in all natural modes. This may be due to the structural geometry of this area and possible some finite element modelling problems that could result in imprecise idealization of the deck-superstructure joint. In the illustrations there is only a significant correlation between sheer strake and upper deck stress values forward of the superstructure, although the sheer line related ones seem to be always slightly larger due to extra stiffness in the centre of the forward upper deck.

It is worth mentioning that the initial expectations were that the stress values for the upper most line will be larger than those of the bottom line. This was not the case and the following offers an explanation as to what might be taking place. Based on the various types of hull-structure interactions referred by Hughes (1988), [6], the present investigation deals with the typical case in which the deckhouse side is not flush with ship side, adding to the fact that there is not intermediate transverse bulkheads, at least effectively continuous from the keel to the upper plating, i.e. none of them are full height, see figure 8.3b). Due to the flexibility of deck beams the deckhouse sides are able to adopt a much larger radius of curvature and consequently they do not carry a part of the flexural bending. Consequently, strain diminishes and the deckhouse is relatively independent from primary bending. These justifies the smaller stress values at deckhouse ceiling plating observed in 8.20, 8.21 and 8.22.

As expected, in terms of horizontal bending, figures 8.23 and 8.24, the boat centre line is recognized as the neutral axis transverse position. Therefore the stress values are shown to be more relevant at the sheer strake.

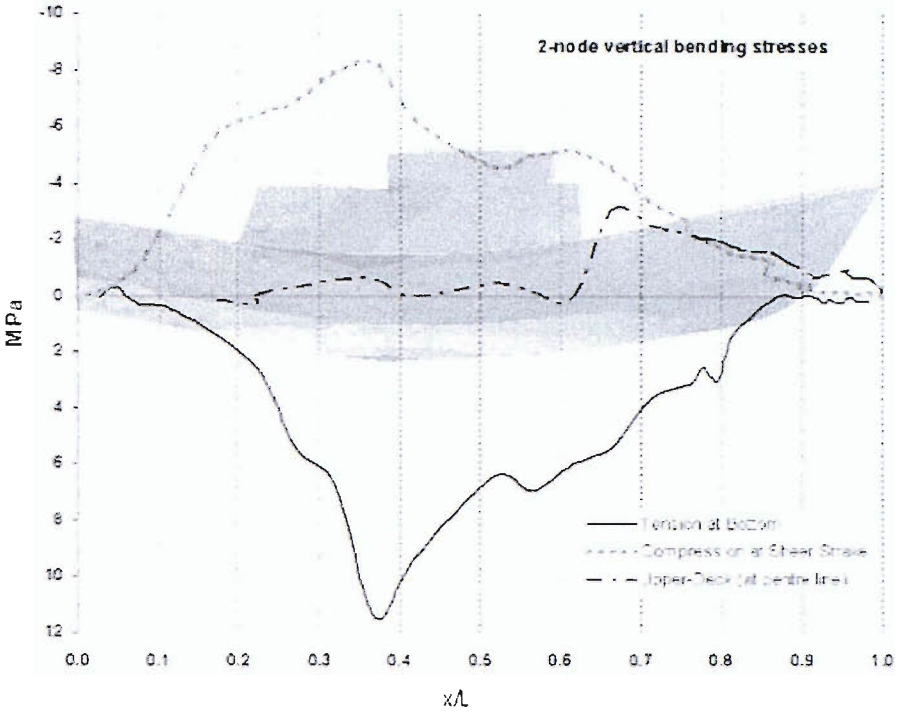

Figure 8.20: 2-node vertical bending

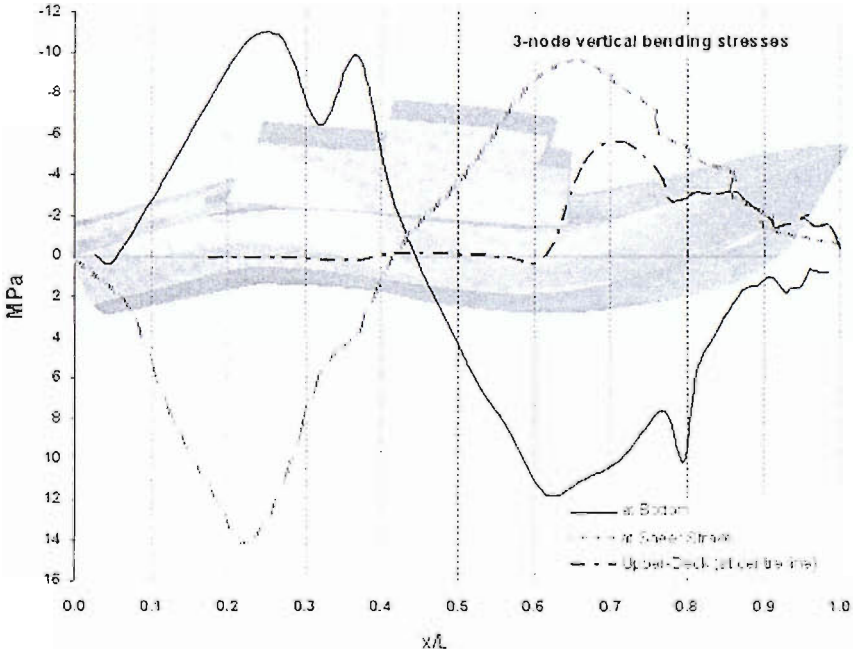

Figure 8.21: 3-node vertical bending

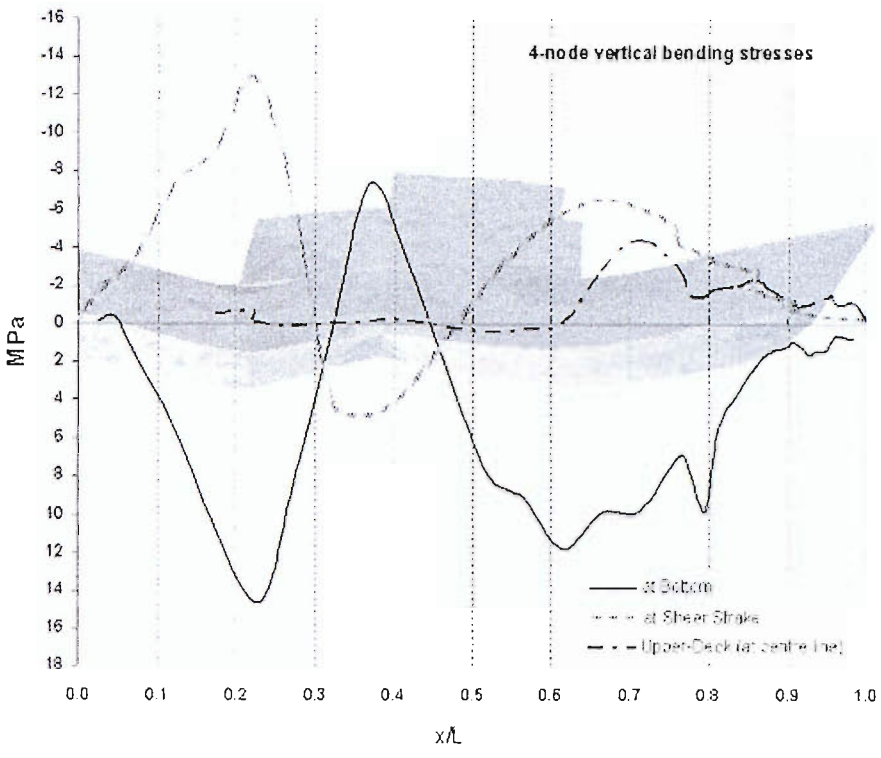

Figure 8.22: 4-node vertical bending

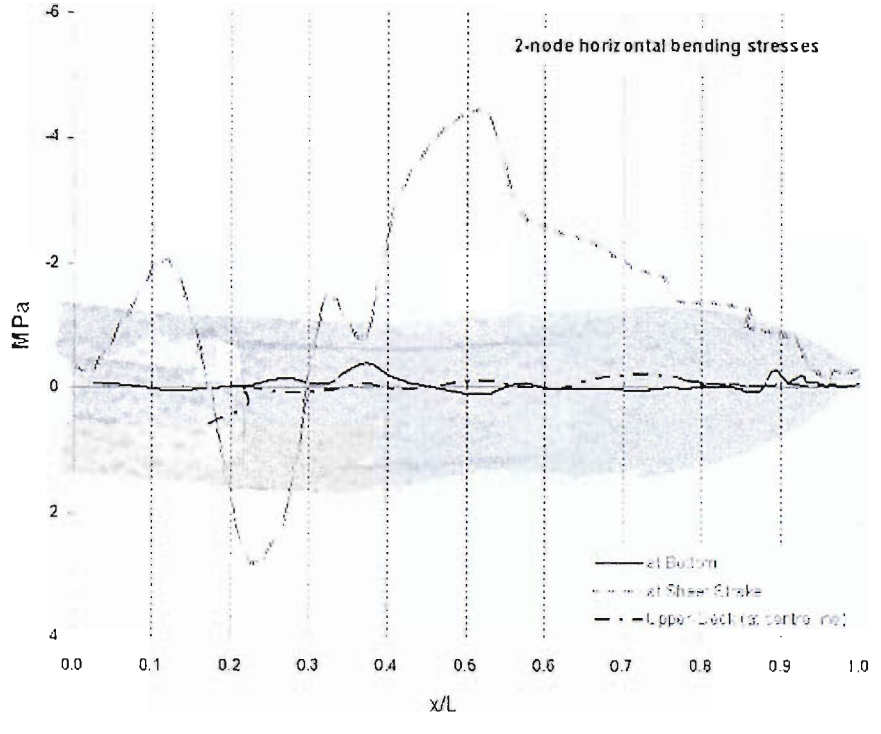

Figure 8.23: 2-node horizontal bending

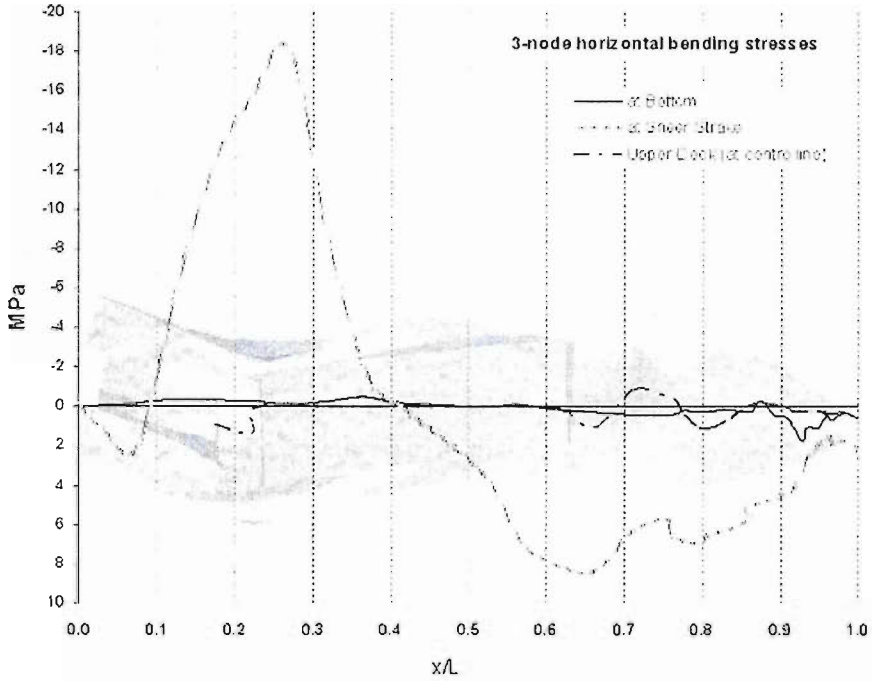

Figure 8.24: 3-node horizontal bending

Chapter 9

Wet Hull Analysis

9.1 Introduction

Methods based on singularity distribution have proven to correctly estimate loading and motion responses of the rigid ship travelling in waves. As already pointed out in the literature review, among others, Hess and Smith (1962) [111] proposed a practical method to estimate a singularity distribution over the mean wetted surface of the structure, represented by quadrilateral elements, i.e. four-cornered panels. More on the issue can be found in the literature review made in chapter 2. Nevertheless, for the present investigation a composite singularity distribution method is used which extensively extends the previous method only for the rigid body, therefore it is possible to determine the singularity strengths for a flexible structure having port and starboard symmetry, obtaining this way a solution for the diffraction and radiation problems in sinusoidal oblique waves, Bishop et al. (1986), [82]. The method used to predict the unknown source strengths is described by an appropriate Green's function corresponding to a pulsating source. Effects due to typical situations during planning in which the transom runs dry, as well as dynamic sinkage and trim, are disregarded according to the speeds chosen for this investigation. Moreover, viscous effects on roll damping were not included in the analysis.

9.2 Numerical Prediction Computer Codes

The description given for the numerical prediction codes is based on the program guides, [112] and [113]. The code *FLXBD* (FLexible BoDy) has been designed as preprocessor for program *HYCOF* (HYdrodynamic COefFicients), the latter doing the unified three-dimensional analysis for regular waves. Figure 9.1 shows the wet panel idealization adopted. The number of panels used is 644, corresponding to both port and

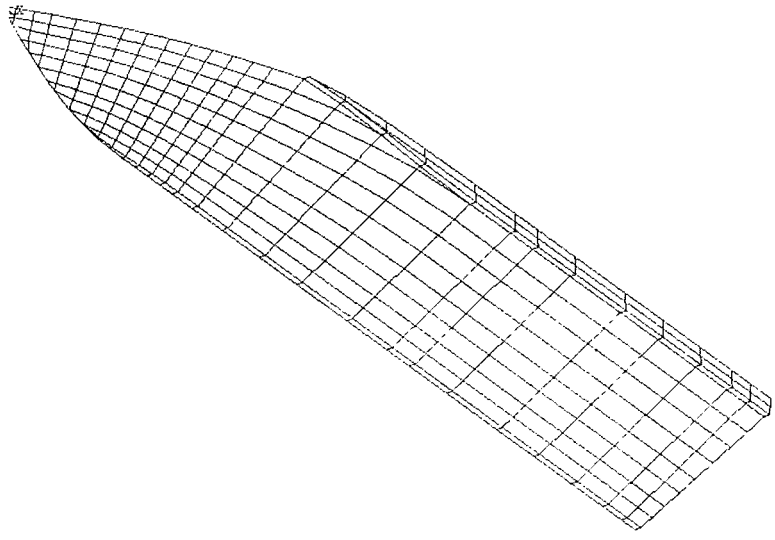

Figure 9.1: Wet Panel Idealization

starboard sides. The four and three cornered panels used have direct correspondence with the finite element model previously developed.

9.2.1 Program Module FLXBD

The program calculates the normal velocity on the wetted surface of a flexible body, defined by four-nodded quadrilateral plate elements. It also calculates relevant functions needed to determine generalised wave exciting forces and hydrodynamic coefficients.

As mentioned earlier, in order to simplify the preparation of the input file, direct correspondence exists between the coordinates position, defining the four and three-nodded quadrilateral plate elements of the finite element model and the idealised wetted panel mesh for *FLXBD*.

Macro commands were developed using the Advanced Parametric Design Language - *APDL*- to collect geometric data from the finite element model, and also the flexible normalised mode shapes for each natural frequency, i.e. collecting for each six DOF node the corresponding deflections and rotations.

Input Data

Some of the relevant data included in the input file can be summarised as follows;

- Hull Main Characteristics
  - Ship Length Between Perpendiculars (LBP)

- Longitudinal and Vertical position of Centre of Gravity, (LCG) and (VCG) respectively.
- Displacement Volume (∇)

- Hull Moments of Inertia
  - Mass Moment of Inertia for roll, pitch and yaw, respectively I_{44}, I_{55} and I_{66}.
  - Product of Inertia for roll into yaw, I_{46}.

- Hydrostatic Coefficients for Rigid Body Motion
  - Restoring Coefficients for heave, roll and pitch, respectively C_{33}, C_{44} and C_{55}.
  - Coupled Restoring Coefficient for Heave and Pitch, C_{35}.

- Three-dimensional Dry hull Analysis Characteristics
  - coordinates defining the four noded quadrilateral plate elements defining the wetted hull surface
  - *in vacuum* normalised flexible mode shapes
  - *in vacuum* undamped natural frequencies, ω_r and both rigid and flexible modes generalised masses, a_{rr}

FLXBD Relevant Input Data and Numerical Results

Table 9.1 compares the hydrostatic input data and the data generated from the mesh defining the hydrodynamic panels calculated by $FLXBD$

	Δ ton	∇ m^3	LCB m	S m^2	LCF m	VCB m	GM_T m	GM_L m
Model C	88.026	85.879	-1.548	140.030	-1.698	-0.450	1.310	49.500
Generated	87.360	85.230	-1.885	136.588	-1.561	-0.481	1.263	50.497
Difference(%)	-0.76	-0.76	1.35	-2.46	-8.07	6.89	-3.59	2.01

Table 9.1: Hydrostatic Values Generated from Hydrodynamic Panel Mesh

The values of longitudinal centre of buoyancy and longitudinal centre of flotation, respectively LCB and LCF, are defined positive forward of amidships, and the vertical position of the centre of buoyancy, VCB, is defined positive above the water line.

A comparison between restoring coefficients, for rigid body motion, calculated from the table of offsets used for the hydrostatic calculations and calculated by the numerical prediction code is made in table 9.2. The objective was to have a term of comparison to understand the level of crudeness of the panel idealisation adopted in this investigation.

The restoring coefficients are calculated based on the still water plane for a normal service condition. Their determination depends upon the salt water density ρ (with a

chosen value of 1025 kg/m^3), the acceleration due to gravity g (9.81 ms^2), the volume of water displaced ∇ (m^3), the water plane area A_w (m^2), the longitudinal position of the centre of flotation LCF (m), from the origin O which is positioned in the same longitudinal position of the vessel centre of mass.

In addition, S_x (in m^3) representing the first waterplane area moment about Oy axis and finally the transverse and metacentric heights, respectively GM_T and GM_L. The expressions for the restoring coefficients are as follows;

$$C_{33} = \rho.g.A_w, \tag{9.1}$$

$$C_{44} = \rho.g.GM_T.\nabla, \tag{9.2}$$

$$C_{55} = \rho.g.\left(GM_L.\nabla + A_w.LCF^2\right), \tag{9.3}$$

and

$$C_{35} = \rho.g.S_x. \tag{9.4}$$

	C_{33} kgs^{-2}	C_{44} kgm^2s^{-2}	C_{55} kgm^2s^{-2}	C_{35} $kgms^{-2}$
From Hydrostatic Properties	1030382	1131230	38683661	-978862
From HYCOF Computer Code	1102020	1082580	43757900	-728542
Difference(%)	6.95	-4.30	13.12	-25.57

Table 9.2: Restoring Coefficients Comparison

Assuming that there were only significant differences in restoring coefficients C_{55} and C_{35}, respectively 13.12 and 25.57 %, and in order to simplify the analysis it is considered that, in general, the coefficients compare relatively well and therefore they will be estimated by HYCOF.

Nevertheless, looking to the flexible restoring coefficients in the output file generated from $FLXBD$ they seem very high. Their influence will have a drastic effect in the calculation of the principal coordinates by program HYCOF. Several verifications were made, but until now it was not possible to identify the problem. It seams that these coefficients are quite sensitive in the normalisation of the modes.

9.2.2 Program Module HYCOF

For given values of forward speed, regular wave amplitudes and heading angles, the program evaluates the potential flow surrounding the flexible body, the hydrodynamic coefficients corresponding to the radiation due to flexible and rigid body motion and the exciting loads induced by waves of sinusoidal form.

The algorithm is based on the composite source distribution method limited for bodies with port-starboard symmetry, [82]. A method using asymptotic and Taylor series serve as basis for the evaluation of the Green's function for the pulsating source. This implies that the method is restricted to waters of infinite depth. In essence, the program performs a unified three-dimensional (i.e. both rigid and flexible body) analysis to obtain motion responses, described by amplitude and phase angles, as well as the principle coordinates.

As mentioned earlier, input parameters are wave amplitude, wave heading angle and constant forward speed. The calculations evaluate the responses for a set of wave frequencies defined by the user. As input data for HYCOF, the segments defining the water line contour (64 wetted panels on Port Side) were identified; once again *APDL* macro commands were used to collect data from *Ansys in vacuum* modal analysis. The maximum speed achieved in the full scale trials, 10.289 m/s (20 knots), was chosen as the reference for the study. Numerical results were obtained for 180, 135 and 90 degrees of heading. Also, a numerical prediction was obtained for a 8.230 m/s forward speed in head waves, in order to have a characterization of the difference between response amplitudes at the same heading. Due to some irregularities observed in the principal coordinates response curves, i.e. for non-dimensional encounter frequencies greater than 5.0, trial numerical evaluations were also obtained for a lower and higher limit speeds of advance, respectively 3.090 and 15.433 m/s.

9.2.3 Hydrodynamic Coefficients

The hydrodynamic coefficients of the wet hull panel idealization of *model C*, referenced in chapter 5, were estimated for several speeds; 3.090, 8.230, 10.289 and 15.433 m/s, corresponding respectively to F_n=0.20, 0.53, 0.66 and 0.99. It can be seen in figure 9.2 and in figure 9.3 the curves representing the symmetric non-dimensional added mass and damping coefficients for all forward speeds range previously mentioned. It is also obvious that the heave added mass and damping coefficients (non-dimensional), respectively A'_{33} and B'_{33} seem to be speed independent, as they should be; the differences seen at higher frequencies are mainly due to the occurrence of irregular frequencies. The pitch added mass and damping coefficients (non-dimensional), respectively A'_{55} and B'_{55}, show a more relevant speed dependency for the lower frequencies. The irregular frequencies are illustrated in the sharp variations observed for the non-dimensional encounter frequencies of approximately 5.4 and 7.4, especially regarding figures 9.2a and 9.3a, representing the heave related coefficients.

For the hydrodynamic non-dimensional damping coefficient, B'_{33}, can still be identified an irregular frequency at approximately 8.6. However it is clearly observed, that it might be recommended a smaller frequency interval for the numerical evaluation for higher speeds in the vicinity of the referenced non-dimensional encounter frequencies.

Although this detailed approach was thought, for the time being, out of the scope of this investigation, since for the case of a forward speed of 15.433 m/s that is not physically achieved by the patrol boat. Nevertheless, it should be noted that the reason behind these numerical evaluations, i.e. for 3.090 and 15.433 m/s, was to observe if there were clear discrepancies in the global behaviour of the hydrodynamic coefficients curves.

The pitch related hydrodynamic coefficients exhibit clear signs of convergence for values greater than 5.0 for non-dimensional encounter frequencies. The speed dependence can be seen to be more relevant for the lower frequencies. These are three identifiable irregular frequencies for the damping coefficient B'_{55}, the first approximately equal to 5.3, which corresponds to the same frequency identified in previously mentioned hydrodynamic coefficients, an the other two at about 7.1 and 8.8. In summary it can be said that the non-dimensional added mass hydrodynamic coefficients appear to be less susceptible to the presence of the irregular frequencies than the damping coefficients. A more detailed discussion of the problem of irregular frequencies can be found in the investigation produced by Du et al., [97], on mathematical models of speed and frequency dependence in seakeeping assessment. This study was carried out on a series 60 hull form, showing that the irregular frequencies presence depend on hull shape and forward speed. In 1950, John, [114] already addressed that irregular frequencies arise when the solution of the integral equation is not unique, leading to the instability of the numerical problem.

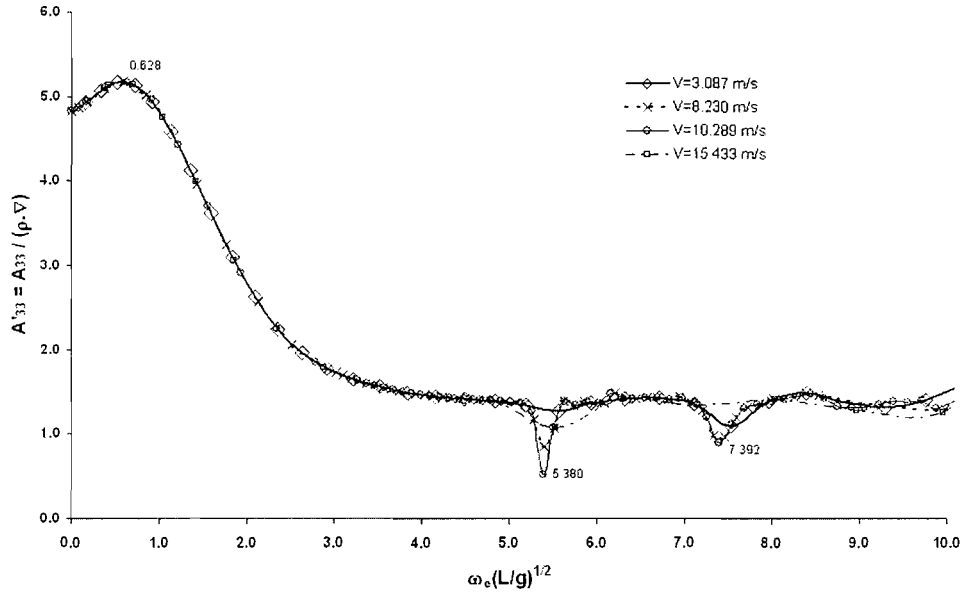

(a)

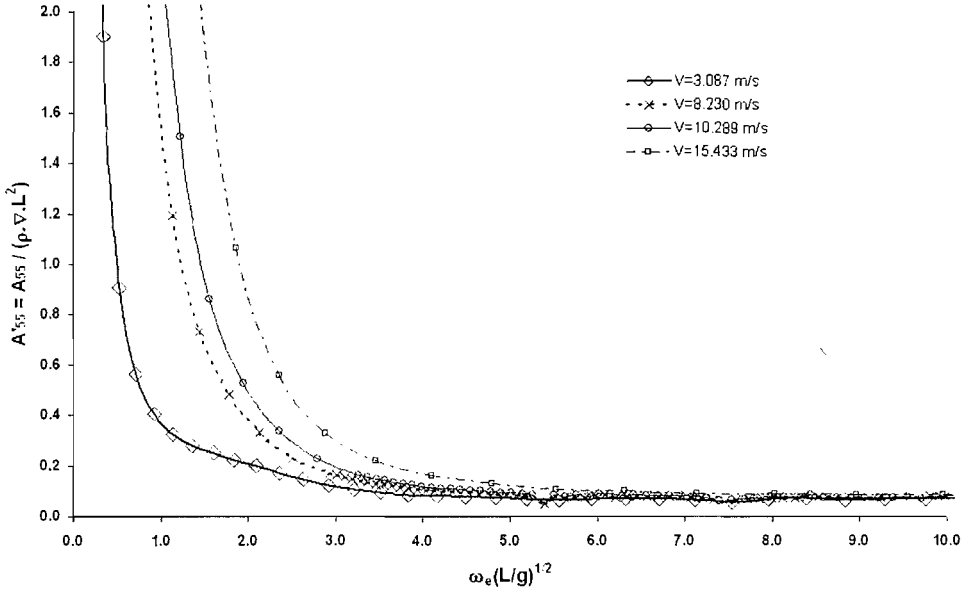

(b)

Figure 9.2: Symmetric Hydrodynamic Non-dimensional Added Mass Coefficients

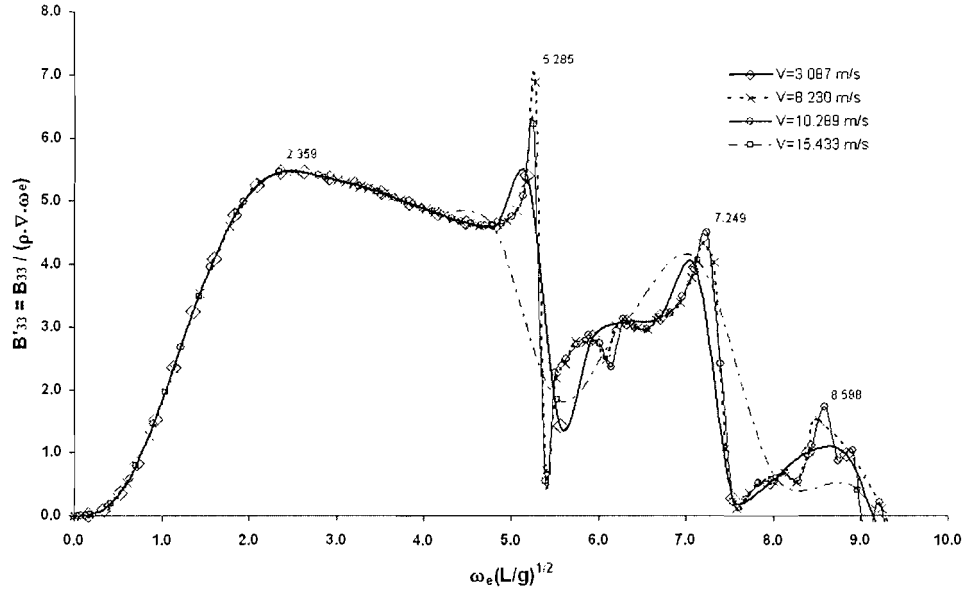

(a)

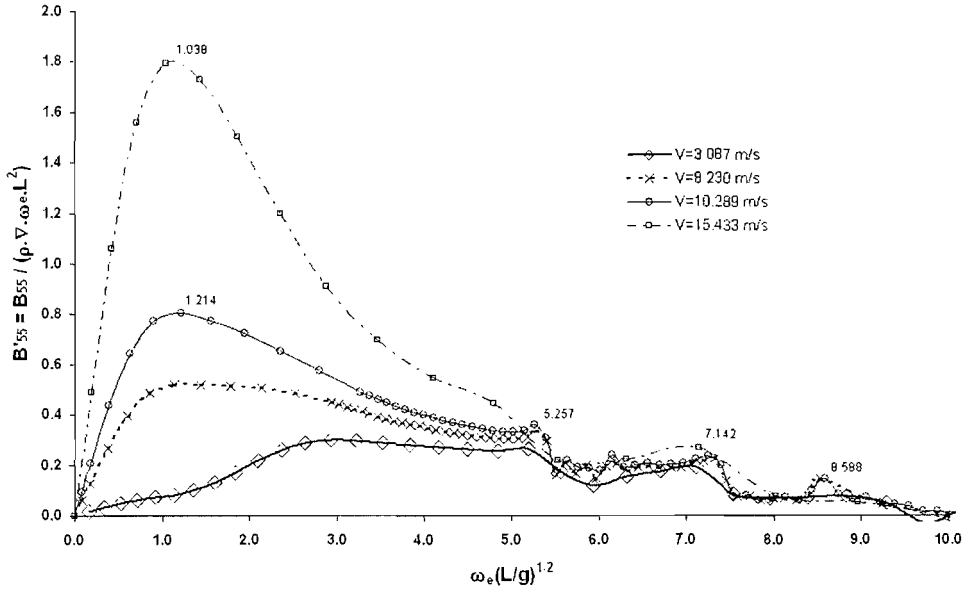

(c)

Figure 9.3: Symmetric Hydrodynamic Non-dimensional Damping Coefficients

9.2.4 Wave Exciting Loads

Results for wave exciting heave forces and pitch moments, respectively $|F_3'|$ and $|F_5'|$, are also presented in figures 9.4a and 9.4b, respectively. For the numerical evaluation of the rigid body responses, the hull is assumed to be travelling in sinusoidal waves, with unit amplitude, at three different headings; 180, 135 and 90 degrees, although only head waves were assumed for the estimation of the wave exciting forces at 3.090 and 15.433 m/s. In order to compare the broadest range of speeds only head waves are used in this document to illustrate the speed dependence of the wave exciting forces. In the frequency domain adopted the variations of the wave exciting forces due to speed dependence are clearly illustrated. Again its noticed, what is to be understood, the presence of a set of irregular frequencies represented by oscillations in the forces for values greater than 4.8, in particular the regions $4.8< \omega_e' <5.8$ and $7.1< \omega_e' <7.5$ for the non-dimensional heave exciting forces.

Again it is noted, that another irregularity is observed for a value of 5.4 for the non-dimensional encounter frequency, identifiable for the pitch wave exciting moment, $|F_5'|$. This curve at the highest speed of advance seems to better behaved, regarding smoothness; however, it should be emphasized that the number of calculated frequencies is far less than the other non-dimensional exciting forces. In other words, the frequency interval is larger, leading possibly to the aliasing of some irregularities. However, for the full scale trials speeds, 8.230 and 10.289 m/s, there are some relevant oscillations on the vicinity of the non-dimensional frequencies 7.4 and 8.5, figure 9.4b.

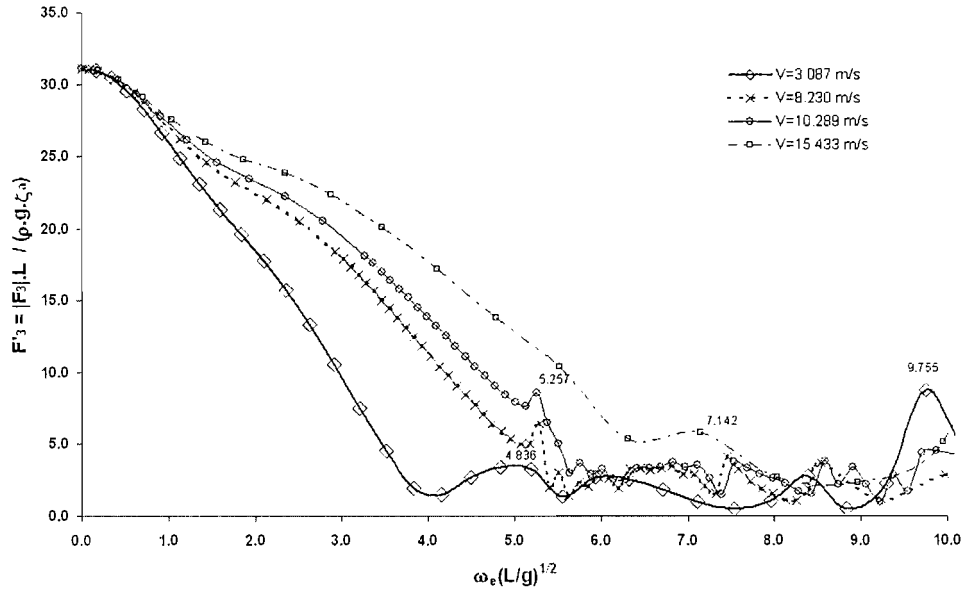

(a)

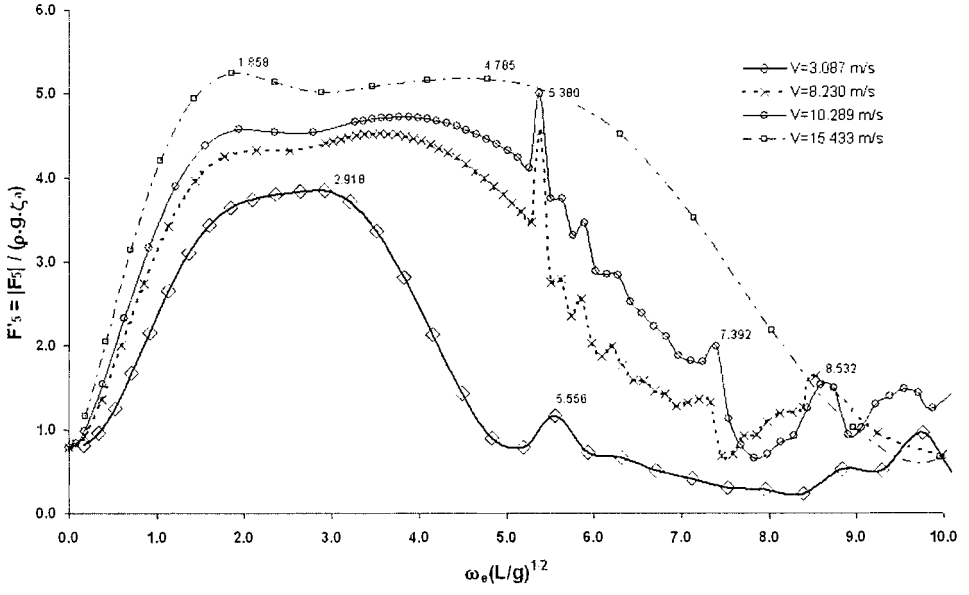

(c)

Figure 9.4: Symmetric Hydrodynamic Non-dimensional Wave Exciting Forces

Chapter 10

Full Scale Trials

10.1 Overview

This chapter describes a comparative study between full scale measurements aboard class *ARGOS* Fast Patrol Boat *NRP Dragao*, and results from a numerical prediction algorithm developed at the Unit of Marine Technology and Engineering. During trials, several runs were conducted at different headings for service and maximum speed. During each run, sea surface elevation, ship motions, and local strains were recorded. This chapter intends to describe the trials' planning, instrumentation procedures, measurements and post processing of the raw data collected.

10.2 Seakeeping Trials Description

During November 2000 sea trials were conducted on board of *NRP Dragao* along the coast line in the areas of South and South-West of Portugal.

Trials' planning included the following operational conditions:

1. Ship in head seas at near zero forward speed
2. Largest possible number of heading angles at service speed
3. Largest possible number of heading angles at maximum allowable speed

The reason for saying forward speed close to zero, in condition 1, relies on the fact that the patrol boat should maintain directional stability in order to properly obtain [1] data from the wave height metre radar installed at the ship's bow and to compare it to a wave buoy readings.

[1] avoiding the reading interference of radiated waves arising from heave motion

Each trial run was conducted with a duration of approximately 30 minutes. This recording time was chosen in order to guarantee that the raw signal included more than 100 cycles, which allows some confidence in statistics, Lloyd (1998), [115].

Headings had a spacing of about 45°, i.e. 180, 135, 90, 45 and 0 degrees. Velocities were chosen according to current operational service speed and maximum possible speed, respectively 16 and 20 knots. This was agreed with the patrol boat main officer due to safety reasons, facing the conditions encountered.

During trials, the patrol boat experienced sea states from 3 to 5, according to the scale adopted by the World Meteorological Organisation.

10.3 Instrumentation for Rigid Body Motions

As already known, the rigid body response of a ship acts like a six degree of freedom system 10.1; however, due to the lack of free channels to record all of them, it was necessary to choose only the most characteristic ship motions which are known to be roll, pitch and heave for conventional vessels.

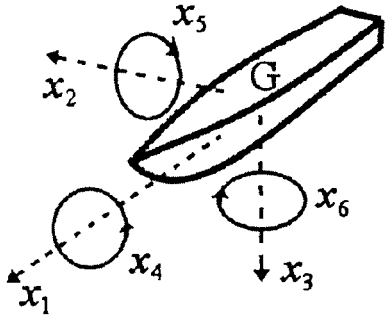

Figure 10.1: Six Degree of Freedom Ship

As said before, a wave height meter was installed at the ship's bow, figure 10.2. The system is based on a microwave radar which beams directly downward into the sea surface. The reflected microwaves suffer a frequency change due to the motion of the sea surface. With the Doppler data, the signal processor unit calculates the wave vertical velocity and integrates to obtain the wave height measurement.

To this end, the latter system only gives information about relative values. To collect absolute values it includes a vertical accelerometer, with a stabilised damped platform, which calculates ship displacement after a double integration by the signal processor unit.

Therefore, to obtain absolute values for wave height ship displacement is subtracted to the relative wave elevation. The former data is then used to calculate the significant

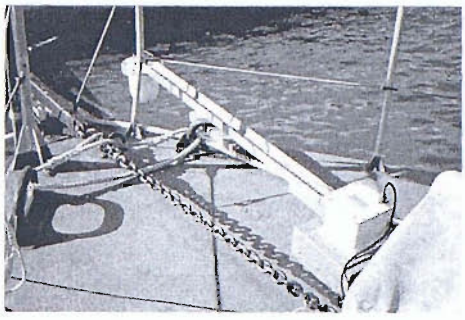

Figure 10.2: Wave Height Meter

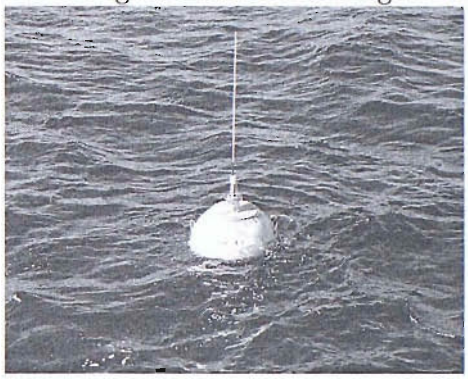

Figure 10.3: Directional Wave Buoy

wave height, SWH, and mean period, T_m. The data is treated for a 6 and 20 minute running average, respectively.

The wave height metre signal processor unit was configured to its maximum resolution, that is 0.1 seconds of sampling interval. The following signals can be collected independently.

Transducer Type	Motion	Reference Name	Units
Accelerometer	Pitch/Heave	SD	$[m]$
Microwave Radar	Relative Wave Elevation	RWH	$[m]$
Digital Integration	Absolute Wave Elevation	WH	$[m]$
Digital Integration	Significant Wave Height	SWH	$[m]$
Digital Integration	Average Wave Period	AWP	$[m]$

Table 10.1: Signals in Wave Height Meter

In practice, finding the exact positioning of the ship's gravity centre has proven to be a difficult task. Therefore, it is most likely that transducers will be positioned in a relatively arbitrary manner. In order to obtain the correction for the readings obtained, away from the ship's centre of gravity in a position with coordinates (x_{B1},x_{B2},x_{B3}), it is necessary to consider the contribution of the various components of the rigid body motion, which relate each other by the system of differential equations 10.1, 10.2 and

10.3.

$$\ddot{x}_1 = \ddot{s}_1 + x_{B2}\ddot{x}_6 - x_{B3}\ddot{x}_5 \qquad m/sec^2 \qquad (10.1)$$

$$\ddot{x}_2 = \ddot{s}_2 + x_{B3}\ddot{x}_4 - x_{B1}\ddot{x}_6 \qquad m/sec^2 \qquad (10.2)$$

$$\ddot{x}_3 = \ddot{s}_3 - x_{B2}\ddot{x}_4 + x_{B1}\ddot{x}_5 \qquad m/sec^2 \qquad (10.3)$$

As well as ship motion transducers, both accelerometers and inclinometers were used, and their positioning is shown in figure 10.5.

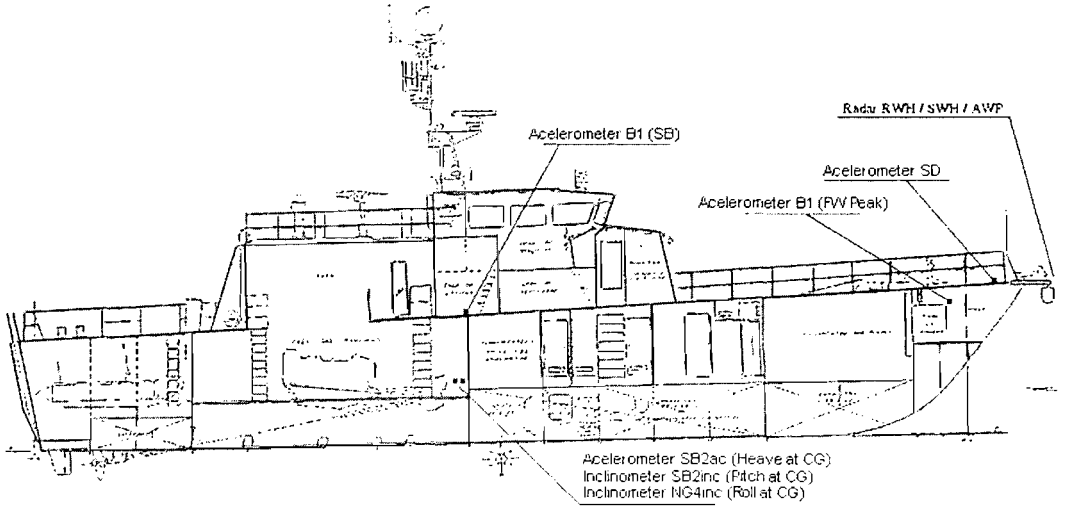

Figure 10.4: Positioning of Motion Transducers Aboard NRP Dragao

The reference names are defined in table 10.2, as well as their measuring units.

Transducer Type	Motion	Reference Name	Units
Accelerometer	Heave	SB2ac	$[m/s^2]$
Inclinometer	Pitch	SB2inc	$[degrees]$
Inclinometer	Roll	SB1inc	$[degrees]$
Accelerometer	Roll/Heave	B1EB	$[m/s^2]$

Table 10.2: Rigid Body Motion Transducers

To fulfil all the tasks included in the instrumentation process, a period of preparation was needed to install the equipment on board, where some of the difficulties encountered are listed below:

- Transducers' positioning and fixation, in order to resist shock, vibration and water;
- Finding solutions for cable passage into water tight compartments;
- Avoiding electromagnetic interference;

- Conditioning of the signal acquisition equipment;
- Reducing, as most as possible, interference with normal crew operation.

All sensors used were protected by watertight steel boxes, figure 10.5, and the power supply unit gave them stabilised and regulated voltage. The readings were obtained, in most cases, from low voltage oscillation, about 5 *Volts*; nonetheless, some cases are from current variations, about 20 *mA*. The signals were then conditioned by a signal processing unit from *National Instruments*. As an example, figure 10.5 shows a detail

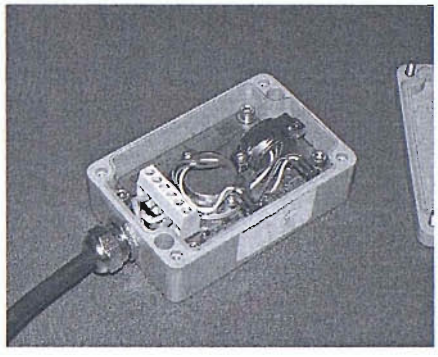

Figure 10.5: Heave and Pitch Transducers Sensor Box

of the pitch inclinometer and heave accelerometer in the same sensor box.

10.4 Instrumentation for Flexible Body Motions

The procedures to obtain flexible body motions are often more arduous than those for the rigid body. If the problem concerns only vibration responses, high frequency accelerometers can easily be installed; however, if the intention is to measure strains, and consequently stresses, the strain gauge installation process in ships is known to be a difficult process. In a few words, it demands some experience in this area. Problems often arise from the fact that the gauges are considerably exposed to the environment, in particular thermic influence, humidity and electromagnetic interference.

Thus, to measure the flexible structure response, 120 ohm strain gauges from *MicroMeasurements* were used in half bridge Wheatstone configuration. Although not exactly proven, it was assumed that principal directions were known due to the limited number of data recording channels; therefore, one of the strain gauges was used as a passive one, just for compensation. The cables connecting the gauges to the signal conditioning unit were shielded and, whenever possible, grounded to the hull.

Due to the relatively small dimensions of the fast patrol boat, there were not too many places where it was possible to avoid the aggressive environment, in particular the high temperatures found in the engine room and the humidity in condensation level in the

forward peak. Hence, surface preparation was a critical process. To minimise damage, after the bonding the gauges were covered with a special neoprene cover.

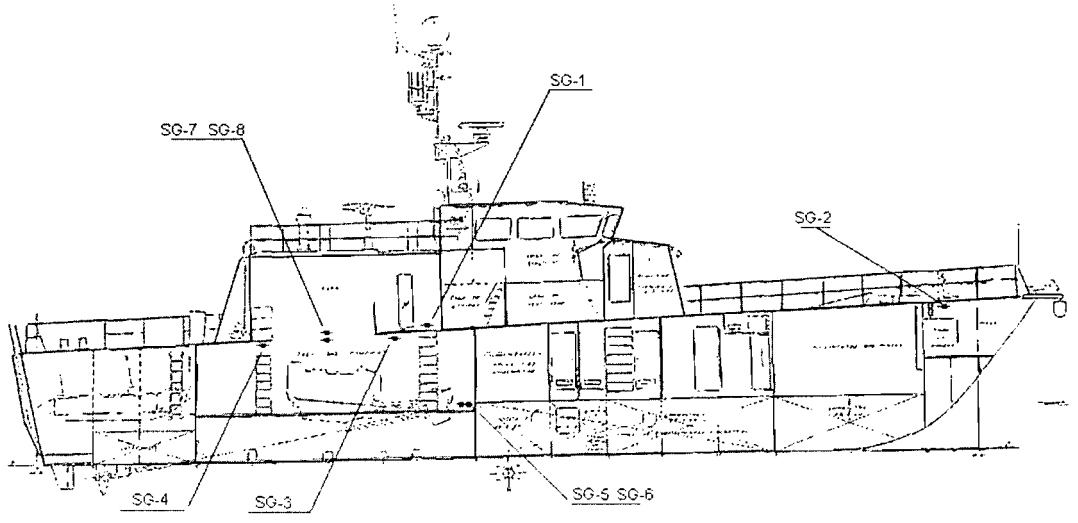

Figure 10.6: Strain Gauges Positioning Aboard NRP Dragao

10.5 Signal Acquisition and Processing

It is known that the seaway which excites the motion of ships can be described as a spectral density function. Therefore, the ship response can be predicted by means of a transfer function that relates the former excitation function with the actual response of the ship in a seaway.

Having this in consideration, the strategy for signal processing is to determine the two spectral density functions, i.e. response and excitation, and define, for each ship motion, like heave, pitch and roll, the corresponding transfer functions.

The software used is based on an object-orientated programming language, developed in *Labview*, which allows tasks like sensor reading and calibration and definition of various data acquisition parameters.

The acquisition system collected data at a 30 Hz sampling frequency. The signal processing was based in a frequency domain spectral analysis for each 30 minute run.

To validate the frequency domain analysis, time domain statistical parameters were calculated. Based on Lloyd's work [115] the mean value of the surface depression is given by,

$$\bar{\zeta} = \sum_{n=1}^{N} \frac{\zeta_n}{N} \quad m \tag{10.4}$$

the variance by,

$$m_0 = \sum_{n=1}^{N} \frac{(\zeta_n - \bar{\zeta})^2}{N} \qquad m^2 \tag{10.5}$$

and the standard deviation relative to mean surface depression, i.e. root mean square (RMS),

$$\sigma_0 = \sqrt{m_0} \qquad m. \tag{10.6}$$

Since, the Fourier series can be expressed in the following form:

$$\zeta(t) = \bar{\zeta} + \sum_{n=1}^{N} \zeta_{n0} \cos(\omega_n t + \epsilon_n) \qquad m \tag{10.7}$$

The spectral ordinates are those determined by dividing the squared ζ_{n0} coefficients by the frequency interval δw,

$$S_\zeta(\omega_n) = \frac{\zeta_{n0}^2}{2\delta\omega} \qquad m^2/(rad/sec) \tag{10.8}$$

Therefore, the variance in frequency domain is given by

$$m_0 = \int_0^\infty S_\zeta(\omega) d\omega = \sum_{n=1}^{\infty} S_\zeta(\omega_n)\delta\omega \qquad m/sec \tag{10.9}$$

In order to calculate the mean periods it was necessary to calculate the spectral moments of order one, two and four, which are given by equation 10.10 in the general form

$$m_n = \int_0^\infty \omega^n S_\zeta(\omega) d\omega \qquad n = 1, 2, 4 \qquad m^2/sec^n \tag{10.10}$$

Spectral moments were calculated using the trapezoidal rule and validated with statistical parameters from the raw data. Therefore, the mean period for the time history is,

$$\bar{T} = \frac{2.\pi.m_0}{m_1} \qquad sec \tag{10.11}$$

The mean period of the peaks,

$$T_p = 2.\pi\sqrt{\frac{m_2}{m_4}} \qquad sec \tag{10.12}$$

and the mean zero crossing period,

$$T_z = 2.\pi\sqrt{\frac{m_0}{m_2}} \qquad sec \tag{10.13}$$

Equations 10.12 and 10.13 are valid if the surface depression has a normal distribution.

Knowing that the average of the highest one-third of all the wave heights represent the significant wave height, this can be expressed by

$$\bar{H}_{1/3} = 4.\sqrt{m_0} \qquad m \tag{10.14}$$

However, if one considers a correction that accounts for the *narrowness* of the spectral density curve, equation 10.14 becomes,

$$\bar{H}_{1/3} = 4.\sqrt{m_0}\sqrt{1 - \frac{\epsilon^2}{2}} \qquad m \tag{10.15}$$

where the bandwidth parameter ϵ, based on the work done by Cartwright and Longuet-Higgins, is given by equation 10.16,

$$\epsilon = \sqrt{1 - \frac{m_2^2}{m_0 m_4}} \tag{10.16}$$

For this particular study the domain of the analysis is based on the encounter frequency given by

$$\omega_e = \omega - \frac{\omega^2.U}{g}.\cos\mu \qquad rad/sec \tag{10.17}$$

The relation between acceleration and displacement spectral density functions is given by equation 10.18, i.e. representing the double integration in the frequency domain,

$$S_{\ddot{\zeta}}(\omega_n) = \omega_n^2.S_{\zeta}(\omega_n) \qquad (m^2/sec^4)/(rad/s) \tag{10.18}$$

Having the real time wave elevation and consequently the measured wave energy spectrum one can find the motion transfer functions for heave, pitch and roll using equations 10.19, 10.20 and 10.21 respectively,

$$\frac{x_{30}}{\zeta_0} = \sqrt{\frac{S_{x3}(\omega_e)}{S_{\zeta}(\omega_e)}} \tag{10.19}$$

$$\frac{x_{40}}{k.\zeta_0} = \sqrt{\frac{S_{x4}(\omega_e)}{S_{\zeta}(\omega_e)}} \tag{10.20}$$

$$\frac{x_{50}}{k.\zeta_0} = \sqrt{\frac{S_{x5}(\omega_e)}{S_{\zeta}(\omega_e)}} \tag{10.21}$$

The signals obtained were filtered using the *Butterworth* low-pass filter, of 8^{th} order with cutting frequencies ranging between 0.020 and 0.037 Hz. The last values were considered in order to avoid the *aliasing* effect and consequently increasing the resolution of the data filtered.

Filtering parameters were the same for each pair of excitation and response, maintaining this way equal phase relations.

In order to obtain the spectral density ordinates, a Fourier transform based algorithm was developed. This algorithm also allows periodogram smoothing using windows, or segments. The triangular, or also known *Bartlett* window was used. This approach is adopted based on the procedure adopted by Grant and Metcalfe (1995), [116].

10.6 Wave Height Meter Validation

Results are here presented comparing the records from the wave buoy of the Portuguese Hydrographic Institute, positioned near Sines coast line, with the data from the wave height meter installed at the ship's bow.

With the kind and professional collaboration of the crew, the patrol boat was positioned heading wind and waves as close as possible to the buoy. At this heading the helmsman tried to maintain a steady position to sea floor according to the precise military *GPS* data. It can be said that the directional stability was achieved with success during all the 20 minute readings. Figure 10.7 shows energy over a wider band of frequencies for

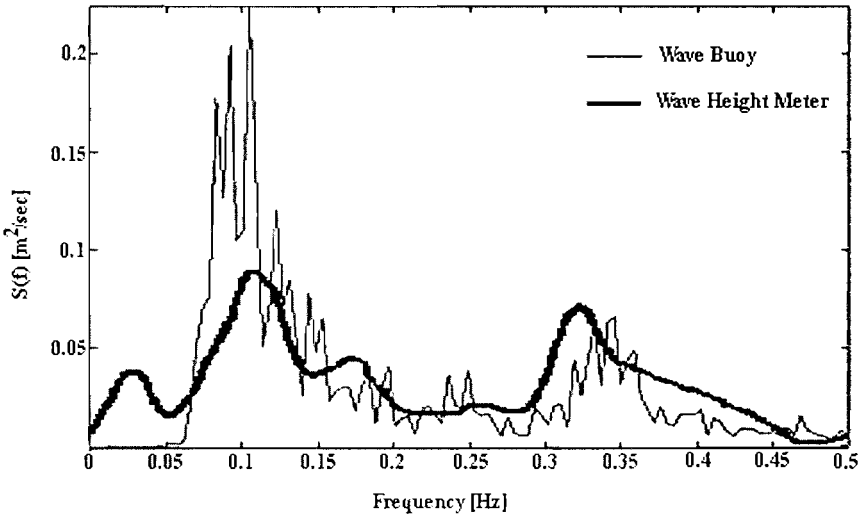

Figure 10.7: Wave Buoy vs Wave Height Meter

the wave height meter spectral density. Also clear is the identification of the two peaks at 0.12 and 0.32 Hz, that compare relatively well with the wave buoy readings.

The analysis of the wave height meter data is shown in figure 10.7.

In table 10.3 $H_{1/3}^{(1)}$, it ignores the bandwidth parameter, on the other side $H_{1/3}^{(2)}$ does not, which is more likely to represent the behaviour of the spectral density curve of figure 10.7.

units	$H_{1/3}^{(1)}$ (m)	$H_{1/3}^{(2)}$ (m)	T_m (sec)	T_z (sec)	T_p (sec)	T_o (sec)	F_o (Hz)
Wave Height	0.5136	0.3959	4.3673	3.7357	2.3797	6.8259	0.1465

Table 10.3: Radar readings at zero forward speed, heading 180 degrees

Quantities T_m, T_z, T_p and T_o represent, respectively, mean period, zero crossing period, peak period and modal period. Similarly, F_o represents the modal frequency.

According to the results provided by the Government Authority, results from the wave buoy are as follows. As figure 10.8 shows, significant wave height has an average value of

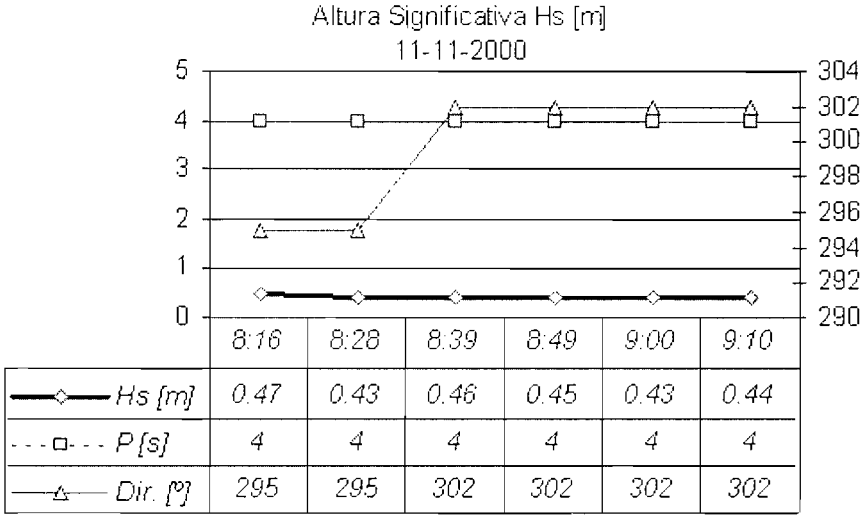

	8:16	8:28	8:39	8:49	9:00	9:10
Hs [m]	0.47	0.43	0.46	0.45	0.43	0.44
P [s]	4	4	4	4	4	4
Dir. [°]	295	295	302	302	302	302

Figure 10.8: Wave Buoy Data

0.45 meters, i.e. for the sampling interval from 8:16 to 9:10 hours, which stands between $H_{1/3}^{(1)}$ and $H_{1/3}^{(2)}$. The 4 second period recorded in the wave buoy compare relatively well with the 4.4 seconds processed in the wave height meter. With these results it can be said that the wave height meter system had a satisfactory behaviour. In the next chapter the processed results of these trials will be compared to the theoretical prediction of rigid body responses obtained by a unified hydroelastic analysis.

Chapter 11

Comparison of Measured Results with Theoretical Predictions

11.1 Rigid Body Response - Response Amplitude Operators

Transfer functions for comparison between full scale trial experiments, carried on board N.R.P. Dragao fast patrol boat, and numerical predictions for rigid body motions, evaluated by a unified hydroelastic analysis are illustrated in figures 11.1, 11.2, 11.3. Reasons regarding filtering procedures, and instrumentation setup, during data recording in the full scale trials did not allow to have the complete raw data for the entire frequency range for the transfer functions, in particular the lowest ones. But, by chance all the range of frequencies that were measurable, and considered to be reliable by the research team, included the characterization of the speed dependent resonant peaks, therefore, the non inclusion of the complete representation of the full scale measurement curves in the illustrations is explained. The theoretical predictions were obtained from the three dimensional model.

In the heave response amplitude operator in head waves, shown in figure 11.1a there is a considerable dynamic amplification for maximum trial speed of 10.289 m/s (F_n=0.66), in which the maximum value for heave motion reaches almost 2.4 times the wave amplitude at non-dimensional encounter frequency 2.389. There is not a clear agreement between numerical estimates and measured results, in which the difference in peak values is as great as 40%, and the same applies to the difference in the non-dimensional resonant frequencies. On the other hand, it seems that for a service speed of 8.230 m/s (F_n=0.53) the curves tend to compare better. Nevertheless there is a difference in frequencies around 14% and in maximum heave response amplitude operator about 25%.

In oblique waves, heading 135°, figure 11.1b, both theoretical and measured results illustrate resonant behaviour, but once again they do not compare relatively well in terms of response amplitudes, with 36% and 45% differences for speeds of 10.289 and 8.230 m/s respectively. To contrast with the previous set of results, the non-dimensional ressonant frequencies show a considerable better agreement in terms of frequency difference, with 1.8% and 0.7% of relative differences for 10.289 and 8.230 m/s of advance speeds, respectively. In the former figure, the identification of irregular frequencies in the theoretical results is clear at a value of 5.36 in both forward speeds.

In beam waves, figure 11.1c, and as expected, only measured results show speed dependent resonances in heave. It is interesting to note that there is a significant greater amplification at service speed, and lowest, compared to the 10.289 m/s. The reason for this seems to be associated with the hydrodynamic behaviour of the vessel at higher speeds in that particular sea state, at the time trials were conducted. Dynamic coupling could have been the principal explanation. Furthermore, studies should be adressed towards the evaluation of the directional wave spectrum that will possibly lead to the identification of some wave spreading that was not observed on board of the patrol boat, i.e. apart from the primary wave direction.

For pitch motion evaluation there is a discrepancy between numerical and measured results, figures 11.2. In head waves, figure 11.2a, the speed dependent resonance is much more notorious in the measured results than in the numerical predictions. The response magnitudes differ between maximum and service speeds, in about 110% for measured results and 11% in numerical predictions. As expected, for oblique waves the speed dependence is less acentuated; however, it still shows a 65% difference and 11% for measured and theorethical results respectively, figure 11.2b.

Finally, regarding roll motion transfer functions, figure 11.3, the magnification amplitude is far more considerable in the numerical predictions than the measurements for beam waves. For instance, figure 11.3b, the theoretically predicted amplitude for maximum speed appears as much as 2.5 times higher than measured results. It is worth noting that there are smaller peaks in the measured maximum speed response amplitude in oblique waves, figure 11.3a, that shows a 2.5% difference in relation to the one obtained in the theorethical calculations, which are smaller than the measured ones.

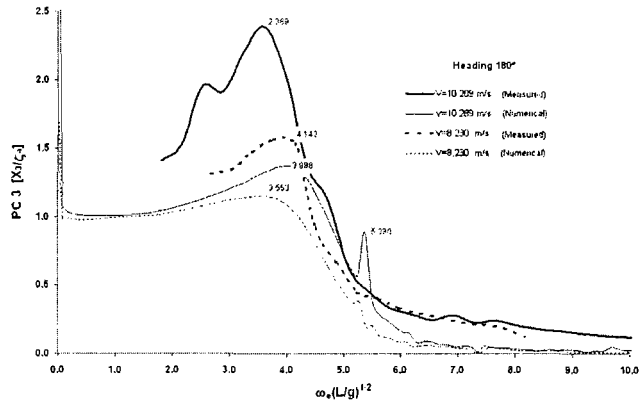

(a)

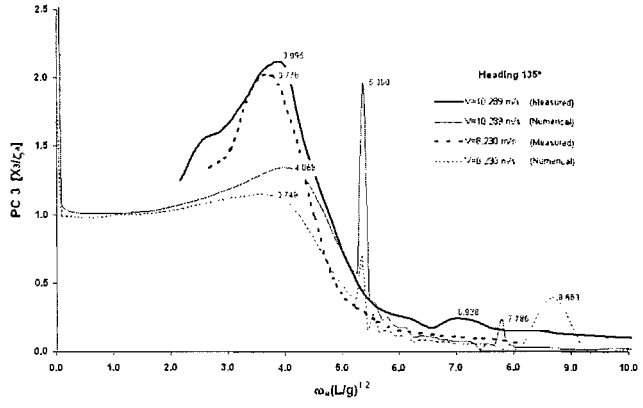

(b)

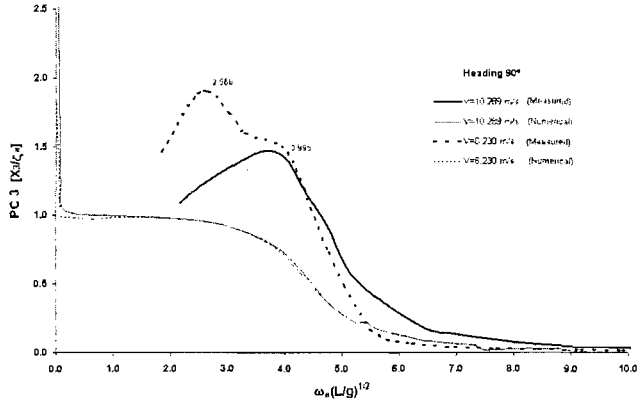

(c)

Figure 11.1: Heave Motion - Numerical Prediction vs Experimental Results

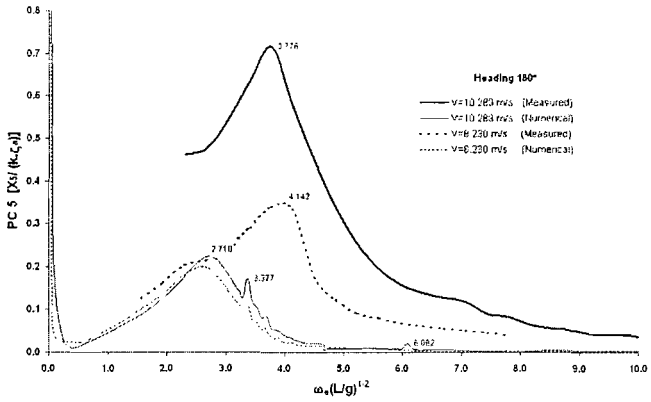

(a)

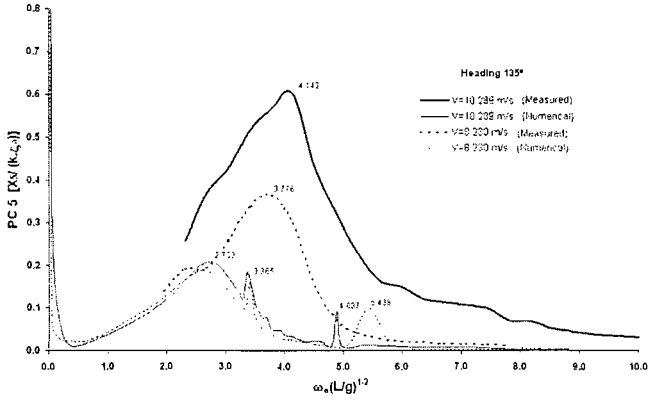

(b)

Figure 11.2: Pitch Motion - Numerical Prediction vs Experimental Results

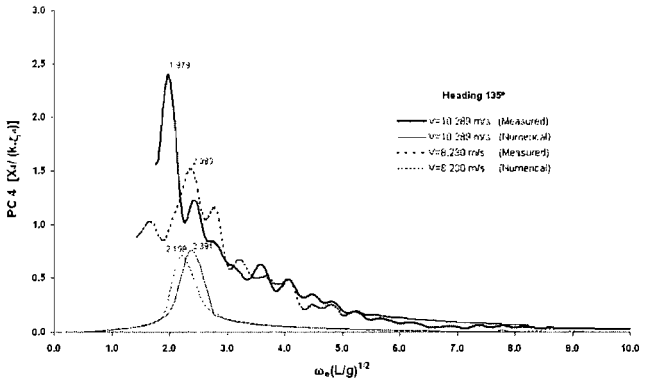

(a)

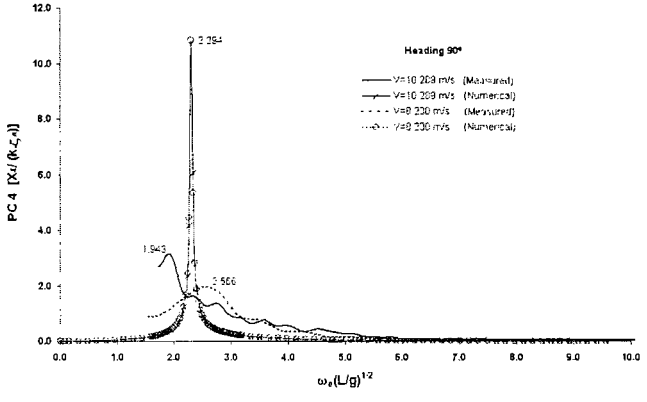

(b)

Figure 11.3: Roll Motion - Numerical Prediction vs Experimental Results

11.2 Flexible Body Responses

Solving the differential equation of motion 4.43, the principal coordinates for the flexible responses were calculated for all four velocities, 3.090, 8.230, 10.289 and 15.433 m/s, for head seas, and additional theoretical predictions for oblique waves, headings 135 and 90°, were obtained for service and maximum speeds, respectively 8.230 and 10.289 m/s. The flexible natural frequencies are relatively large and outside the range adopted in this investigation, that considered a limit value of 10 as the maximum non-dimensional encounter frequency ($\omega'_e = \omega_e(L/g)^{1/2}$). The first frequency of resonance due to FSI occurs at a non-dimensional encounter frequency of 111, with an equivalent wave length $\lambda = 0.023.L$ for head waves. That fact largely reduces the influence of the structural damping factors, due to the limited frequency domain here adopted.

Theoretical predictions are presented for the two-dimensional beam model idealization presented in chapter 7 and the three-dimensional plate model, referred as *model C* in the hull idealization adopted in chapters 8 and 9. For all the models; 2D-Beam, 3D-Beam and 3D-Plate numerical predictions are evaluated using three-dimensional potential flow analysis. The hull surface is idealized with 644 four cornered panels in which are applied

a singularity distribution (pulsating source) over the mean wetted surface area. This demonstrates the capacity, and versatility, of a three-dimensional hydroelasticity analysis on dealing with fluid-structure interaction on more simplified beam structural models, this type of approach as also already been taken by Price et al.(2002),[89].

The first three symmetrical principal coordinate amplitudes (2-, 3- and 4-node vertical) are plotted in figure 11.4 in order to compare the two- and three-dimensional, beam and plate models respectively, for three different headings.

For the two node vertical bending at an advance speed of 8.230 m/s, figure 11.4a, the two-dimensional (2D) beam model seems to be overestimated comparatively to the three-dimensional (3D) plate model. The differences in principal coordinate amplitudes reach as far as 41% in head waves at the resonance peaks (associated with rigid body motions), that differ to each other by approximatly 2.3%. Also, heading dependence shows to be more accentuated for the 2D-Beam model idealisatíon than for the 3D-Plate model. Peaks occurring in the vicinity of $\omega_e' \approx 8$ for the 2D-Beam model are not numerically predicted by the 3D-Plate model. On the other hand, in figure 11.4b, for maximum trial speed, there is a much better agreement in the curves relating to both models. However, in spite of a noticable difference in non-dimensional encounter frequencies representing the resonance peak for beam waves, the amplitudes of principal coordinates seem to be both of the same order of magnitude.

As expected, the amplitude is reduced for the three-node vertical bending principal coordinates, figures 11.4c and 11.4d, but it seems that the non-dimensional frequencies related to peak positioning are almost the same for both models, in particular $\omega_e' = 4.1290$ for 8.230 m/s and $\omega_e' = 4.3177$ for 10.289 m/s. Although principal coordinate amplitudes for the 2D-Beam model are in average 50% greater than the ones estimated for the 3D-Plate model. As previously demonstrated for the two-node vertical bending, heading dependence is not so significant when changing from 180 to 135 degrees. Again the 2D-Beam model predicts, for both advance speeds, a peak in the neighbourhood of $\omega_e' \approx 8$.

In figures 11.4e and 11.4f, representing the principal coordinate amplitudes for the 4-node vertical bending, the 3D-Plate model largely predicts reduced values against some overestimates by the 2D-Beam model, that demonstrates that there might be a possible numerical instability for frequencies grater than $\omega_e' \approx 5$. These latter figures show some indications that the three-dimensional plate model seems to be more suitable for the theoretical prediction of the fluid structure interaction, i.e. regarding the predicted principal coordinate amplitude reduction as a function of the increase of the mode shape index.

For both service and maximum speed achieved in full scale trials, respectively 8.230 m/s (F_n=0.53) and 10.289 m/s (F_n=0.66), a more detailed observation on heading angle dependence of the first three symmetrical principal coordinates amplitudes is illustrated

in figures 11.5 and 11.6. For the symmetric modes presented in this investigation it can be seen that the principal coordinates have their maximum amplitude value, disregarding irregular frequencies, always for head sea conditions. Overall, it can be seen that comparing headings of 180 and 135 degrees the 3D-Plate model predictions are closer than the case of the 2D-Beam model. Although, they decrease considerably towards beam waves. Increasing mode shape index, or in other words its complexity, the heading dependence increases progressively for the 3D-Plate model, but the same can not be said to the 2D-Beam model at F_n=0.66, in particular observing the numerical results presented in figure 11.6. Nevertheless, the heading dependence follows the same trend for both advance speeds for the 3D-Plate model.

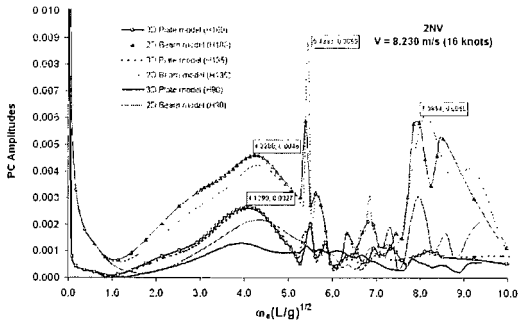

(a) 2-node vertical bending mode at V=8.230 m/s

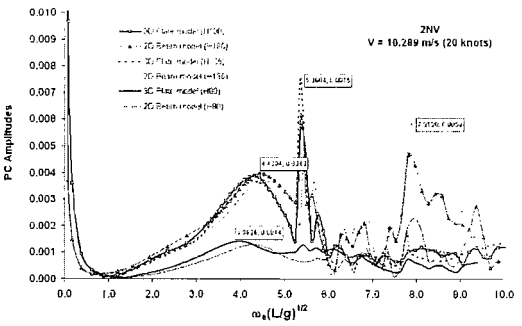

(b) 2-node vertical bending mode at V=10.289 m/s

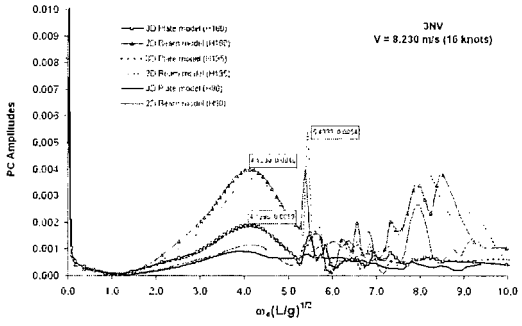

(c) 3-node vertical bending mode at V=8.230 m/s

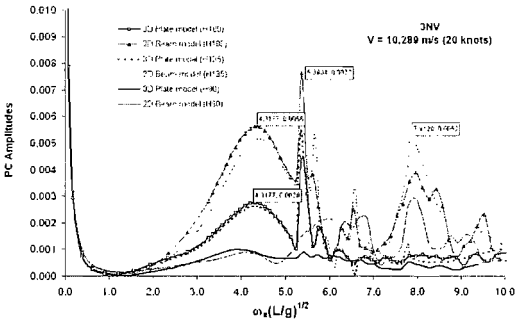

(d) 3-node vertical bending mode at V=10.289 m/s

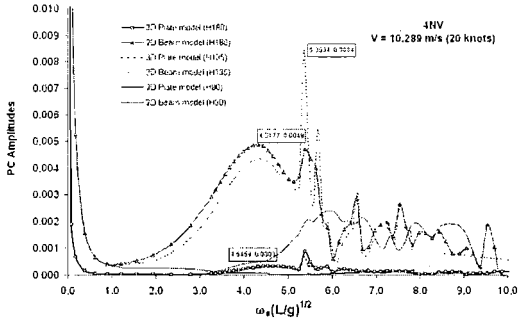

(e) 4-node vertical bending mode at V=10.289 m/s

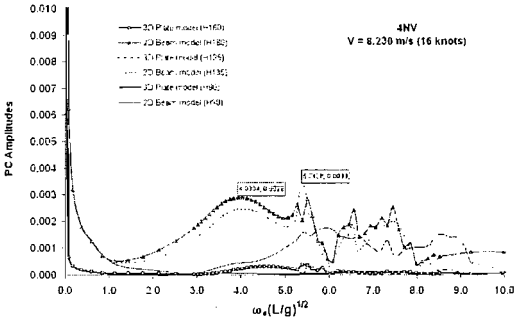

(f) 4-node vertical bending mode at V=8.230 m/s

Figure 11.4: Symmetrical Principal Coordinates Amplitudes 2D-Beam vs 3D-Plate

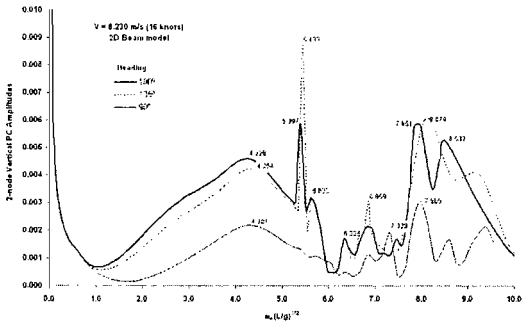

(a) r=2: Beam 2-node vertical bending mode

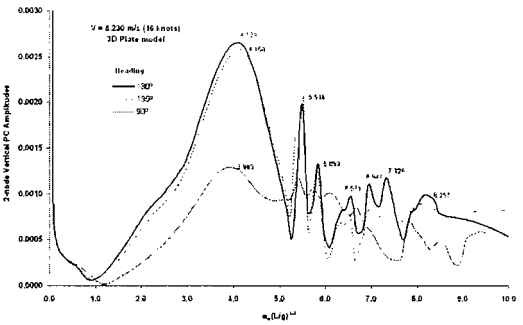

(b) r=8: Plate 2-node vertical bending mode

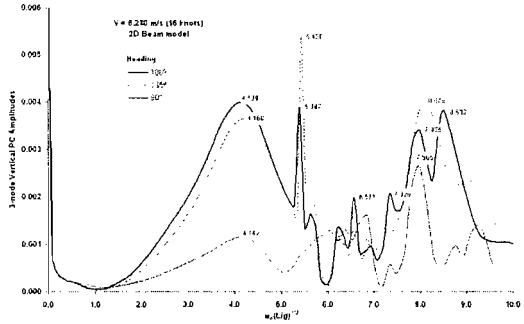

(c) r=3: Beam 3-node vertical bending mode

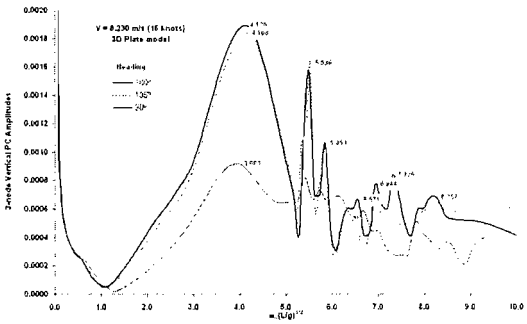

(d) r=12: Plate 3-node vertical bending mode

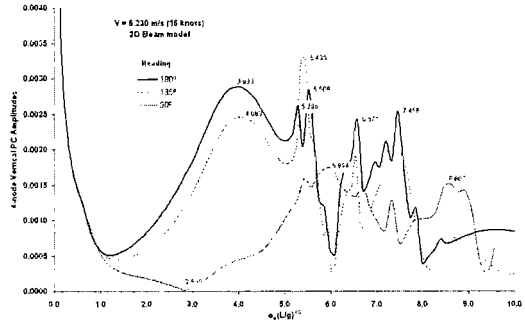

(e) r=4: Beam 4-node vertical bending mode

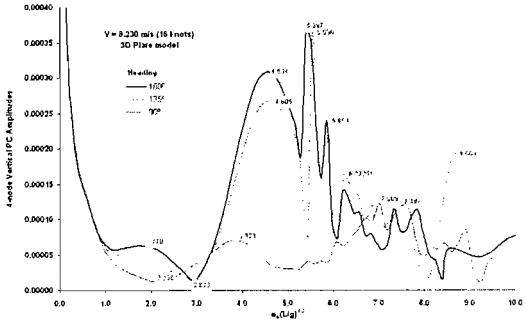

(f) r=14: Plate 4-node vertical bending mode

Figure 11.5: Principal Coordinates Amplitudes for F_n=0.53

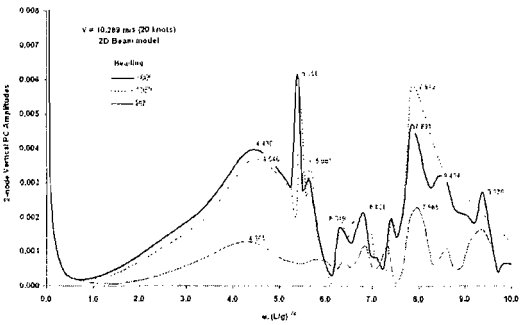

(a) r=2: Beam 2-node vertical bending mode

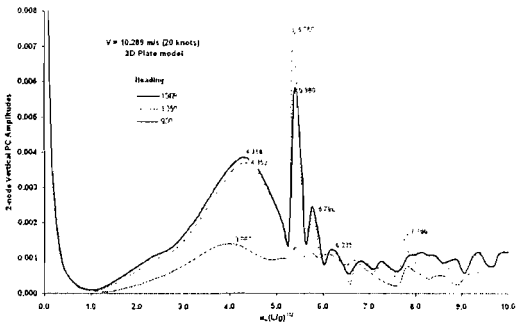

(b) r=8: Plate 2-node vertical bending mode

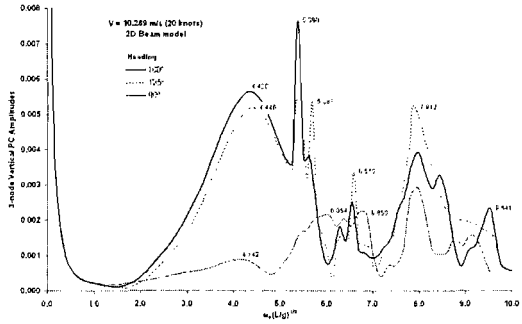

(c) r=3: Beam 3-node vertical bending mode

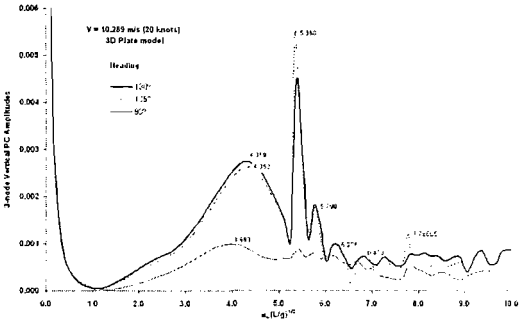

(d) r=12: Plate 3-node vertical bending mode

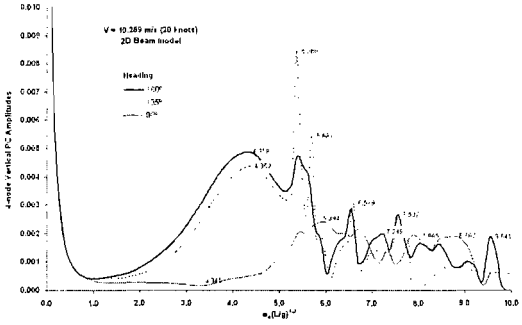

(e) r=4: Beam 4-node vertical bending mode

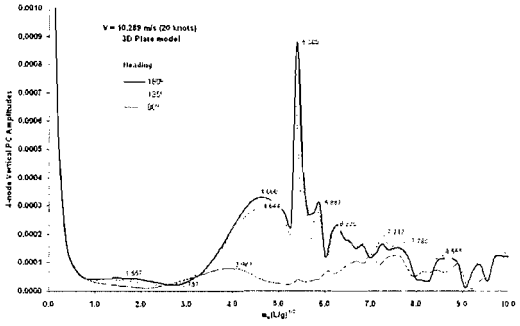

(f) r=14: Plate 4-node vertical bending mode

Figure 11.6: Principal Coordinates Amplitudes for F_n=0.66

Chapter 12

Conclusions

12.1 Overview

In this investigation, a general three-dimensional hydroelastic analysis has been applied to characterize the fluid structure interaction phenomena of a monohull, fast patrol boat made of fibre reinforced plastic, travelling in regular waves.

The research presented is divided in six distinct phases;

The **first** one gives an overall interpretation of the particular discipline of hydroelasticity, by means of a literature review, followed by the formulation of the theoretical problem combining structural dynamics with potential flow hydrodynamics. The background research and presentation of the mathematical theories are presented in the chapters 2, 3 and 4.

A **second** phase, and probably the most time consuming, presents all the steps thought to be necessary for the evaluation of the dry hull modal characterization. These steps include model idealisation and three-dimensional geometry validation, in terms of hydrostatic characterization and structural components distribution. Three different models were studied: model A, B, and C, in which the order follows the increasing detail regarding particular emphasis made to the docking space that occupies the aft body and cross-section dissimilitudes in the chine area of the underwater hull. The potential for using the most simplified wetted hull shape was investigated, although the choice finally fell in the more detailed model C, that predictably was the only one that satisfied all loading conditions, and respective hydrostatic characteristics, that actually are described in the intact stability data of the vessel.

Evaluation of mechanical properties of a considerable number of different laminates, that constitute the global structure of this patrol boat, was made using methodologies based in solid mechanics applied to composite structures. An equivalent two-dimensional

non-uniform hull beam idealization was also prepared in order to compare modal characteristics with a far more complex three-dimensional finite element model.

In the two-dimensional dry hull analysis (Beam model), data presented for the hull girder section is evaluated from the most detailed *Model C* divided into 23 sections. The Prohl-Myklestad method was the sequence of calculations adopted to estimate the flexible response. Corrections made for shear deflections were used. Vertical positioning of the shear centres for different sections were estimated, especially in order to correctly characterize the large deck opening present over the main engine room. In this preliminary investigation results were presented for the first four symmetrical flexible mode shapes. Results obtained by mode summation and numerical integration (still water longitudinal strength) analyses compare relatively well; however, it is possible that using two more symmetric mode shapes could lead to a relatively better convergence of values in the shear force and bending moment diagrams. A three-dimensional beam model, with also 23 beam elements, was generated using *ANSYS*. *In vacuo* modal characteristics were collected and comparisons were made, first towards the more rudimentary analytical approach previously described, and finally with the more complex three-dimensional model.

In the three-dimensional dry hull analysis all structural elements were referenced due to the full set of structural drawings made available for this research. In the generation of the finite element model a special effort was made trying to avoid, as much as possible, the *inclusion* of stiffeners' effectiveness in equivalent thickness shell elements. The idea behind this choice was to have a model that, in future working developments, would allow detailed local finite element analysis for areas considered to be of critical interest.

The use of lumped masses was also adopted to model masses, considered to be significant like the twin main propulsion engines and some significant auxiliary machinery like for instance generators. Structural pillars in the crew living compartments were accounted in the analysis. The effect of including the elements previously mentioned was studied in several alternative trial runs and their importance is considerable in the determination of the hull natural frequencies.

Results have shown some discrepancies relating non-dimensional natural frequencies of all the models, in which only the 3-node vertical bending mode seems to be in closer agreement in all the three models, i.e. 3D-Plate, 3D-Beam and 2D-Beam. In general sense, results for the 2D-Beam models compare relatively well until the third symmetric bending mode, and that was the reason for only using this more rudimentary, and faster to evaluate, model in the wet hull analysis. However, non-dimensional generalised masses demonstrate a slight difference in value for the 3-node symmetrical vertical natural frequency. Results for the three-dimensional plate model demonstrate consistently that the structure appears to be more rigid resulting in higher natural frequencies, possibly showing the true difficulty of evaluating precise structural data for a two-dimensional

beam idealization. Furthermore, the approach adopted in terms of using larger size finite elements to define the superstructure was not the correct choice. An extra panel stiffness could arise from that fact leading to limitations in accounting for the shear lag effect. A more precise convergence study of mesh refinement should be made to produce a more accurate model to compare with the two-dimensional case. Results of the longitudinal modal internal actions are presented for the three dimensional model, once again reflecting the importance of the large deck opening over the main engine room area.

A **third** phase, in which full scale trials were run on board the patrol boat at two distinct speeds, one at service speed and another at maximum possible speed at the time of the trials' conduction. Due to real-time wave height recordings and instrumentation measurements of ship motions, it was possible to present several transfer functions to be later compared to theoretical predictions. This phase involved significant preparation due to the well known difficulties of on board instrumentation. Sea state validation, comparing wave buoy data with the on board wave height meter, is also presented. Along with these trials, strain measurements were obtained, although difficulties have arisen because of temperature influence in most of the gauge readings obtained in the so important engine room ceiling, that altered the calibration values.

A **fourth** phase, where the actual wet hull analysis is evaluated by means of a computer code based on three-dimensional potential flow analysis, that uses singularity distributions, as pulsating sources over quadrilateral panels, numerically predicting relevant functions needed to determine generalised wave exciting forces and hydrodynamic coefficients due to regular waves incidence. Several trial runs were conducted to produce sufficient small frequency intervals in resonance zones, considered to be of interest for the present investigation. However, fore a more extended study in this issue would have been more accurate to produce also a convergence study in terms of elementary wet panel size. This could be made in terms of linear interpolation of coordinates and degrees of freedom without changing dry hull finite element. Nevertheless, with some additional work, the later finite element mesh could also be refined, if an overall analysis is to be produced.

A **fifth** phase illustrates comparisons between rigid body responses numerically predicted with measured results. Hydrodynamic coefficients were estimated for four distinct speeds, F_n=0.20, F_n=0.53, F_n=0.66 and F_n=0.99, in order to identify numerical instabilities. At this stage of the investigation, principal coordinate amplitudes are presented only for 2- 3- and 4-node symmetric vertical modes, at two different speeds, F_n=0.53 and F_n=0.66, and three different headings, 180, 135 and 90 degrees. It is shown that the non-dimensional heave added mass and heave damping coefficients seem to be speed independent for lower encounter frequencies and slightly independent for higher encounter frequencies. The non-dimensional pitch added mass and pitch damping coefficients show

a more relevant speed dependency for the lower frequencies. Irregular frequencies are illustrated in the sharp variations in all the results, in particular for values of $\omega'_e > 5$.

In the determination of the heave response amplitude operators, in head waves, numerical predictions underestimate the dynamic amplification of the resonance peaks. There is not clear agreement between numerical estimates and measured results for the non-dimensional frequencies but comparisons tend to improve for lower speeds of advance. In oblique waves, heading 135°, theoretical and measured results do not relate satisfactory in terms of response amplitude, observed in particular at the resonance vicinity. However, the non-dimensional resonant frequencies show a considerable better agreement with less than 2% of relative difference. For beam waves, and as expected, only measured results show speed dependent resonances in heave, in which dynamic coupling could have been the principal explanation. Again, for numerical predictions of pitch motion there is a discrepancy between numerical and measured results, and in particular for head waves the speed dependent resonance is much more significant for the measured results than the numerical predictions. Finally, regarding roll motion transfer functions. The magnification amplitude is far more considerable in the numerical predictions than the full scale measurements in beam seas, probably due to the inherent dispersion induced by irregular seas. The measured non-dimensional resonance frequency shows on average, 2.5% difference in relation to the one obtained in the theorethical calculations. The reasons for the observed discrepancies between measured and numerical three dimensional predictions can be attributed to the unsuitability of the pulsating source formulation to these relatively high speeds ($F_n = 0.53$ and 0.66) and the idealisation of the complex chine hull form. In the case of roll motion, the inaccuracy of potential flow damping is the main reason for the discrepancies.

And finally in the **sixth** phase, results of the principal coordinates for the flexible responses are presented. They were calculated for all four velocities, 3.090, 8.230, 10.289 and 15.433 m/s, for head seas, and additional theoretical predictions for oblique waves, headings 135 and 90°, respectively for 8.230 and 10.289 m/s. Theoretical predictions are presented for the two-dimensional beam-strip model idealization, and the three-dimensional plate-panel model, referred as *model C*. The first three symmetrical principal coordinate amplitudes (2-, 3- and 4-node vertical) were evaluated for the three different headings.

Symmetrical principal coordinates amplitudes seem to be overestimated by the two-dimensional beam model comparatively to the three-dimensional plate model. However, this tendency appears to change as the forward speed increases. As expected, the principal coordinate amplitudes reduce as the flexible mode indexes increase. Non-dimensional frequencies related to resonance and other peak positioning are almost the same for the two models in oblique waves for the 3-node vertical mode.

The principal coordinate amplitudes for the 4-node vertical bending in the 3D-Plate

model largely reduce their magnitudes against some overestimate of the 2D-Beam model. It demonstrates that there might be a possible numerical instability for frequencies greater than $\omega'_e \approx 5$. It should also be noted that differences between the natural frequencies obtained by 2D-Beam and 3D-Plate models are large from the 3-node mode forwards. These figures show some indications that the three-dimensional plate model seems to be more adequate for the theoretical prediction of the fluid structure interaction.

For the symmetric modes presented in this investigation the principal coordinates have their maximum amplitude value always for head sea conditions, disregarding irregular frequencies. Globally, comparing head waves with oblique ones, the 3D-Plate model shares smaller variations than the case of the 2D-Beam model.

The present study attempts to be an humble contribution for the research of the dynamic behaviour of monohulls with a small length to beam ratios, regarding a unified hydroelastic analysis. The study has shown some inherent limitations, to a beamlike approach for this particular type of vessels.

12.2 Recommendations for Future Work

The following are recommended, as they will contribute to furthering the understanding of this field of study. The comparison of the antisymmetric modes evaluated for the beam models with the ones already obtained on the three-dimensional dry hull analysis is carried out.

- Wave induced loads should be evaluated for the hull spatial positions considered as critical. They would ideally include calculations for vertical and horizontal bending moments, vertical shear force and torsional moment. This will lead to the numerical evaluation of the longitudinal direct stresses, and since strain readings were obtained successfully they can be used for a complete comparison with measured data.

- Apart from some drift of the calibration curves of the strain gauges in the engine room, mainly due to thermal influence, the oscillatory responses, stationary and transient strains were obtained, making possible to identify, in future studies, some natural frequencies, and to estimate almost quantitatively some structural damping, recorded in this particularly interesting area of the Patrol Boat.

- Measured data, from the full-scale trials conducted in this investigation, also include following seas that could be compared to rigid body numerical predictions. Furthermore, based on the wave buoy data at the full-scale trial's date, studies can be addressed towards the evaluation of the directional wave spectrum that will possible lead to the identification of some wave spreading that was not observed on board of the patrol boat during sea trials.

Appendix A

AutoHydro Results

A.1 Hull Data (with appendages)

Hull Condition

- Baseline Draft:1.434 at Origin
- Trim: 0.03 deg
- Heel: zero

Dimensions

- Length Overall: 27.014 m
- LWL: 24.896 m
- Beam: 5.940 m
- BWL: 5.720 m
- Volume: 85.879 m^3
- Displacement: 88.026 MT

Coefficients

- Prismatic: 0.773
- Block: 0.421
- Midship: 0.544
- Waterplane: 0.720

Ratios

- Length/Beam: 4.548
- Displacement/length: 158.971
- Beam/Draft: 4.143
- MT/cm Immersion: 1.050

Areas

- Waterplane: 102.472 m^2
- Wetted Surface: 140.030 m^2
- Under Water Lateral Plane: 33.752 m^2
- Above Water Lateral Plane: 80.982 m^2

Centroids

- Buoyancy: LCB = 10.901 fwd
- TCB =0.000 port
- VCB = 0.930
- Flotation: LCF = 11.604 fwd
- Under Water LP: 11.867 fwd of Origin, 0.697 below waterline.
- Above Water LP: 13.117 fwd of Origin, 1.826 above waterline.

Note: All values in meters and coefficients are calculated based on waterline length at a given draft.

A.2 Hydrostatic Properties

Draft is from Baseline with VCG equal to 2.212 meters. [1]

LCF Draft(m)	Displ (MT)	LCB (m)	VCB (m)	LCF (m)	TPcm (MT/cm)	MTcm (MT-m/deg)	KML (m)	KMT (m)
0.100	0.454	9.733f	0.067	9.938f	0.09	5.48	693.042	0.382
0.200	1.835	9.975f	0.134	10.132f	0.18	11.47	360.523	0.756
0.300	4.145	10.067f	0.201	10.160f	0.28	17.29	241.141	1.129
0.400	7.396	10.125f	0.267	10.212f	0.37	23.46	183.923	1.501
0.500	11.594	10.171f	0.334	10.252f	0.47	29.77	149.313	1.873
0.600	16.748	10.209f	0.401	10.285f	0.56	36.21	126.086	2.243
0.700	22.848	10.234f	0.468	10.291f	0.66	42.46	108.681	2.614
0.800	29.902	10.254f	0.535	10.309f	0.75	48.99	96.071	2.985
0.900	37.920	10.280f	0.602	11.351f	0.76	42.89	67.011	3.247
1.000	45.966	10.460f	0.664	11.253f	0.85	49.63	64.070	3.688
1.100	54.976	10.585f	0.727	11.184f	0.95	56.32	60.901	4.122
1.200	64.681	10.689f	0.791	11.352f	0.99	59.94	55.302	3.918
1.300	74.717	10.787f	0.853	11.476f	1.02	63.25	50.708	3.724
1.400	85.042	10.877f	0.913	11.576f	1.04	66.49	47.006	3.572
1.500	95.591	10.959f	0.972	11.671f	1.06	68.77	43.428	3.418
1.600	106.321	11.035f	1.031	11.747f	1.08	70.82	40.373	3.295
1.700	117.207	11.104f	1.088	11.802f	1.10	72.57	37.684	3.197
1.800	128.234	11.167f	1.145	11.848f	1.11	74.18	35.352	3.121
1.900	139.398	11.224f	1.202	11.890f	1.12	75.75	33.343	3.065
2.000	150.695	11.276f	1.258	11.927f	1.13	77.20	31.559	3.025
2.100	162.112	11.324f	1.314	11.969f	1.15	78.83	30.070	2.997
2.200	173.665	11.368f	1.370	12.011f	1.16	80.51	28.771	2.980
2.300	185.354	11.410f	1.425	12.053f	1.18	82.24	27.630	2.972
2.400	197.182	11.450f	1.481	12.096f	1.19	84.02	26.622	2.971
2.500	209.149	11.488f	1.536	12.139f	1.20	85.84	25.725	2.976
2.600	221.257	11.526f	1.592	12.183f	1.22	87.72	24.924	2.986
2.700	233.508	11.562f	1.648	12.226f	1.23	89.64	24.205	3.001
2.800	245.903	11.597f	1.703	12.270f	1.25	91.62	23.557	3.020
2.900	258.436	11.631f	1.759	12.309f	1.26	93.49	22.936	3.043
3.000	271.097	11.664f	1.815	12.452f	1.26	92.77	21.816	3.049

Table A.1: Hydrostatic Properties

[1] Water Specific Gravity = 1.025 kg/L

A.3 Weight Distribution

Weight Position (m)				Weight Longitudinal Limits	
Weight (ton)	LCG	TCG	VCG	L1	L2
0.05	0.11a	0.00	2.05	0.00f	0.21a
0.63	0.11f	0.00	1.52	0.21f	0.01f
1.60	0.87f	0.00	1.54	1.50f	0.21f
1.57	2.13f	0.00	1.56	2.75f	1.50f
1.90	3.52f	0.00	1.58	4.25f	2.75f
3.10	5.01f	0.00	2.40	5.75f	4.25f
3.31	6.76f	0.00	2.22	7.75f	5.75f
2.83	8.51f	0.00	2.24	9.25f	7.75f
2.51	9.70f	0.00	2.41	10.15f	9.20f
2.79	10.96f	0.00	2.66	11.75f	10.15f
2.99	12.76f	0.00	2.71	13.75f	11.75f
2.69	14.52f	0.00	2.72	15.25f	13.75f
2.59	16.01f	0.00	2.46	16.75f	15.25f
1.20	17.36f	0.00	1.69	17.95f	16.75f
0.85	18.10f	0.00	1.93	18.25f	17.95f
1.96	19.02f	0.00	1.98	19.75f	18.25f
1.01	20.26f	0.00	2.13	20.75f	19.75f
1.41	21.26f	0.00	2.19	21.75f	20.75f
0.83	22.26f	0.00	2.28	22.75f	21.75f
1.24	23.26f	0.00	2.43	23.75f	22.75f
0.71	24.12f	0.00	2.57	24.48f	23.75f
0.61	24.84f	0.00	2.89	25.20f	24.48f
0.38	26.00f	0.00	3.45	26.80f	25.20f
11.24	7.88f	0.00	2.00	11.63f	4.13f
1.21	16.63f	0.00	0.90	19.13f	14.13f
2.00	12.26f	0.00	0.90	14.13f	10.38f
5.79	20.38f	0.00	0.80	22.88f	17.88f
1.00	11.01f	0.00	4.70	11.63f	10.38f
1.25	13.51f	0.00	3.20	15.38f	11.63f
1.30	9.76f	0.00	4.71	11.63f	7.88f
25.50	8.14f	0.00	2.43	23.75f	0.00f

Table A.2: Weight Distribution

A.4 Longitudinal Loading

Location(m)	Weight(MT)	Buoyancy(MT/m)	Shear(MT)	Bending(MT·m)
26.80f	0.000	0.000	0.00	0
26.80f	0.238	0.000	0.00	0
25.20f	0.238	0.000	-0.38	0
25.20f	0.847	0.000	-0.38	0
24.68f	0.847	0.000	-0.82	1
24.48f	0.847	0.036	-0.99	1
24.48f	1.013	0.036	-0.99	1
24.47f	1.012	0.037	-0.99	1
23.75f	0.933	0.418	-1.53	2
23.75f	1.375	0.418	-1.53	2
22.88f	1.320	1.080	-2.05	3
22.88f	2.478	1.080	-2.05	3
22.75f	2.469	1.179	-2.23	4
22.75f	2.184	1.179	-2.23	4
21.75f	2.169	1.908	-2.86	6
21.75f	2.884	1.908	-2.86	6
20.75f	2.800	2.450	-3.52	9
20.75f	2.545	2.450	-3.52	9
19.75f	2.509	2.903	-3.37	13
19.75f	2.971	2.903	-3.37	13
19.13f	2.938	3.151	-3.33	15
19.13f	3.180	3.151	-3.33	15
18.25f	3.132	3.502	-3.18	18
18.25f	4.763	3.502	-3.18	18
17.95f	4.789	3.611	-3.54	19
17.95f	3.005	3.611	-3.54	19
17.88f	3.006	3.630	-3.50	19
17.88f	1.848	3.630	-3.50	19
16.75f	1.850	3.946	-1.31	22
16.75f	2.696	3.946	-1.31	22
15.38f	**2.686**	**4.245**	**0.62**	**22**
15.38f	3.022	4.245	0.62	22
15.25f	3.021	4.274	0.78	22
15.25f	3.300	4.274	0.78	22
14.13f	3.180	4.422	2.02	21
14.13f	3.476	4.422	2.02	21
13.75f	3.434	4.473	2.39	20
13.75f	3.324	4.473	2.39	20
11.75f	3.398	4.560	4.71	13
11.75f	3.757	4.560	4.71	13
11.63f	3.756	4.561	4.80	12
11.63f	6.093	4.561	4.80	12
10.38f	6.055	4.564	2.91	7
10.38f	4.745	4.564	2.91	7
10.15f	4.745	4.564	2.87	7
10.15f	5.856	4.564	2.87	7
9.25f	5.931	4.567	1.68	5
9.25f	5.104	4.567	1.68	5
7.88f	5.081	4.570	0.96	3
7.88f	4.737	4.570	0.96	3
7.75f	4.735	4.570	0.94	3
7.75f	4.629	4.570	0.94	3
5.75f	4.700	4.575	0.75	1
5.75f	5.244	4.575	0.75	1
4.26f	5.207	4.579	-0.21	1
4.25f	5.207	3.379	-0.22	1
4.25f	4.591	3.379	-0.22	1
4.13f	4.585	3.379	-0.37	1
4.13f	3.086	3.379	-0.37	1
2.75f	3.018	3.381	0.08	1
2.75f	3.138	3.381	0.08	1
1.50f	3.185	3.383	0.36	1
1.50f	3.286	3.383	0.36	1
0.21f	3.223	3.385	0.53	0
0.21f	5.219	3.385	0.53	0
0.01f	5.236	1.111	-0.07	0
0.01f	2.086	1.111	-0.07	0
0.00	2.087	0.996	-0.08	0
0.00	0.204	0.996	-0.08	0
-0.21a	0.272	0.211	0.00	0
-0.21a	0.000	0.098	0.00	0

Table A.3: Longitudinal Loading

Max. Shear 4.80 MT at 11.630f Max. Bending Moment 22 MT·m at 15.380f (Hogging)

A.5 Righting Arms

Heel Angle(deg)	Trim Angle(deg)	Origin Depth(m)	Righting Arm(m)
0.00	0.03a	1.434	0.000
5.00s	0.03a	1.427	0.115
10.00s	0.05a	1.402	0.221
15.00s	0.02a	1.338	0.297
20.00s	0.07f	1.237	0.350
25.00s	0.19f	1.106	0.389
30.00s	0.30f	0.956	0.425
35.00s	0.42f	0.785	0.463
40.00s	0.51f	0.598	0.508
45.00s	0.54f	0.413	0.548
50.00s	0.52f	0.238	0.568
52.76s	0.49f	0.144	0.570
55.00s	0.46f	0.069	0.569
60.00s	0.39f	-0.095	0.556

Table A.4: Righting Arms vs Heel Angle

Appendix B

Combined Linearised Free-Surface Boundary Condition

It is possible to obtain the boundary conditions at the mean free-surface, $z = 0$, from the free-surface position $z = \zeta(x, y, t)$ by means of a Taylor expansion.Thus keeping the linear terms obtained in equations 4.10 and 4.13 the kinematic boundary condition for the mean free-surface becomes

$$\frac{\partial \zeta}{\partial t} = \frac{\partial \Phi}{\partial z}, \tag{B.1}$$

and the dynamic boundary condition,

$$g\zeta + \frac{\partial \Phi}{\partial t} = 0. \tag{B.2}$$

Solving equation B.2 for the wave elevation, ζ, and combining the result with equation B.1 the single boundary condition for the mean free-surface, $z = 0$, is then given by

$$\frac{\partial^2 \Phi}{\partial t^2} + g\frac{\partial \Phi}{\partial z} = 0. \tag{B.3}$$

Assuming harmonic oscillation, of the velocity potential Φ, equation B.3 assumes the following form,

$$-\omega^2 \Phi + g\frac{\partial \Phi}{\partial z} = 0, \tag{B.4}$$

where ω represents the circular frequency of oscillation.

Appendix C

Cross Section Properties of Model C

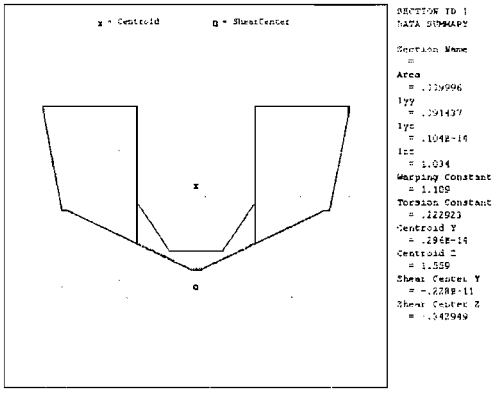

Figure C.1: Cross Section at x=1.50 m

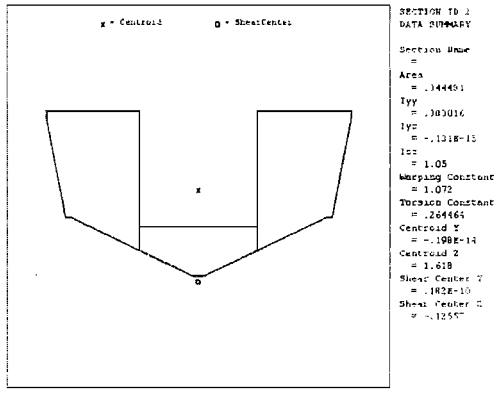

Figure C.2: Cross Section at x=2.75 m

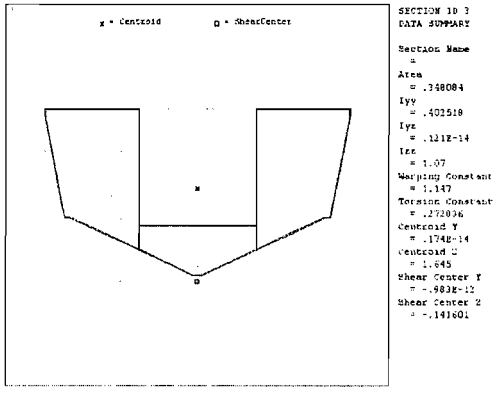

Figure C.3: Cross Section at x=4.25 m

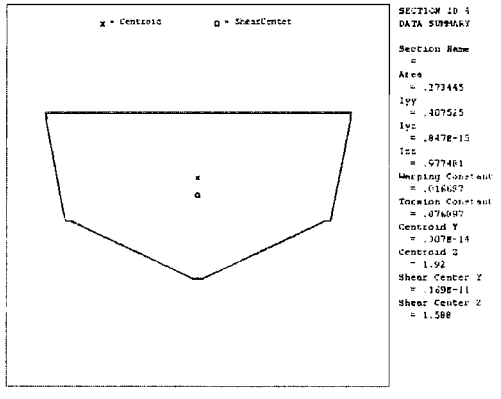

Figure C.4: Cross Section at x=5.75 m

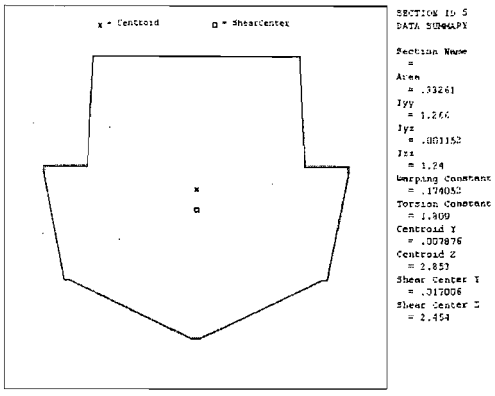

Figure C.5: Cross Section at x=7.75 m

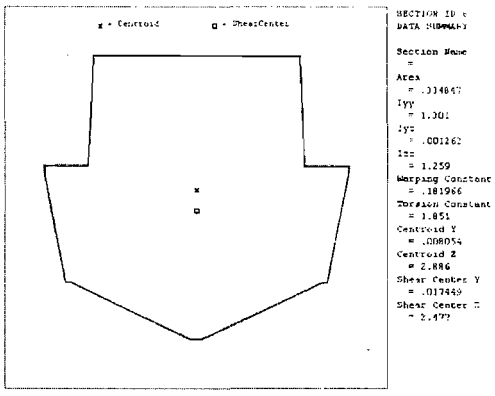

Figure C.6: Cross Section at x=9.25 m

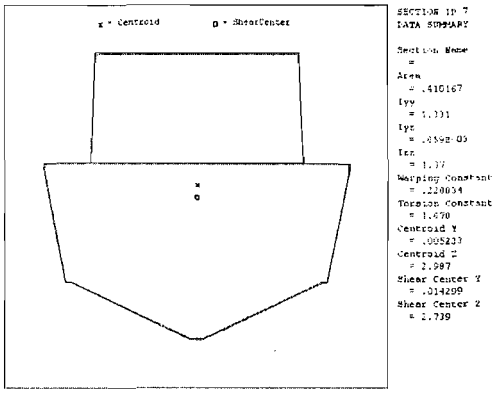

Figure C.7: Cross Section at x=10.15 m

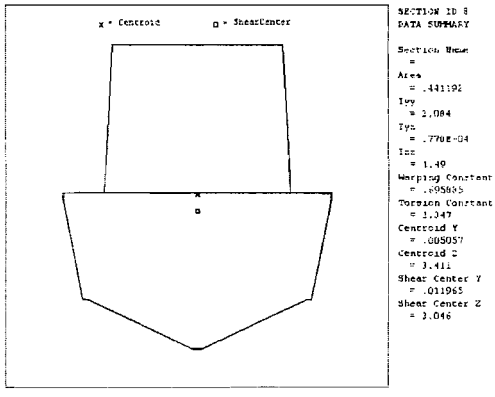

Figure C.8: Cross Section at x=11.75 m

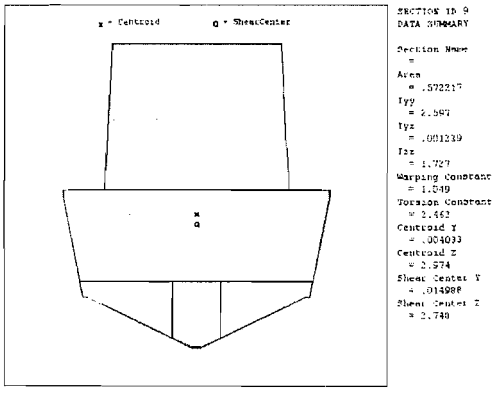

Figure C.9: Cross Section at x=13.75 m

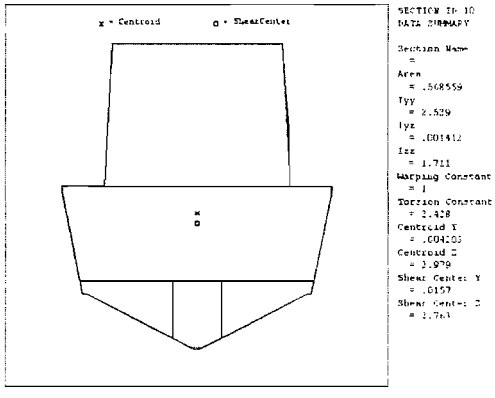

Figure C.10: Cross Section at x=15.25 m

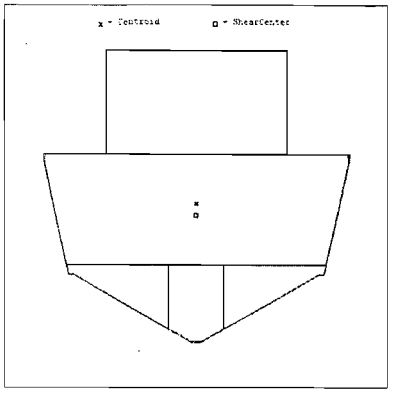

Figure C.11: Cross Section at x=16.75 m

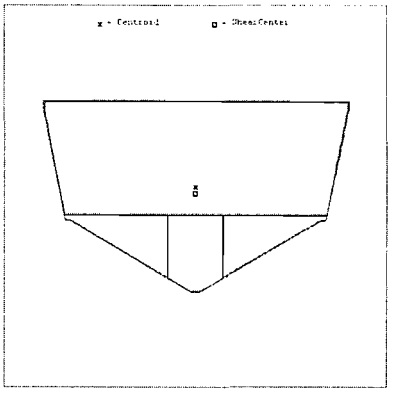

Figure C.12: Cross Section at x=17.95 m

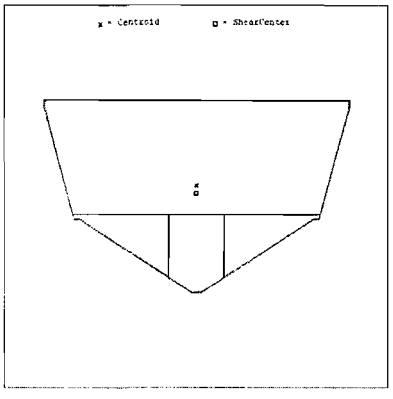

Figure C.13: Cross Section at x=18.25 m

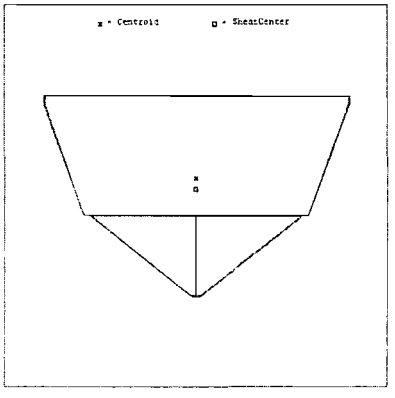

Figure C.14: Cross Section at x=19.75 m

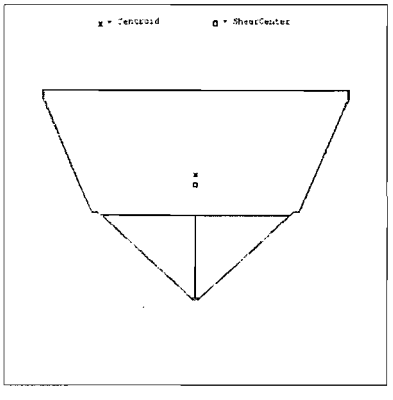

Figure C.15: Cross Section at x=20.75 m

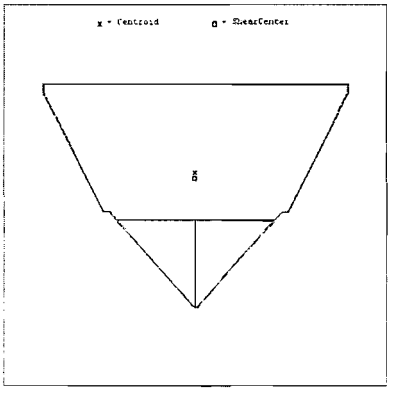

Figure C.16: Cross Section at x=21.75 m

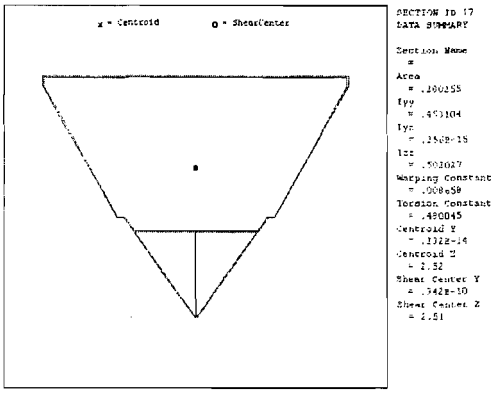

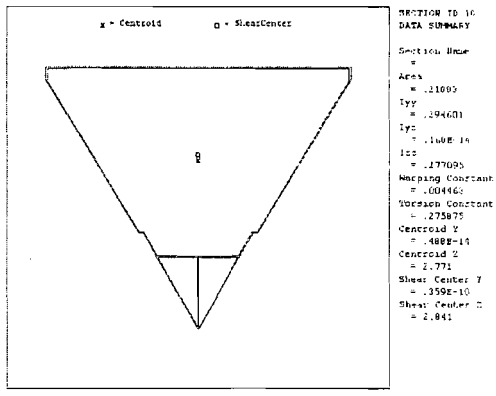

Figure C.17: Cross Section at x=22.75 m Figure C.18: Cross Section at x=23.75 m

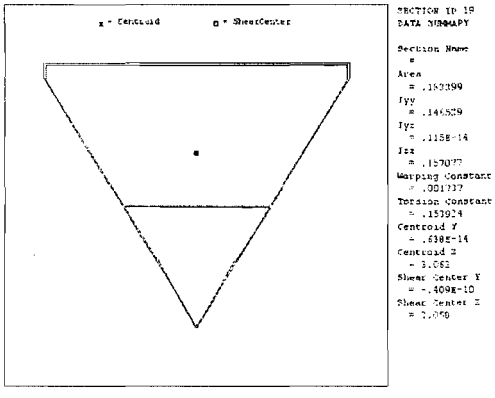

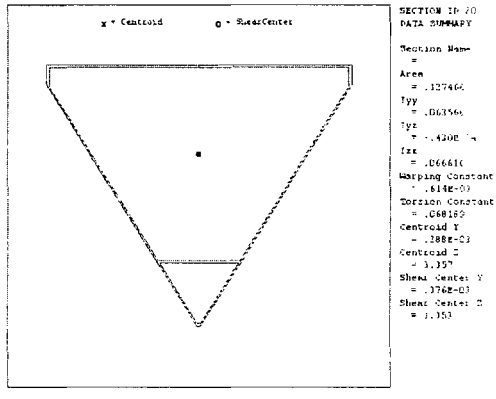

Figure C.19: Cross Section at x=24.48 m Figure C.20: Cross Section at x=25.20 m

Bibliography

[1] Bishop, R.E.D. & Price, W.G. 1979. *Hydroelasticity of Ships.* Cambridge University Press.

[2] Bergan, P.G., Nestgard, A. & Skeie, G. 1999. *On the solution of Fluid Structure Interaction Problems in the Maritime Industries.* European Conference on Computational Mechanics (ECCM). Munich, Germany.

[3] Faltinsen, O. M. 1990 *Sea loads on ships and offshore structures.* Cambridge University Press, New York.

[4] Spyridon, E. H. 2002 *Hydroelastic modelling for the prediction of wave induced loads on bulk carriers.* Southampton University PhD Thesis.

[5] Gorbatov, Y. 1998 *Reliability of Maintained Ship Structures Subjected to Corrosion and Fatigue.* Technical University of Lisbon, PhD thesis Instituto Superior Técnico.

[6] Hughes, O.F. 1988 *Ship Structural Design - A Rationally-Based, Computer-Aided Optimization Approach.* The Society of Naval Architects and Marine Engineers.

[7] Kaminski, M.L., Amdahl, J., Fasano, E.,Frieze, P.A., Gordo, J.M., Grundy, P., Hess, P.E., Kawamoto, Y., Kujala, P., Paik, J.K., Rohr, U., Simonsen, B.C. 2000 *Ultimate Strength, Technical Committee III.1.* 14th International Ship and Offshore Structures Congress, Nagasaki, Japan.

[8] Gibson, R.F. 1994. *Principles of Composite Material Mechanics.* Mc Graw-Hill International Editions.

[9] Heller, S.R. and Jasper, N.H. 1961. *On the Structural Design of Planning Craft.* Trans. RINA, 103, pp.49.

[10] Savitsky, D. and Brown, P.W., 1976. *Procedures for the Hydrodynamic Evaluation of Planning Craft in Smooth and Rough Water.* Marine Technology, 13(4).

[11] Allen, R.G. and Jones, R.R., 1978. *A Simplified Method for Determining Structural Design Limit Pressures on High Performance Marine Vehicles.* Proc. AIAA/SNAME Advanced Marine Vehicles Conf. San Diego, CA.

[12] Smith, C.S. 1990. *Design of Marine Structures in Composite Materials.* Elsevier Science Publishers Ltd.

[13] Lloyds Register of Shipping, 1978. *Rules and Regulations for the Classification of Yachts and Small Craft*, London.

[14] det Norske Veritas, 1981. *Rules for the Construction and Certification of Boats*, Norway.

[15] American Bureau of Shipping, 1978. *Rules for Building and Classing Reinforced Plastic Vessels*, New York.

[16] Registro Italiano Navale, 1977. *Rules for Pleasure Boats and Ships*, Genoa.

[17] European Association of Classification Societies, 1982. *Rules for Pleasure Boats-GRP Hulls*, London.

[18] Bureau Veritas, 1979. *Rules and Regulations for the Construction and Classification of Textile Glass Reinforced Polyester Vessels*, Paris.

[19] Recreational Craft Sectoral Group (RSG), 1994. *Recreational Craft Directive 94/25/EC.*

[20] Froude, W., 1861. *On the Rolling of Ships*, Transactions the Institute of Naval Architects, London, Vol.2 pp.180-229.

[21] Froude, W., 1955. *The Papers of William Froude*, The Institute of Naval Architects, London.

[22] Korvin-Kroukovsky, B.V., 1961. *Theory of Seakeeping*, Society of Naval Architects and Marine Engineers, New York.

[23] Comstock, J.P., 1967. *Principles of Naval Architecture*, Society of Naval Architects and Marine Engineers, New York.

[24] Newman, J.N., 1978. *The theory of ship motions*, Adv Appl Mech, Vol 18, pp 221-283.

[25] Bishop, R.E.D., Price, W.G., 1991. *Some Comments on Present-Day Ship Dynamics*, Philosophical Transactions, R. Soc. London, A334, pp.187-197.

[26] Krilov, A., 1896. *A New Theory of the Pitching Motion of the Ships on Waves, and of the Stresses Produced by this Motion*, Transactions the Institute of Naval Architects, London, Vol.65 pp.590-632.

[27] Michell, J.H., 1898. *The Wave Resistance of a Ship*, Phil. Magazine, Vol.45 pp.106-123.

[28] Haskind, M.D, 1964. *The Hydrodynamic Theory of Ship Oscillations in Rolling and Pitching*, Research Bulletin of the Society of Naval Architects and Marine Engineers, No.1-12, pp.3-43.

[29] Peters, A.S., and Stoker, J.J., 1957. *The Motion of a Ship, as Floating Rigid Body, in a Sway*, Communications Pure Applied Mathematics, Vol.10 pp.399-490.

[30] Newman, J.N., 1961. *A Linearized Theory for the Motion of a Thin Ship in Regular Waves.* Journal of Ship Research, Vol.3, No.1, pp.1-19.

[31] Maruo, H., 1962. *Calculation of the Wave Resistance of Ships, the Draught of Which is as Small as the Beam.* Journal Zosen Kiokai, The Society of Naval Architects of Japan, Vol.112, pp.67-102.

[32] Ursell, F., 1962. *Slender Oscillating Ships at Zero Forward Speed.* Journal of Fluid Mechanics, Vol.19, pp.496-516.

[33] Tuck, E.O., 1964. *A Systematic Asymptotic Expansion Procedure for Slender Ships.* Journal of Ship Research, No.8, pp.15-23.

[34] Newman, J.N. and Sclavounos, P.D. 1980. *The Unified Theory for Ship Motions.* Proceedings 13th Symposium Naval Hydrodynamics, Tokyo.

[35] Maruo, H. and Tokura, J. 1978. *Prediction of Hydrodynamic Forces and Moments Acting on Ships in Heaving and Pitching Oscillations by Means of an Improvement of the Slender Ship Theory.* Journal of the Society of Naval Architects of Japan, Vol.143, pp.111-120.

[36] Mays, J.H. 1978. *Wave Radiation and Diffraction by a Floating Slender Body.* Ph.D. Thesis, Department of Ocean Engineering Massachusetts Institute of Technology, Cambridge, Massachusetts.

[37] Korvin-Kroukovsky, B.V., 1955. *Investigation of Ship Motions in Regular Waves*, Transactions of the Society of Naval Architects and Marine Engineers, Vol.63, pp.385-435.

[38] Timman, R. and Newman, J.N. 1962. *The Coupled Damping Coefficients of Symmetric Ships*, Journal of Ship Research, Vol.5, No.4.

[39] Ogilvie, T.F. and Tuck, E.O. 1969. *A Rational Strip Theory for Ship Motions*, Report No. 013 of the Department of Naval Architects and Marine Engineers, University of Michigan, Ann Arbor.

[40] Fonseca, N., 2001. *Hidrodinâmica dos Movimentos e Esforços Induzidos em Navios por Ondas de Grande Amplitude.* Technical University of Lisbon, PhD thesis Instituto Superior Técnico.

[41] Gerritsma, J. and Beukelman, W., 1967. *Analysis of the Modified Strip Theory for the Calculation of Ship Motions and Wave Bending Moments.* International Shipbuilding Progress, Vol.14, No.156, pp.319-337.

[42] Salvesen, N., Tuck, E.O. and Faltisen, O., 1970. *Ship Motions and Sea Loads*, Transactions of the Society of Naval Architects and Marine Engineers, Vol.78, pp.250-287.

[43] Kaplan, P., Sargent, T.P., and Raff, A.I., 1969. *An Investigation of the Utility of Computer Simulation to Predict Ship Structural Response*, Report SSC-197, Second Technical Progress Report from Project Sr-147, Ship Computer Response to the Ship Structures Committee, U.S. Coast Guard.

[44] Jensen, J.J. and Pedersen, P.T., 1979. *Wave-Induced Bending Moments in Ships- a Quadratic Theory*, Transactions of the Royal Institute of Naval Architects, Vol.121, pp.151-165.

[45] Paulling, J.R. and Wood, P.D. 1974. *Ship Motions and Capsizing in Astern Seas.* Proceedings of the 10th Symposium of Naval Hydrodynamics ,pp.93-109.

[46] Xia, J. and Wang, Z. 1997. *Time-Domain Hydro-Elasticity Theory of Ships Responding to Waves.* Journal of Ship Research, Vol.41, No.4, pp.286-300.

[47] Xia, J., Wang, Z. and Jensen, J.J. 1998. *Non-Linear Wave Loads and Ship responses by a Time-Domain Strip Theory.* Marine Structures, Vol.11, No.3, pp.101-123.

[48] Fonseca, N. and Guedes Soares, C., 1998a. *Time-Domain Analysis of Large-Amplitude Vertical Motions and Wave Loads.* Journal of Ship Research, Vol.42, No.2, pp.100-113.

[49] Fonseca, N. and Guedes Soares, C., 1998b. *Non-Linear Wave Induced Responses of Ships in Irregular seas.* Proceedings of the 12th International Conference on Offshore Mechanics and Artic Engineering (OMAE'98), ASME, Article No. 98, New York.

[50] Ogilvie, T.F. 1972. *The Wave Generated by a Fine Ship Bow*, Proceedings of the 5th Symposium on Naval Hydrodynamics, pp.3-128, Washington D.C.

[51] Faltinsen, O.M. and Zhao, R. 1991. *Numerical Predictions of Ship Motions at High Forward Speed.* Philosophical Transactions: Physical Sciences and Engineering, Royal Society London, Vol.A 334, pp.241-252.

[52] Chapman, R.B. 1975. *Free Surface Effects for Hydrodynamic Forces on a Surface-Piercing Plating Oscillating in Yaw and Sway.* Proceedings 1st International Conference of Numerical Ship Hydrodynamics, pp.333-350, David W. Taylor Ship R&D Center, Bethesda, Maryland.

[53] Zhao, R. 1997. *A complete Linear Time-Domain Analysis for Predicting Ship Motions at Higher Froude Number.* International Shipbuilding Progress, Vol.44, No.440, pp.341-361.

[54] Hess, J.L. and Smith A.M.O. 1964. *Calculation of Non-Lifting Potential Flow about Three-dimensional Bodies.* Journal of Ship Research, No.8, pp.22-44.

[55] Hess, J.L. and Smith A.M.O. 1967. *Calculation of Potential Flow about Arbitrary Bodies.* Progress in Aeronautical Sciences, Vol.8, pp.1-138.

[56] Faltinsen, O.M. and Michelsen, F.C. 1974. *Motions of Large Structures in Waves at Zero Froude Number.* Dynamics of Marine Vehicles and Structures in Waves, R.E.D. Bishop and W.g. Price (Editors), Institute of Mechanical Engineers, London, pp.91-112.

[57] Faltinsen, C.I. 1978. *Hydrodynamic Loading of Large Structures: Three Dimensional Source Distribution Methods.* Numerical Methods in Offshore Engineering, pp.87-140.

[58] Eatock Taylor, R. and Waite, J.B., 1978. *The Dynamics of Offshore Structure Evaluated by Boundary Integral Techniques.* International Journal of Numerical Methods, Vol.13 pp.73-92.

[59] Newman, J.N. and Sclavounos, P.D., 1988. *The Computation of Wave Loads on Large Offshore Structures.* Proceedings International Behaviour of Offshore Structures, T. Moan, N. Janbu and O. Faltinsen (Editors), Trondheim, pp.605-622.

[60] Chang, M.S., 1977. *Computations of Three-dimensional Ship Motions with Forward Speed.* Proceedings 2nd International Numerical Ship Hydrodynamics, University of California, Berkeley, pp.124-135.

[61] Inglis, R.B. and Price, W.G., 1981a. *A Three-dimensional Ship Motion Theory - Comparison Between Theoretical Prediction and Experimental Data of the Hydrodynamic Coefficients with Forward Speed.* Transactions of the Royal Institution of Naval Architects, Vol.124, pp.141-157.

[62] Inglis, R.B. and Price, W.G., 1981b. *The Influence of Speed Independent Boundary Conditions in Three-dimensional Ship Motion Problems.* International Shipbuilding Progress, No.28(318), pp.22-29.

[63] Guevel, P. and Bougis, R., 1982. *Ship Motions with Forward Speed in Infinite Depth.* International Shipbuilding Progress, No.29, pp.20-33.

[64] Ba, M. and Guilbaud, M., 1995. *A fast Method of Evaluation for the Translating and Pulsating Green's Function.* Ship Technology Research Bulletin (SNAME), No.42.

[65] Lin, W.M. and Yue, D., 1990. *Numerical Solutions for Large-Amplitude Ship Motions in the Time Domain.* Proceedings of the 18th Symposium on Naval Hydrodynamics, Ann Harbor, pp.41-66.

[66] Lin, W.M. and Yue, D., 1993. *Time-domain analysis for floating bodies in mild-slope waves of large amplitude.* Proceedings of the 8th International Workshop on Water Waves and Floating Bodies, St. Johns, Newfoundland, Canada.

[67] Bingham, H., Korsmeyer, F. Newman, J.N., 1993. *The Simulation of Ship Motions.* Proceedings of the 6th International Conference on Numerical Ship Hydrodynamics, Iowa City, pp.561-579.

[68] Bingham, H., Korsmeyer, F. Newman, J.N., 1994. *Prediction of the Seakeeping Characteristics of Ships.* Proceedings of the 20th Symposium on Naval Hydrodynamics, Santa Barbara, California, USA, pp.19-38.

[69] Magee, A.R., 1994. *Seakeeping Calculations using a Time Domain Method.* ings of the 20th Symposium on Naval Hydrodynamics, Santa Barbara, California, USA.

[70] Inglis, C.E., 1929. *Natural Frequencies and Modes of Vibration in Beams of Non-Uniform Mass and Section.* Transactions of the Royal Institution of Naval Architects, Vol.2, pp.145-166.

[71] Heller, S.R. and Ambramson, H.N. 1959. *Hydroelasticity - A New Naval Science.* Journal of the American Society of Naval Engineers, Vol.71, pp.205-209.

[72] Bishop, R.E.D., Price, W.G. & Temarel, P. 1980. *A Unified Dynamic Analysis of Antisymmetric Ship Responses to Waves.* Transactions from The Royal Institution of Naval Architects, 122, 349-365.

[73] Bishop, R.E.D., Chalmers, D.W., Price, W.G. & Temarel, P. 1986. *The Dynamic Characteristics of Unsymmetrical Ship Structures.* Transactions from The Royal Institution of Naval Architects, 128, 205-215.

[74] Bishop, R.E.D., Price, W.G. & Tam, P.K.Y 1978. *On the Dynamics of Slamming.* Transactions from The Royal Institution of Naval Architects, 120, 259-280.

[75] Belik, O., Bishop, R.E.D. and Price, W.G., 1980. *On the Slamming Response of Ships to Regular Head Waves*, Transactions of the Royal Institute of Naval Architects, Vol.122, pp.325-337.

[76] Belik, O., Bishop, R.E.D. and Price, W.G., 1983. *A Simulation of Ship Responses due to Slamming in Irregular Head Waves*, Transactions of the Royal Institute of Naval Architects, Vol.125, pp.237-253.

[77] Bishop, R.E.D., Clarke, J.D. & Price, W.G. 1984. *Comparison of Full Scale and Predicted Responses of Two Frigates in a Severe Weather Trial.* Transactions from The Royal Institution of Naval Architects, 126, 153-166.

[78] Guedes Soares, C., 1989. *Transient Response of Ship Hulls to Wave Impact.* International Shipbuilding Progress, Vol.36, No.406 ,pp.137-156.

[79] Aksu, S., Price W. G., Suhrbier, K. R., Temarel, P. 1993 *A Comparative Study of the Dynamic Behaviour of a Fast Patrol Boat Travelling in Rough Seas.* Marine Structures, Elsevier Science Publishers Ltd, United Kingdom.

[80] Xia, J., Wang, Z. and Jensen, J.J. 1998. *Non-linear Wave Loads and Ship Responses by a Time Domain Strip Theory.* Marine Structures, 11, pp.101-123.

[81] Wu, Y.S., 1984. *Hydroelasticity of Floating Bodies*, Ph.D. thesis, Brunel University, UK.

[82] Bishop, R.E.D., Price, W.G. & Wu, Y. 1986. *A General Linear Hydroelasticity of Floating Structures Moving in a Seaway.* Phil. Trans. Royal Soc. of London, Series A 316, pp. 375-425.

[83] Aksu, S., Price W. G. & Temarel, P. 1991. *A Three-dimensional theory of Ship Slamming in Irregular Oblique Seaways.* International Symposium on the Dynamiocs of Marine vehicles and Structures in Waves, W.G. Price et al. (Editors) Elsiever Science Publishers, UK.

[84] Aksu, S., Price W. G. & Temarel, P. 1991. *A Comparison of Two-dimensional and Three-dimensional Hydroelasticity Theories Including the Effects of Slamming.* Proceedings of IMechE, 205, pp.3-15.

[85] Miao, S.H., Price, W.G. & Temarel, P. 1997 *The Hydroelastic Behaviour of Multi-Hulls Travelling in a Seaway.* Proceedings of the 3rd International Conference in Advances in Marine Structures.

[86] Louarn, F. & Temarel, P. 1999. *An Investigaton of the Structural Dynamics of a Racing Yacht.* 14th Chesapeake Sailing Yacht Symposium, USA.

[87] Keane, A.J., Temarel, P., Wu, X.J. & Wu, Y. 1991 *Hydroelasticity of Non-Beamlike Ships in Waves.* Transactions of the Royal Society, London, United Kingdom.

[88] Louarn, F. 1998. *Hyroelastic Behaviour of a Sailing Yacht in Waves - M.Phil. to Ph. D. Transfer Document.* University of Southampton, Department of Ship Science, United Kingdom.

[89] Price, W.G., Salas Inzunza, M., Temarel, P. 2002 *The Dynamic Behaviour of a Mono-Hull in Oblique Waves Using Two- and Three-Dimensional Fluid-Structure Interaction Models.* The Royal Institution of Naval Architects, United Kingdom.

[90] Craig, Roy R., Jr. 1981 *Structural Dynamics - An Introduction to Computer Methods.* John Wiley & Sons.

[91] Rayleigh, Lord. 1894. *The Theory of Sound.* Macmillan, London. 2nd Edition, art.4.

[92] Lagrange, J. L. 1888-89. *Mécanique analytique*, 4. ed., 2 vols. Paris: Gauthier-Villars et fils.

[93] Newman, J.N., 1977. *Marine Hydrodynamics.* Cambridge, Massachusetts: The MIT Press.

[94] Aris, R. 1962. *Vectors, Tensors, and the Basic Equations of Fluid Mechanics.* Englewood Cliffs, N.J., Prentice-Hall.

[95] Sommerfeld, A., 1949. *Partial differential equations in physics*, N Y: Academic Press.

[96] Salvesen, N., Tuck, E.O. Faltinsen, O. 1971 *Ship Motions and Sea Loads.* Publication No.75, Det Norske Veritas.

[97] Du, S.X., Hudson, D.A., Price, W.G. & Temarel, P. 2000. *A Validation Study on Mathematical Models of Speed and Frequency Dependence in Seakeeping.* Proc. Instn. Mech. Engrs., Vol 214, Part C.

[98] Halpin, J.C. and Tsai, S.W. 1969 *Effects of Environmental Factors on Composite Materials.* AFML-TR67-423.

[99] Halpin, J.C. and Kardos, J.L. 1976 *The Halpin-Tsai equations: a review.* Polym. Eng. Sci., 16, pp.344.

[100] Agarwal, B.D. and Broutman, L.J. 1980 *Analysis and Performance of Fiber Composites.* Wiley, New York.

[101] Hull, D. 1981 *An Introduction to Composite Materials.* Cambridge University Press, United Kingdom.

[102] Benham, P.P. & Crawford, R. J 1996. *Mechanics of Engineering Materials.* Longman Group.

[103] Barbero, E.J., Lopez-Anido, R. & Davalos, J.F. 1993 *On the Mechanics of Thin-walled Laminated Composite Beams.* Journal of Composite Materials, 27, 806-829.

[104] Cowper, G.R. 1966 *The Shear Coefficient in Timoshenko's Beam Theory.*Journal of Applied Mechanics, pp.335-340.

[105] Help System Release 5.4, 1997 *Ansys Reference Manual.* ANSYS, Inc.

[106] Thomson, W.T. 1993 *Theory of Vibration with Applications.*Prentice Hall, New Jersey.

[107] Lewis Edward, V. 1988 *Principles of Naval Architecture, Vol.2: Resistance, Propulsion and Vibration.*Society of Naval Architects and Marine Engineers, Jersey City, N.J..

[108] Meirovitch, L. 1986 *Elements of Vibration Analysis.* McGraw-Hill.

[109] Imaoka, S. 2000 *ANSYS Tips & Tricks: Structural SHELL Elements, Part 1.* Collaborative Solutions, Inc.

[110] Petyt, M. 1990 *Introduction to Finite Element Vibration Analysis* Cambridge University Press, United Kingdom.

[111] Hess, J.L., and Smith , A.M.O. 1962 *Calculation of Non-Lifting Potential Flow about Arbitrary Three Dimensional Bodies* Douglas Aircraft, rep. E.S.40622.

[112] Ship Science 1998 *Input Guide for Program FLXBD.*University of Southampton, The Faculty of Engineering and Applied Science, United Kingdom.

[113] Ship Science 1998 *Input Guide for Program HYCOF.*University of Southampton, The Faculty of Engineering and Applied Science, United Kingdom.

[114] John, F. 1950 *On the Motion of Floating Bodies.*Communs on Pure and Appl. Maths, No.3, pp.45-101.

[115] Lloyd, A.R.J.M. 1998 *Seakeeping - Ship Behaviour in Rough Weather.* ARJM Lloyd.

[116] Hearn, G. H., Metcalfe A. V. 1995 *Spectral Analysis in Engineering - Concepts and Cases.*Arnold, a member of the Hodder Headline Group.

[117] ISO 2631 1978 *Guide for the Evaluation of Human Exposure to Whole-Body Vibration.*

[118] Berg, P., Bråfelt, O., Folkeson, C. 1985 *Noise and Vibration on Board.* Joint Industrial Safety Council, Stockholm.

[119] Harris, C. M. 1995 *Shock and Vibration Handbook.* Mc Graw-Hill International Editions.

[120] Abrahamsen, K. A. 1997 *Requirements for Noise and Vibration: Prediction and Measurements.* WEGEMT Association 23^{rd} School. Full Scale Surveys of the Performance of Ships and Platforms. Genoa.

[121] St Denis, M. Pierson, W.J. 1953 *On The Motions of Ships in Confused Seas.* Transactions of the Society of Naval Architects and Marine Engineers.